UNIVERSITY OF SOUTHAMPTON

FACULTY OF PHYSICAL SCIENCES AND ENGINEERING

OPTOELECTRONICS RESEARCH CENTRE

FIBRE LASER SOURCES WITH LOW QUANTUM DEFECT

by

Tianfu Yao

Thesis for the degree of Doctor of Philosophy

December 2014

UNIVERSITY OF SOUTHAMPTON

ABSTRACT

FACULTY OF PHYSICAL SCIENCES AND ENGINEERING

OPTOELECTRONICS RESEARCH CENTRE

Doctor of Philosophy

FIBRE LASER SOURCES WITH LOW QUANTUM DEFECT

Tianfu Yao

High power fibre lasers with efficient amplification of optical signals have been widely used for various applications for many years. A great advantage of fibres is their thermal properties, which are so good that fibres are often quoted as being immune to thermal degradation. However, powers keep increasing and the fibre geometry is becoming more similar to their "bulk" (non-waveguiding) counterparts. Thermal problems are severe in bulk lasers, and are, unsurprisingly, becoming more important also for fibres. Heating is inevitable in the laser cycle due to the energy difference (quantum defect) between pump and signal photons. Nevertheless, there is substantial room to reduce the heating by minimising the quantum defect, with pump and signal wavelengths as close as possible.

In this thesis, I demonstrate low-quantum-defect fibre amplifiers and lasers based on two different energy conversion processes, i.e., in high-brightness (tandem) pumped ytterbium-doped fibre and in short-wavelength-pumped Raman fibre. The latter approach increases the photon energy relative to the thermal energy and vibrational energy of the host.

Firstly, as it comes to tandem-pumping of ytterbium-doped fibre amplifiers, the challenge is to make the pump and signal wavelengths as close as possible, while keeping the signal gain and pump absorption sufficiently high. With the optimum average ytterbium excitation level and high pump brightness, the quantum defect can be as small as 0.6% when pumped at 1030 nm, according to theoretical calculations. Subsequently, an experimental amplifier core-pumped by a single-mode laser source is presented. A 2% quantum defect is reached, with pump and signal wavelengths at 1030 nm and 1050 nm, respectively. The slope efficiency reaches 95% to 96%. Initial investigations show low photodarkening with tandem-pumping, with some dependence on the dependence on ytterbium ions concentration.

Secondly, Raman conversion of pulses in a diode-pumped highly nonlinear fibre is studied in a ring-laser cavity configuration. The quantum defect is 3.5% with 806 nm pump and 835 nm Stokes wavelengths. A slope efficiency of 65% is obtained with 600 m long fibre and 100 ns pulse width. Then, I study experimentally and theoretically 975 nm continuous-wave-pumped fibre Raman lasers based on a graded-index and a double-clad fibre. Both lasers emit at 1019 nm (4.3% quantum defect) with improved brightness. A record laser output of 6 W and 19% slope efficiency from the double-clad Raman fibre and 20 W from the graded-index fibre shows further scaling of single-mode power is possible with improved cavity and fibre design.

Table of Contents

List of symbols

- Area size A
- Beam propagation factor M^2
- Beam/fibre core radius w_0
- Brightness B
- Brightness enhancement η_B
- Cladding area A_{cl}
- Convective heat transfer coefficient h'
- Coolant temperature T_c
- Core radius a
- Cross section σ
- Divergence half-angle Θ
- Effective area A_{eff}
- Effective length L_{eff}
- Fibre background loss α
- Fibre length L
- Fluorescence lifetime τ_l
- Frequency ω
- Frequency ν
- Glass radius b
- Heat deposition density Q
- Ions population density N
- Laser threshold $P^p_{threshold}$
- Longitudinal coordinate z
- Non-radiative decay rate W_{NR}
- Numerical aperture NA
- Number of pulses NP
- Optical intensity I
- Optimised fibre length L_{opt}
- Orbital angular momentum l
- Planck's constant h
- Polarisation constant K
- Power/amplitude P
- Pulse building-up factor M
- Radial coordinate r
- Raman critical pump $P^p_{critical}$
- Raman gain coefficient g_R
- Reflectivity of the mirrors R_1 *and* R_2
- Refractive index n
- Re-launching efficiency η_1 *and* η_2
- Small- signal net gain G_{net}
- Solid-angle Ω
- Spin angular momentum s
- Tangential angle φ
- Temperature T
- The fraction of excited ions $\overline{n_2}$
- Thermal conductivity κ
- Total angular momentum J

▪ Transverse mode field distribution	F
▪ Transverse modes overlap coefficient or ratio of effective areas	Γ
▪ Wavelength	λ
▪ Wave vector	k

List of abbreviations and acronyms

▪ Aluminosilicate	Al
▪ Amplified spontaneous emission	ASE
▪ Bandpass filter	BPF
▪ Beam parameter product	BPP
▪ Cladding pumped	CP
▪ Continuous wave	CW
▪ Dichroic mirror	DM
▪ Distributed feedback	DFB
▪ Double clad Raman fibre	DCRF
▪ Double-clad fibre	DCF
▪ Erbium	Er
▪ Erbium doped fibre amplifier	EDFA
▪ Erbium doped fibre laser	EDFL
▪ Excited state absorption	ESA
▪ Fibre Bragg grating	FBG
▪ Fibre Raman amplifiers	FRA
▪ Fibre Raman lasers	FRL
▪ Full width at half maximum	FWHM
▪ Germanium	Ge
▪ Graded-index	GRIN
▪ High power fibre laser	HPFL
▪ Highly nonlinear fibre	HNLF
▪ High reflection	HR
▪ Holmium	Ho
▪ Large-mode-area	LMA
▪ Laser diode	LD
▪ Light Detection And Ranging	LIDAR
▪ Master oscillator power amplifier	MOPA
▪ Modified chemical vapour deposition	MCVD
▪ Multi-mode	MM
▪ Multi-mode fibre	MMF
▪ Neodymium	Nd
▪ Optoelectronics research centre	ORC
▪ Phosphosilicate	P
▪ Photodarkening	PD
▪ Polarisation mode dispersion	PMD
▪ Polarising beam splitter	PBS
▪ Quantum defect	QD
▪ Quantum efficiency	QE
▪ Rare-earth	RE
▪ Refractive index profile	RIP
▪ Single-mode fibre	SMF
▪ States of polarisation	SOP
▪ Step-index	SI
▪ Stimulated Raman scattering	SRS
▪ Tapered fibre bundle	TFB
▪ Three dimensional	3D

▪ Thulium	Tm
▪ Volume Bragg grating	VBG
▪ Wavelength-division-multiplexing	WDM
▪ White light source	WLS
▪ Yb doped fibre	YDF
▪ Ytterbium	Yb
▪ Ytterbium doped fibre laser or amplifier	YDFL or YDFA

List of tables

List of figures

DECLARATION OF AUTHORSHIP

I, ...Tianfu Yao.....

declare that this thesis entitled

….FIBRE LASER SOURCES WITH LOW QUANTUM DEFECT …..

and the work presented in it are my own and has been generated by me as the result of my own original research. I confirm that:

1. This work was done wholly or mainly while in candidature for a research degree at this University;
2. Where any part of this thesis has previously been submitted for a degree or any other qualification at this University or any other institution, this has been clearly stated;
3. Where I have consulted the published work of others, this is always clearly attributed;
4. Where I have quoted from the work of others, the source is always given. With the exception of such quotations, this thesis is entirely my own work;
5. I have acknowledged all main sources of help;
6. Where the thesis is based on work done by myself jointly with others, I have made clear exactly what was done by others and what I have contributed myself;
7. Parts of this work have been published as: [list references]:

Signed: .....

Date: .....

Acknowledgements

In the first place, I would like to thank my supervisor Prof. Johan Nilsson for his supervision and encouragement, which has helped me from the beginning to the end. He tells me how a good scientist should be. I am also grateful to Dr. Christophe Codemard and Dr. Youmin Chang for all the discussions and suggestions on fibre lasers. Thank for their other help during my study.

My gratitude also goes to other present and previous members of the High Power Fibre Laser Group, including, Dr. Junhua Ji, Dr. Luis Vazquez-Zuniga, Dr. Gysbert van der Westhuizen, Dr Yutong Feng, Dr Xuan Wu, and Mr. Harish Achar for sharing labs and equipments. I am also grateful to Prof. Jayanta. K. Sahu and other members at Silica Fibre Fabrication Group for drawing excellent fibres and rewinding long fibres used in this thesis. I am indebted to Mr. Simon Butler and Mr. Jamie Cook, who helped me to manufacture mechanical components.

I would like to extend my gratitude to all stuff and students, for their discussions and support with equipment, including Dr. Shaif-ul Alam, Dr. Seongwoo Yoo, Dr. Ee Leong Lim, Dr. Jakub Szela, Dr. Priyanth Mehta, and Dr. Jae Daniel. I would like to express my gratitude to ORC providing the opportunity to meet and study with outstanding people. I would like to thank all those who have helped me from time to time.

In addition, I would like to thank my parents for their constant encouragement and endless love during the past years. Particularly grateful to my boyfriend Liangjin Huang for his companionship though my whole study. He lets me know a better world.

Finally, I would like to acknowledge CSC and ORC for funding my PhD. Also, I would like to thank my supervisor Prof. Johan Nilsson to sponsor me during part of my study.

Chapter 1: Introduction

This thesis describes how to design and realise high power fibre sources with pump and signal wavelength chosen for low quantum defect (QD). The QD, defined as the energy difference between pump and signal photons, is significant for low thermal load. High brightness pumping and the amplification scheme are the central themes. Therefore, it is essential to select the pump and signal wavelengths, which further affect the pump threshold, signal gain and other laser properties. They will eventually enable efficient conversion and realisation of low QD, i.e., low heat generation. The subjects covered by this thesis are not limited to rare-earth (RE) doped optical fibres with limited absorption and emission band, but also include fibre Raman lasers (FRL) with unique advantages for low QD operation. Furthermore, besides of the core pumping, cladding pumping is also considered as a means to scale up the output power of Raman lasers. With these, it is attractive to pump with semiconductor diodes not only for power-scaling, but also for targeting hard-to-get wavelengths.

In the first chapter, I will summarise the history of fibre lasers as well as motives and contents of this thesis. An overview of ytterbium doped fibre lasers (YDFL) and FRL is introduced in the section 1.1. Then I will motivate the study of low QD in fibre lasers. Finally section 1.2 outlines the thesis.

1.1 Fibre lasers overview

1.1.1 History of fibre lasers

The first laser was demonstrated in 1960 by T. H. Maiman at the Hughes Research Laboratory [1]. Optical radiation at 694 nm was achieved by pumping a ruby crystal with a high-power flash lamp. Also during this period, E. Snitzer started to recognize the potential advantages of an optical fibre cavity and constructed the first fibre laser using neodymium (Nd) ions in 1963 [2 - 4]. Pumped by a flash lamp, the fibre laser emitted around 1060 nm with multimode (MM) output. At the time, the only economically viable optical pump sources were lamps, which required transverse pumping. Besides, the active sample was very “lossy” and multimoded. This meant long length could not be used and a lot of power from the broadband flash-lamp was not absorbed, making the laser inefficient. Fibre lasers are not well suitable to transverse

pumping. As a result, the progress of RE-doped fibre was hindered over the next two decades, until the mid-1980s. It still needs to be mentioned the first longitudinally pumped fibre laser, pumped by a laser diode (LD), was demonstrated by Stone and Burrus in 1973 [5] .With laser sources, longitudinal pumping can be employed instead of side pumping with “bulky” flash lamps.

Stimulated Raman scattering (SRS) was first reported and later confirmed by E. J. Woodbury, W. K. Ng and their colleagues in 1962, when they operated a ruby laser and observed optical emission at a wavelength of 767 nm [6, 7]. While the initial discovery of spontaneous Raman scattering in liquids was reported by C. V. Raman and K. S. Krishnan in 1928, it took the advent of the laser before SRS was observed [8]. However, research on SRS was slow due to the difficulties in finding pump source in excess of 10 kW, a massive amount at that time. In 1970, a breakthrough in lowering the power threshold was achieved by confining the pump laser radiation in a waveguide using a liquid-core fibre by E. P. Ippen at Bell Labs [9]. Shortly afterwards in 1971, Ippen along with co-workers R. H. Stolen and A. R. Tynes observed SRS in an all-glass optical fibre for the first time [10]. They recognized the potential of using SRS in glass fibres to construct broadband amplifiers and tuneable lasers due to its broad Raman gain bandwidth. Throughout the 1970s and 1980s, a considerable amount of research was carried out on SRS and other nonlinear effects in fibres [11, 12]. But they also emphasised that fibres with low background loss and thus in longer lengths could be used to further reduce SRS threshold.

Those two decades were also an intense period of research into developing low-loss optical fibres for use in optical fibre communication systems. Throughout the 1980s, the interest in optical amplifiers started to grow thanks to the mature optical fibre communication systems [13]. Initial systems used electro-optic repeaters to raise the power of attenuated signals, leading to a lot of cost and unwanted complexity.

Fibre Raman amplifiers (FRAs) and RE-doped fibre amplifiers were both seen as potential candidates for use in optical fibre communications systems. The realisation of low-loss optical fibres benefitted Raman generation, but for RE-doped amplifiers it was still hard to achieve sufficiently low loss when RE-ions were incorporated. However, FRAs were always going to be hindered by the high threshold powers and the lack of reliable, high power, compact pump sources in communication systems [14]. Eventually

the race to provide an optical amplifier in optical fibre communication systems was won by a RE-doped fibre amplifier. In 1985, Poole, Payne and Fermann at the University of Southampton reported an improvement in the fabrication of low-loss RE-doped silica fibres, i.e., the development of solution-doping as a way to incorporate rare earths into preforms fabricated with a novel extension to the modified chemical vapour deposition (MCVD) process [15]. In the same year, Mears, Reekie, Poole and Payne demonstrated a Nd-doped silica single-mode fibre (SMF) laser [16]. Later on, they reported an erbium (Er) doped fibre laser (EDFL) and an Er-doped fibre amplifier (EDFA) in the 1.5 μm band [17, 18]. Since then fibre lasers made with various RE-doped fibres including Nd, Er, ytterbium (Yb), holmium (Ho) and thulium (Tm) using MCVD solution doping have been investigated [19]. However, the EDFA emission wavelength just happened to overlap with the low loss 3rd window of optical fibre communication systems, which coupled with its intrinsic fibre compatibility made the EDFA one of the most significant discoveries of recent years.

During this time, there were significant developments of optical components and LD technology, which was the only practical electrically powered pump source for RE-doped fibres. In 1992, the EDFA started to be commercialized. In addition, fibre Raman amplification was developed to complement EDFAs and to extend the reach of optical signals in long-haul transmission. Meanwhile, practical Fibre Bragg Gratings (FBG) and other fibre based components were also developed [20, 21].

Optical communication remains the most important fibre application but there has also been a lot of focus on other aspects of fibre devices and in particular, high power operation.

1.1.2 Further step to output power scaling

Thanks to the progress of high-power MM LDs and the invention of the double-clad fibre (DCF), continuous wave (cw) high-power fibre amplifiers and lasers have been extensively studied and increasingly developed [22, 23]. Single-mode operation of RE-doped fibres have become available at power levels that make them prime candidates in cutting, engraving, soldering and many other applications normally addressed by solid-state lasers or semiconductor lasers. And with the ever-increasing advances in fibre design and fabrication, the future for fibre-based light sources looks bright and very

interesting with plenty of opportunities for further development and interesting new concepts.

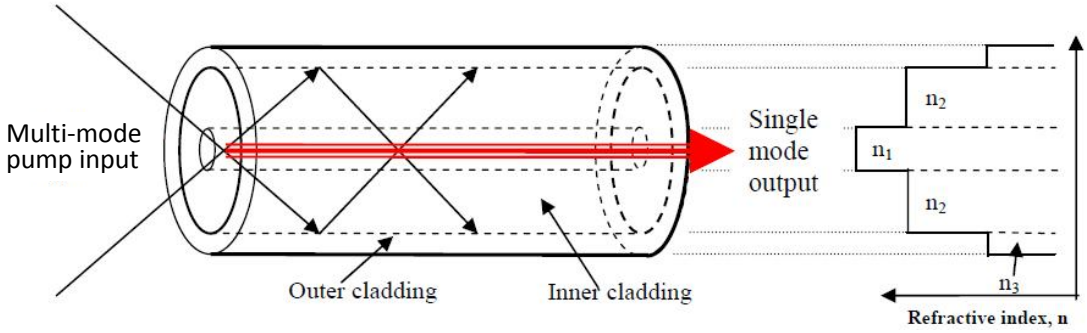

Figure 1.1 Schematic of ray propagation in DCF and the refractive index profile.

Figure 1.1 shows the DCF structure, which consists of a fibre whose so-called inner cladding is surrounded by a lower-index outer cladding and then forms a waveguide around the primary core waveguide. It enables pump-LDs with relatively low brightness to be coupled into the fibre's inner cladding while maintaining a laser output with enhanced brightness [24]. Several RE ions have been investigated for their use in high power fibre lasers, notably Yb, Nd, Er, Ho and Tm. Since then, by using so-called large-mode-area (LMA) Yb doped fibres (YDFs), the historical first-ever YDFL reaching the kW level with good beam quality was reported by Y. Jeong et al., at the University of Southampton in 2004 [25]. Currently, the highest reported single-mode fibre laser is beyond 20 kW, from IPG Photonics [26]. YDFs are superbly suited to power scaling, thanks to the excellent characteristics of Yb ions, such as a wide absorption wavelength range, simple two-level energy system, resilience to concentration quenching, small QD, and more.

Power-scaling of fibre lasers is researched by several groups around the world, such as High Power Fibre Laser (HPFL) group and others at Optoelectronics Research Centre (ORC), University of Southampton, and other groups such as the Friedrich Schiller University of Jena, University of the Michigan, SPI Lasers and IPG Photonics. It is possible to further increase the output power of fibre lasers with diffraction-limited beam. However, the scaling becomes increasingly challenging and is ultimately limited by several factors, i.e., thermal effects, nonlinear effects, and materials damage [27, 28].

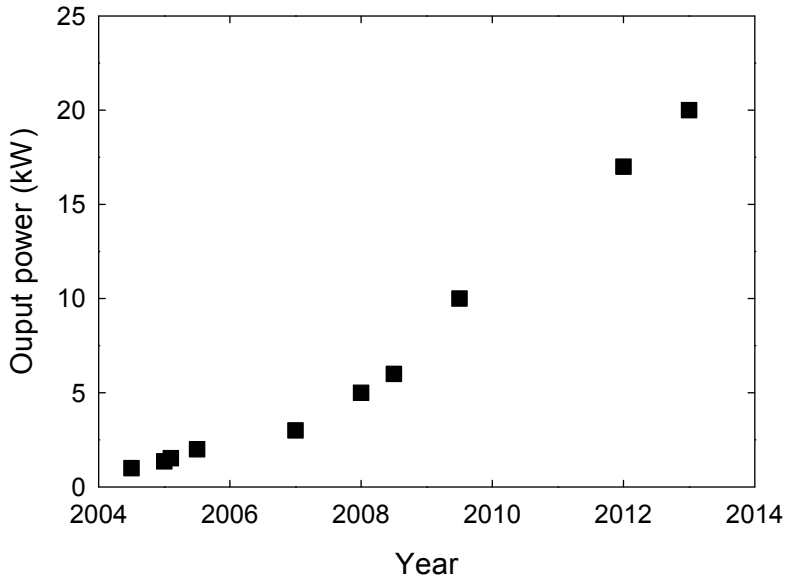

Figure 1.2 The power evolution of cw diffraction-limited YDFLs since 2004.

Pumped by the high power YDFLs with good beam quality, the output power from FRAs and FRLs has also increased [35]. The updated output power record of core-pumped FRAs was presented by M. Rekas, reaching above 200 W of output power at 1125 nm from an amplifier [29].The published record of core-pumped FRLs based on cascaded SRS is 300 W at 1.5 μm in 2013 [30].

The first CP FRL was reported by J. Nilsson and co-workers at the University of Southampton in 2002 [31]. Based on a double-clad Raman fibre (DCRF), they reached over 50 mW of average output power at peak wavelength of 1680-1690 nm, when synchronously pulse-pumped by a Q-switched Er-Yb co-doped fibre laser. In 2006, the first cw CP FRL was demonstrated by C. A. Codemard and his colleagues, achieving 10.2 W output power at 1660 nm with excellent brightness enhancement [32]. Later on, they increased the cw output power to over 100 W while maintaining a good beam quality [33]. In the pulsed regime, J. Ji demonstrated the FRAs pumped by a Q-switched Nd:YAG laser for the first time in 2010, obtaining 2.15 kW record peak power and 1 mJ record energy with M^2 parameter of 1.69 [34]. He also realised a pulse-pumped CP FRA with 75% peak power conversion and 60% energy conversion efficiency into the 1st Stokes. The corresponding brightness gain is 8.7 [35]. In terms of efficient operation in the cw regime, he achieved a slope efficiency as high as 81% and 91%, respectively, in 4%-100% and 4%-4% reflecting linear laser cavity configurations, while the brightness enhancement was estimated to be 11.5 [36]. According to the simulation results, the

inner-cladding-to-core area ratio is limited to 8, to ensure a high threshold of unwanted 2nd order Stokes [34]. With such high powers available in a single-mode beam and further advances on low-loss, high Raman gain fibres, the output power from FRAs and FRLs has also increased, opening up new potential applications such as harmonic generation to visible wavelengths for bio-medical applications and laser guide-star programs [37].

1.2 Motivations

The motivation for this thesis is to investigate ways of exploiting the low thermal load and low QD by taking advantage of recent advances in high-brightness and in-band pumping of RE-doped fibres. For core-pumped YDFs, by appropriately choosing the pump wavelength and fibre length, it is possible to obtain a low QD. As for SRS, pumping at short wavelength contributes to low QD as well, which is another aspect of my research.

The heat generation is always one of the biggest enemies at high powers, resulting in the thermal lensing, thermally-induced stresses and fibre damage [38, 27]. In practice, one can remove the heat by state-of-the-art heatsinking with a high surface-to-volume ratio. This method is efficient and intrinsic to the structure of fibre lasers [39]. Another way is to eliminate thermal load by minimising QD. This is becoming increasingly necessary as the power level of fibre lasers increases.

1.2.1 Tandem pumped YDFLs

Compared to direct LD-pumping, a tandem-pumping architecture, in which YDFLs emitting at around 1 μm pump another YDF operating at a longer wavelength, enables higher-brightness pumping. As mentioned in the previous section, the power of fibre sources with diffraction limited output has already reached 20 kW [26]. This was a tandem-pumped master oscillator – power amplifier (MOPA) with a fibre-laser seed source (i.e., master oscillator).

As discussed, YDFs tandem-pumped at relatively long wavelengths show the potential for decreasing the QD. Besides, the excitation level can also be controlled by the tandem-pumping mechanism, which consequently limits the excess gain in large-core ytterbium doped fibre amplifier (YDFAs). This reduces the unsaturated gain and

perhaps also self-pulsing and unwanted build-up of higher-order modes [40]. This should allow for better beam quality from large MM cores as well as for further scaling of the core area, albeit at the cost of a smaller inner cladding and therefore higher brightness requirement on the pump source. In combination with a possible lower rate of photodarkening (PD), this makes tandem pumping attractive for further power scaling of YDF devices in different regimes of operation [40, 41].

The theoretical analysis shows the minimum QD can be achieved with unity area ratio between the pump and signal, combined with a proper fibre length. Although there is a lack of published details on this source, tandem-pumping is clearly very promising for power scaling of fibre lasers, Yb-doped as well as other ones.

1.2.2 Directly LD-pumped FRLs

Optical amplification obtained by SRS provides some exciting advantages and differences, while keeping most advantages of RE-doped fibre devices. Raman scattering occurs in most materials, including all solid materials. Therefore, optical fibres without any active dopant can also generate gain, through a nonlinear interaction between pump and signal photons and material vibrations, in case of SRS [42]. Furthermore, emission is possible for a much broader continuous range of wavelengths than for RE-doped fibre lasers. Figure 1.3 shows the wavelength bands of some RE elements and SRS in silica fibre.

In addition, SRS is an instantaneous process without the intermediate energy-storage that occurs in RE-doped gain media, and without the need to store energy to create gain. Other further attractions are the freedom in materials and the longer interaction length, which reduces the impact of the heating on the waveguiding.

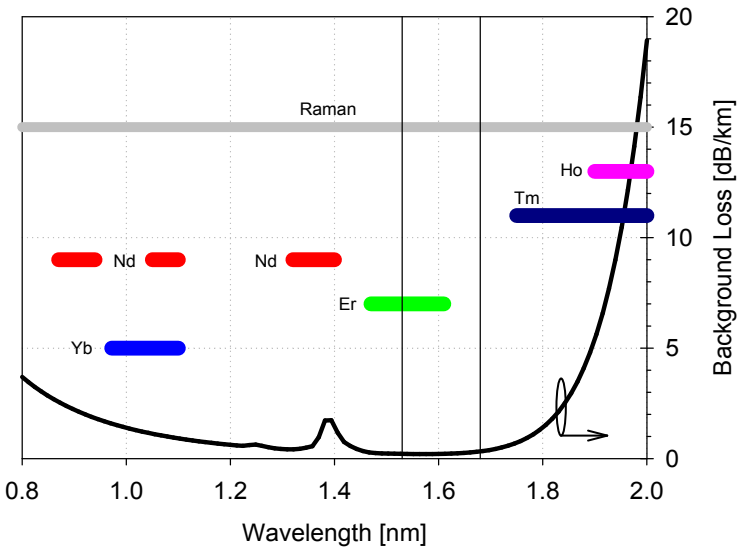

Figure 1.3 Background loss and emission bands of some RE dopants in the 0.8 - 2.0 μm wavelength range in silica. Raman gain can be achieved across that wavelength range [36].

Thus, CP FRLs represent an appealing solution to transforming MM pump light into cw as well as pulsed single-mode laser output. Such a laser source benefits from the wavelength flexibility of SRS. Furthermore, this allows for a wide range of high-brightness pump sources, such as RE-doped fibre devices, and potentially also semiconductor lasers emitting at short wavelength such as 808 nm or 975 nm.

Especially within the last decade, the rapid improvement of high-power, high-brightness, semiconductor LDs has provided significant opportunities for improving HPFLs. For directly diode-pumped fibre Raman devices, the high diode brightness is needed to reach the pump intensity to the level where the Raman gain becomes sufficient. Furthermore, the availability of such diodes at short wavelength also reduces the relative QD, as the photon energy increases but the Stokes shift remains constant. Moreover, high-brightness LDs help to reduce the complexity. Besides, LDs can be combined spatially, in polarisation, and spectrally, for pumping at higher powers. It is straightforward to run LDs in cw and pulsed mode and thus electrically control the temporal format of the output. With diode-pumping, Raman lasers open up an efficient route to wavelengths shorter than what is available from high-power fibre lasers. Furthermore, at short wavelengths, PD is a big concern, and RFs are likely to be more resilient to PD than RE-doped fibres. Therefore, it is very attractive to investigate FRLs cladding-pumped directly by diodes.

1.3 Thesis outline

This thesis is divided into five chapters in addition to this chapter. The second chapter provides the background theory to the thesis. This begins with laser beam quality and brightness, highlighting their importance for fibre amplifiers and lasers. Secondly, the relevant Raman theory is presented, focussing on SRS in optical fibres and the general properties of FRLs. This is followed by the spectroscopy of Yb-ions in optical fibre, focussing on the potential of tandem pumping scheme. Finally, thermal effects and temperature distribution along the optical fibre will be discussed with an emphasis on low QD.

Chapter 3 - 5 present my analytical and experimental results. Chapter 3 covers tandem-pumping. Theoretical calculations show the minimum QD in tandem-pumped YDFs. In experiments, with 1030 nm pump and 1050 nm seed wavelengths, the lowest QD of 2% was achieved in a core-pumped YDF. The slope efficiency reached over 95%. PD-measurements on tandem-pumped YDFAs indicate the importance of Yb concentration and host compositions even with low Yb excitation level.

In Chapter 4 the focus shifts to the Raman laser work and an investigation into the special concern of short-wavelength operation. The chapter first introduces the details of a silica-based highly nonlinear fibre (HNLF) for the FRL which was fabricated by Sumitomo Electric Industries. The construction of the FRLs pulse-pumped by a high-brightness diode at 806 nm is presented. The FRLs are analysed in terms of several key characteristics, i.e., output power, threshold and efficiency. And the use of polarisation control is discussed.

Chapter 5 builds on the results achieved in Chapter 4 and describes the work on power-scaling of cw FRLs by wavelength-multiplexing two pump diodes emitting around 975 nm. The experimental and theoretical study of SRS conversion in a MM FRL is presented. The challenges and limitations of power-scaling of diode pumped FRLs are discussed.

Finally, Chapter 6 concludes this thesis with a summary of the main results achieved before finishing with comments for the possibilities for future work. There is also an appendix containing a list of the publications arising from my work during my Ph.D. study at the ORC.

1.4 References

1 T. H. Maiman, “Stimulated optical radiation in ruby masers,” Nature, 187, 493, (1960).

2 E. Snitzer, “Optical maser action of Nd3+ in a barium crown glass,” Phys. Rev. Lett., 7, 444-446, (1961).

3 E. Snitzer, “Proposed fiber cavities for optical lasers,” J. Appl. Phys., 32, 36-39, (1961).

4 C. J. Koester, and E. Snitzer, “Amplification in a fiber laser,” Appl. Opt., 3, 1182-1186, (1964).

5 J. Stone, and C. A. Burrus, “Neodymium-Doped Silica Lasers in End-Pumped Fibre Geometry,” Appl. Phys. Lett., 23(7), 388-389, (1973).

6 E. J. Woodbury and W. K. Ng, “Ruby laser operation in the near IR,” Proc. IRE., 50, 2367, (1962).

7 G. Eckhardt, R. W. Hellwarth, F. J. McClung, S. E. Schwarz, D. Weiner, and E. J. Woodbury, “Stimulated Raman scattering from organic liquids,” Phys. Rev. Lett., 9(11), 455-457, (1962).

8 C. V. Raman and K. S. Krishnan, “A new type of secondary radiation,” Nature, 121, 501-502, (1928).

9 E. P. Ippen, “Low-power quasi-cw Raman oscillator,” Appl. Phys. Lett., 16(8), 303-305, (1970).

10 R. H. Stolen, E. P. Ippen, and A. R. Tynes, “Raman oscillation in glass optical waveguide,” Appl. Phys. Lett., 20(2), 62-64, (1972).

11 R. H. Stolen, “Nonlinear properties of optical fibers”, in Optical Fibre Telecommunications, (S. E. Miller and A. G. Chynoweth, Eds. New York: Academic, 1974).

12 R. H. Stolen, “Nonlinearity in fiber transmission,” Proc. IEEE, 68(10), 1232-1236 (1980).

13 J. Hecht, “The evolution of Optical amplifiers,” Optics and Photonics News, 13(8), 36-39, 2002.

14 E. Desurvire, M. Papuchon, J. P. Pocholle, J. Raffy, and D. B. Ostrowsky, “High-gain optical amplification of laser diode signal by Raman scattering in single-mode fibres,” Electron. Lett., 19(19), 751-753, (1983).

15 S. B. Poole, D. N. Payne, and M. E. Fermann, “Fabrication of low-loss optical fibres containing rare-earth ions,” Electron. Lett., 21(17), 737-738, (1985).

16 R. J. Mears, L. Reekie, S. B. Poole, and D. N. Payne, “Neodymium-doped silica singlemode fibre laser,” Electron. Lett., 21(17), 738-740, (1985).

17 R. J. Mears, L. Reekie, S. B. Poole, and D. N. Payne, “Low-Threshold Tunable-Cw and Q-Switched Fiber Laser Operating at 1.55 mm,” Electron. Lett., 22(3), 159-160, (1986).

18 R. J. Mears, L. Reekie, S. B. Poole, and D. N. Payne, “Low-noise erbium-doped fibre amplifier operating at 1.54μm,” Electron. Lett., 23(19), 1026-1028, (1987).

19 J. E. Townsend, S. B. Poole, and D. N. Payne, “Solution-doping technique for fabrication of rare-earth-doped optical fibres,” Electron. Lett., 23(7), 329-331, (1987).

20 K. O. Hill, B. Malo, F. Bilodeau, D. C. Johnson, and J. Albert, “Bragg gratings fabricated in monomode photosensitive optical fiber by UV exposure through a phase mask,” Appl. Phys. Lett., 62(10), 1035-1037, (1993).

21 J. T. Kringlebotn, J. L. Archambault, L. Reekie, and D. N. Payne, “Er^{3+}:Yb^{3+}-Codoped Fiber Distributed-Feedback Laser,” Opt. Lett., 19(24), 2101-2103, (1994).

22 E. Snitzer, H. Po, F. Hakimi, R. Tumminelli, and B. C. McCollum, “Double-clad, offset core Nd fiber laser,” in Proc. Opt. Fiber Sensors, PD5, New Orleans, USA, 1988.

23 J. Kafka, “Laser diode pumped fiber laser with pump cavity,” US patent 4, 829, 529 (1989).

24 R. D. Maurer, “Optical waveguide light source,” US patent 3, 808, 549 (1974).

25 Y. Jeong, J. K. Sahu, D. N. Payne, and J. Nilsson, “Ytterbium-doped large-core fiber laser with 1.36 kW continuous-wave output power,” Opt. Express, 12(25), 6088-6092, (2004).

26 Bill Shiner, “High power fiber laser technology,” presentation at Annual Department of Energy Laser Safety Officer (DOE LSO) Workshop, September 10, (2013).

27 J. W. Dawson, M. J. Messerly, R. J. Beach, M. Y. Shverdin, E. A. Stappaerts, A. K. Sridharan, P. H. Pax, J. E. Heebner, C. W. Siders, and C. P. J. Barty, “Analysis of the scalability of diffraction-limited fiber lasers and amplifiers to high average power,” Opt. Express, 16(17), 13240-13266, (2008).

28 C. Jauregui, J. Limpert, and A. Tünnermann, “High-power fibre lasers,” Nature Photonics, 7, 861-867, (2013).

29 Miroslaw Rekas, Oliver Schmidt, Stephan Rhein, Hagen Zimer, Thomas Schreiber, Ramona Eberhardt, and Andreas Tuennermann, “Raman Amplifier with > 200 W Average Power Based on a Step-index Fused Silica Fibre,” Frontiers in Optics (FiO), FTuW2, San Jose, US, 2011.

30 V. R. Supradeepa and J. W. Nicholson, “Power scaling of high-efficiency 1.5 μm cascaded Raman fiber lasers,” Opt. Lett. 38 (14), 2538–2541 (2013).

31 J. Nilsson, J. K. Sahu, J. N. Jang, R. Selvas, D. C. Hanna, and A. B. Grudinin, "Cladding-pumped Raman fiber amplifier," in Proc. Optical Amplifiers and Their Applications (OAA 2002), paper PD2-1/2/3, Vancouver, Canada 2002.

32 C. A. Codemard, P. Dupriez, Y. Jeong, J. K. Sahu, M. Ibsen, and J. Nilsson, "High-power continuous-wave cladding-pumped Raman fiber laser," Opt. Lett., 31(15), 2290-2292, (2006).

33 C. A. Codemard, J. Ji, J. K. Sahu, and J. Nilsson, "100 W CW cladding-pumped Raman fiber laser at 1120 nm," in Proc. of Photonics West, 7580, 58, San Francisco, US, 2010.

34 J. Ji, C. A. Codemard, Jayanta K. Sahu, and J. Nilsson, "Design, performance, and limitations of fibers for cladding-pumped Raman lasers," Opt. Fiber Technol. 16, 428-441 (2010).

35 J. Ji, C. A. Codemard, J. K. Sahu, and J. Nilsson, "Pulsed cladding-pumped large mode area fiber Raman amplifier," in Proc. of Photonics West, 7598-47, San Francisco, US, 2010.

36 J. Ji, "Cladding-pumped Raman fibre laser sources," Thesis, ORC, University of Southampton, (2011).

37 J. T. Murray, W. T. Roberts, W. L. Austin, R. C. Powell, and D. Bonaccini, "Fiber Raman laser for sodium guide star," Proc. SPIE 3353, 330-339, (1998).

38 M. S. Kuznetsov, O. L. Antipov, A. A. Fotiadi, and P. Megret, "Electronic and thermal refractive index changes in Ytterbium-doped fiber amplifiers," Opt. Express, 21(19), 22374-22388, (2013).

39 M.-A. Lapointe, S. Chatigny, M. Piché, M. Cain-Skaff, and J.-N. Maran, "Thermal effects in high-power cw fiber lasers," Proc. SPIE, 7195(1), 71951U, (2009).

40 C. Codemard, J. K. Sahu, and J. Nilsson, "Tandem cladding-pumping for control of excess gain in ytterbium-doped fiber amplifiers," IEEE J. Quantum Electron., 46(12), 1860-1869, (2010).

41 Shinichi Matsubara, Kyousuke Uno, Yoshiaki Nakajima, Sakae Kawato, Takao Kobayashi, and Akira Shirakawa, “Low quantum-defect laser oscillation by high intensity pumping at room temperature”, Quantum Electronics and Laser Science Conference, JWA81, 2007.

42 G. P. Agrawal, Nonlinear Fiber Optics, (4th Ed., Academic Press Inc., San Diego CA, 2007).

Chapter 2: Background

This chapter is divided into several sections that present an overview of theory and information required to understand the later chapters and put them in relevant theoretical context. Section 2.1 describes laser brightness and its relation to the beam quality of fibre laser sources. Then, in section 2.2, Raman scattering in optical fibre that arises from high-intensity optical fields is introduced, with a particular attention to Raman gain and threshold when pumping with MM diodes. The spectroscopic properties of Yb ions and amplification in YDFs are presented in section 2.3. These help in modelling of low QD by tandem-pumping with longer pump wavelengths and high pump brightness. Finally, section 2.4 introduces expressions for the QD and simulation results on thermal distribution, which are important since the related thermal effects are critical in HPFLs.

2.1 Beam quality and brightness enhancement

Fibre lasers based on DCF which convert light from MM semiconductor pump sources into diffraction limited output beam are examples of lasers that can be optically pumped by high-power, low-brightness beams. Consequently, they can be seen as brightness converters. Fibre lasers are now among the brightest laser sources in existence. In terms of applications, such fibre laser sources with high beam quality enable tight focusing of a beam, for example, in laser material processing, three dimensional (3D) printing, marking, cutting and drilling, as well as long working distances and low divergence beams, such as in Light Detection And Ranging (LIDAR) or frequency conversion.

The concepts of brightness and beam quality are generally well known. Indeed the term “high brightness” indicates a high power output and/or a high beam quality. The beam quality of a laser, which is independent of the optical power, corresponds to the degree to which the beam can be focused for a given beam divergence (or convergence) angle. In general, the beam quality can be described by the beam propagation factor (or parameter) M^2 [1]

$$M^2 = \frac{\Theta w_0}{\lambda/\pi} \tag{2. 1}$$

where Θ is the divergence half-angle in the far field of the light emerging through the focal point and w_0 is the beam radius at the waist of the light beam [2]. Note that normally, the beam forms a waist at the fibre end. Hence, the in-fibre beam radius can be used for w_0. The beam parameter product (*BPP*) is another quantity used to describe the beam quality:

$$BPP = \Theta w_0 = M^2 \frac{\lambda}{\pi} \tag{2. 2}$$

For a diffraction-limited Gaussian beam, the *BPP* equals λ/π. The M^2 factor of a laser source equals the ratio between its *BPP* and that of a diffraction-limited Gaussian beam with the same wavelength. Thus, the M^2 factor is unity for a diffraction-limited beam. A single-mode step-index (SI) fibre typically has an M^2-value of 1.05. Thus, even though the light distribution constitutes a single mode in the fibre, it is not quite diffraction-limited, nor does it correspond a single free-space mode. Still, the fundamental mode of a fibre is normally considered to be diffraction-limited, since its beam quality is only a few percent worse than diffraction-limited.

Together with the optical power, the M^2 factor determines the brightness, which is also called the radiance and is defined as the amount of light that passes through or is emitted from a particular area, and falls within a given solid angle. Rather than the power, brightness determines the power density achievable in a focused beam. Brightness is expressed in $W/(sr \cdot m^2)$. Therefore, in an optical fibre, in the small angle approximation, the brightness *B* can be defined by [3]:

$$B = \frac{P}{\Omega A} = \frac{P}{M_x^2 M_y^2 \lambda^2} \tag{2. 3}$$

where *B* is the fibre brightness, *P* is the radiant power from an area of size *A* in a solid-angle Ω, and M_x^2 and M_y^2 are the beam propagation factors in orthogonal planes. Both brightness and beam quality are invariants through an imaging optical system without loss or aberrations. Note also that although the radiance can be considered to be a local quantity that can vary across an emitter, M^2 is strictly defined with integral expressions over the whole laser beam. Thus Eq. (2.3) is no longer a local quantity but applies to the laser source as a whole. In the case of a beam of radius w_0 emerging from a circular fibre, according to Eq. (2.1) and Eq. (2.3), the brightness can also be expressed as,

$$B = \frac{P}{M_x^2 M_y^2 \lambda^2} = \frac{P}{\pi^2 \Theta^2 w_0^2} \approx \frac{P}{\pi^2 NA^2 w_0^2} \quad (2.4)$$

Many types of lasers can be thought of as brightness converter, including CP fibre lasers. In these devices, a MM pump source with lower brightness is converted to an output beam (signal) with higher brightness. By applying this fibre structure, the brightness of the output can be enhanced. The brightness enhancement, or brightness gain, η_B, can be easily calculated based on Eq. (2.4):

$$\eta_B = \frac{B_s}{B_p} \approx \frac{P_s}{P_p}\left(\frac{\pi NA_{cl} w_{cl0}}{\lambda_s M_s^2}\right)^2 \quad (2.5)$$

In Eq. (2.5), the subscripts *cl* stands for inner cladding while subscripts *s* and *p* are for signal and pump, respectively. In a recent result by J. Ji, a state-of-the-art DCRF was used to generate 2.7 kW peak output power with a M^2 factor of 2.2 [4]. The fibre had a 0.07 NA, 40 μm diameter core and a 0.2 NA, 107 μm diameter inner cladding. The maximum average power conversion efficiency into 1st Stokes at 1120 nm was around 43%. Thus, in this case, the brightness was enhanced 80 times. One of the important parts of my research is the development of Raman fibre devices based on graded index fibre or DCRF that increase the brightness, relative to that of the pump diodes [5, 6]. Since the output power of a laser is always lower than the pump power, an improvement of the brightness also means that the beam quality improves. However the opposite is not true.

2.2 Raman scattering in optical fibres

The basic Raman process is an inelastic light-scattering process, which leads to energy from a pump wave being transferred to a lower-frequency Stokes wave and / or a higher-frequency anti-Stokes wave through the interaction between the pump wave and the vibrational states of a material [7]. Furthermore, the presence of a Stokes wave leads to so-called SRS and thus much quicker Raman conversion. The rate of energy transfer is proportional to the pump and Stokes intensity. It follows that SRS is a third-order nonlinear process in which the Stokes wave, which may be an optical signal, is amplified at a rate proportional to the pump intensity. The intensity must be high for SRS to be significant. To describe SRS, one of the important characteristics is the

Raman gain spectrum, as shown in Figure 2.1 for silica and germanium (Ge). The Raman gain spectrum is independent of the pump frequency. The Raman gain coefficient g_R extends up to around 40 THz [8] in silica fibre. The broad peak is located around 13 THz.

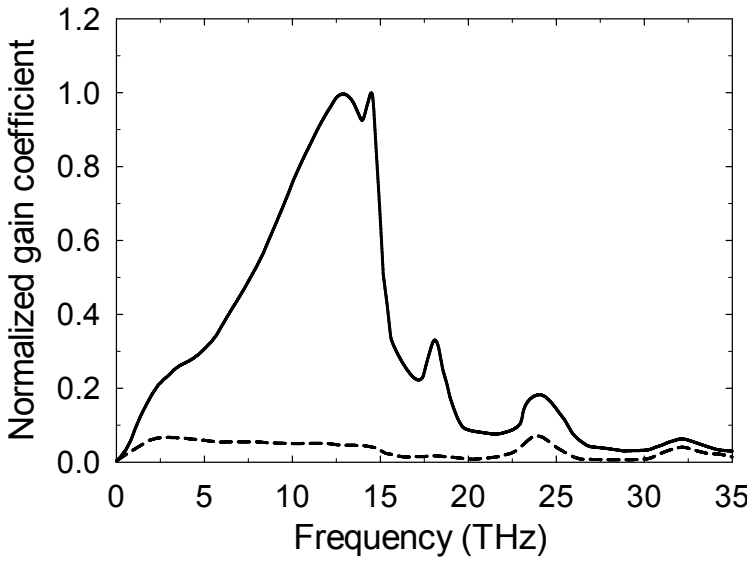

(a)

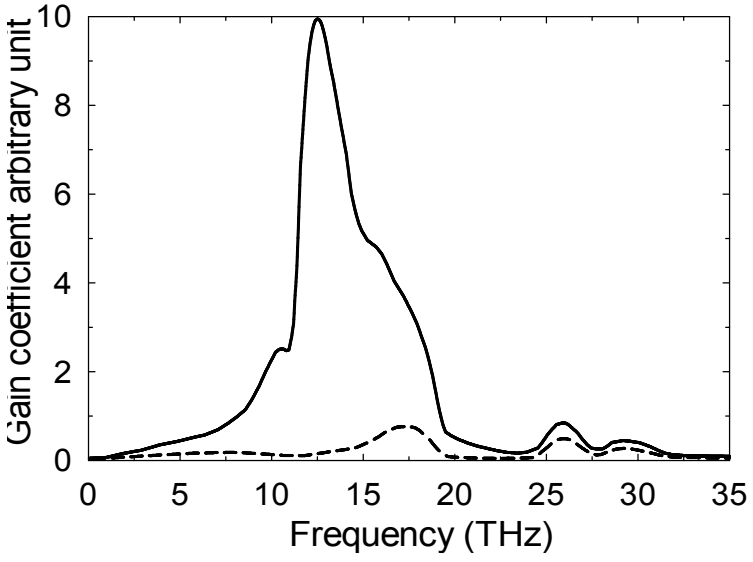

(b)

Figure 2.1 Raman-gain spectra for (a) fused silica and (b) GeO_2 at a pump wavelength λ_p of 1 μm [8,9].

Due to a wide and continuous gain range, silica fibre can act as the gain medium for broadband Raman amplifiers and lasers. Since SRS is a nearly instantaneous process with time constant below ~100 fs in silica [10], the signal and pump beams must

overlap in time. Furthermore, since SRS can be viewed as a quite weak nonlinearity, a strong interaction requires intense beams over significant lengths. This makes optical fibres particularly well suited for SRS, despite the low value of the Raman gain coefficient in glass.

2.2.1 SRS in single-mode optical fibre

In a simple approach valid under cw and quasi-cw conditions, the nonlinear interaction between the pump and Stokes waves through SRS process along a length of SMF can be described by two coupled equations [11]

$$\frac{dP_s}{dz} = \frac{1}{A_{eff}} \frac{g_R}{K} P_p P_s - \alpha_s P_s \tag{2. 6}$$

$$\frac{dP_p}{dz} = -\frac{1}{A_{eff}} \frac{\lambda_s}{\lambda_p} \frac{g_R}{K} P_p P_s - \alpha_p P_p \tag{2. 7}$$

where P_i, α_i, and λ_i are the beam power, linear attenuation coefficient and wavelength, respectively, with $i = s, p$ denoting the Stokes and pump wave. Considering the influence of the polarisation of the Stokes and pump waves, a constant K is added with value 1 if the polarisations are linear and parallel or 2 if the waves are depolarised [11, 12]. g_R is the Raman gain coefficient as exemplified by Figure 2.1. A_{eff} is the effective area, which is the inverse of the mode overlap integrals, defined as

$$A_{eff} = \frac{\int\int_{-\infty}^{+\infty} |F_p(x,y)|^2 |F_s(x,y)|^2 \, dxdy}{(\int\int_{-\infty}^{+\infty} |F_p(x,y)|^2 \, dxdy)(\int\int_{-\infty}^{+\infty} |F_s(x,y)|^2 \, dxdy)} \tag{2. 8}$$

where, F_i is the transverse mode field distribution with $i = s, p$ denoting the Stokes and pump wave.

If the signal power is small enough for the pump depletion to be negligible, then the pump evolution is trivially found Eq. (2. 7). Subsequently we can directly get an analytic solution for the signal power P_s by substituting the pump evolution into Eq. (2. 6):

$$P_s(z) = P_s(0)\exp\left(\frac{g_R}{K}\frac{1}{A_{eff}}\int_0^z P_p(u)du - \alpha_s z\right)$$
$$= P_s(0)\exp\left(\frac{g_R}{K}\frac{P_p(0)}{A_{eff}}L_{eff}(z) - \alpha_s z\right) \quad (2.9)$$

where $P_i(0)$ and $P_i(z)$ are the power at the injection point and the power at a distance z from the injection point respectively, $L_{eff}(z)$ is the effective length up to the point z. Through the propagation along the optical fibre, the pump power is reduced by the attenuation and the SRS. The solution to Eq. (2. 9) shows because of the background loss, the effective SRS interaction length is reduced from the actual fibre length L to effective length. Therefore, considering the whole fibre length rather than just the length up to a point z, the effective length of the pump wave is defined as

$$L_{eff} = \frac{\int_0^L P_p(z)dz}{P_p(0)} = \frac{1}{P_p(0)}\int_0^L P_p(0)e^{-\alpha_p z}dz = \frac{1-e^{-\alpha_p L}}{\alpha_p} \quad (2.10)$$

This assumes that the pump power is only attenuated by the background loss. In this regime, if the fibre is long enough, L_{eff} approximates a finite value of α^{-1}, while the effective length approaches the real fibre length L if the background loss is negligible.

In the absence of pump depletion, the small-signal net gain G_{net} follows directly from Eq. (2. 9):

$$G_{net} = 4.343\left(\frac{g_R}{K}\frac{P_p(0)}{A_{eff}}L_{eff} - \alpha_s L\right) \quad (2.11)$$

The small-signal net gain G_{net} is in decibels. By reducing the effective area, increasing the pump power or the effective fibre length, or using a fibre with a higher Raman gain coefficient, a higher Raman gain can be obtained. Furthermore, they can be traded against each other, so that a high value of one of these parameters can relax the requirement for a high value for the others.

2.2.2 Raman critical power or threshold in FRL

Even if the Stokes wave is not seeded, it will still build up from spontaneous Raman scattering (or equivalently, from noise or so-called vacuum fluctuations) [13]. The

Raman critical power is defined as the input pump power at which the unseeded Stokes output power in a specific fibre end becomes equal to the pump power in that end. The critical power can be used to roughly estimate the parameters needed for Raman conversion in many cases. It can also be used to estimate when unwanted SRS starts to appear, e.g., in RE-doped fibre devices although the SRS tolerated in a RE-doped fibre may be much lower. In silica, the critical pump power for a single-pass SRS process approximates to [11, 13]

$$P_{critical}^{p} \approx 16\frac{A_{eff}K}{g_R L_{eff}} \tag{2. 12}$$

$$P_{critical}^{p} \approx 20\frac{A_{eff}K}{g_R L_{eff}} \tag{2. 13}$$

for forward and backward propagation directions, respectively. The expression for the co-propagating case is valid for both cw and pulsed light. If walk-off is negligible then the expression applies for the instantaneous power, whereas it applies to the average power if the walk-off is large compared to the period. The expression for the counter-propagating case applies for cw light, for pulses that are long compared to the fibre transit time, and for pulses with period much shorter than the transit time (in this case the average rather than the instantaneous power should be used).

The counter-propagating case of Eq. (2. 13) comes across as a theoretical abnormality, relying on assumptions that are rarely, if ever, encountered in practice [11]. Specifically, the equations assume that there is only Stokes power in one propagation direction. In fact, the local Raman gain at any one point is practically identical in all directions (in an isotropic material such as fused silica). Thus, in case of cw pump light, the forward and backward Raman gain will be the same, and the forward and backward Stokes wave will carry the same amount of power in a simplified ideal case. This would suggest that the unseeded Stokes power is the same or similar in both directions, with a similar threshold. However, in many practical cases there are likely to be fluctuations in the pump power (when the pump coherence length is shorter than the fibre length), and this makes the forward-propagating Stokes power higher than the backward propagating power. Thus, due to the pump fluctuations mentioned above, the forward Stokes wave will build up before or at least not later than the backward Stokes wave, so the

assumption of Eq. (2. 13) of a dominating backward Stokes wave is not realised in practice. This is actually suggested by the higher critical power for the counter-propagating case of Eq. (2. 13), although this is, incorrectly, on the basis of pump depletion. The real reason is temporal pump fluctuations.

The 1st Stokes power can be amplified to the point where it starts to generate the next Stokes order. The 1st Stokes acts as a pump for the 2nd Stokes, and its power eventually starts to decrease as the 2nd Stokes power builds up. The energy is then rapidly transferred to the 2nd Stokes beam. The process can continue in a cascaded fashion, so that even higher-order Stokes radiation can be generated, provided that the input pump power is sufficiently high. However, my work focuses on generating a high power, high-brightness, 1st Raman Stokes laser, and avoiding cascaded Raman scattering.

In the case of a FRL, the threshold pump power corresponds to the pump power at which Raman amplification during a roundtrip is large enough to balance the cavity loss (as for any laser). In a simple Fabry-Perot resonator with mirrors (or gratings), the signal propagation loss along the fibre, together with the transmission loss at the mirrors and coupling losses at the two ends of the fibre, mainly compose the roundtrip loss in a FRL. Thus the expression of the pump threshold of a FRL is given by [14]

$$P_{threshold}^{p} = \left(\alpha_s L - \frac{1}{2} \ln\left(R_1 R_2 \right) \right) \frac{A_{eff} K}{g_R L_{eff}} \qquad (2.\ 14)$$

where, R_1 and R_2 are the reflectivity of the mirrors at the pump launching end and far end of the fibre respectively, and the other terms have already been defined and listed.

2.2.3 Multimode-pumped SRS

In a multi-mode fibre (MMF), SRS is similar but more complicated than that in a SMF, described by the equations given in section 2.2.1. The pump and / or Stokes beams are transported by several modes in a MMF. The power of each mode then creates an optical power distribution that generates Raman gain in proportion to the local intensity. Thus, it is necessary to consider all modes involved in the SRS process [15]. In the cw or quasi-cw regime, the intensity evolution of each propagating mode at different wavelengths under Raman scattering can be modified from Eq. (2. 6) and Eq. (2. 7).

It is justified to neglect the interference of the pump modes. The reason is the SRS gain is small over a characteristic length expressed by the inverse of $k_{max} - k_{min}$ (assumed $\approx 2\pi\ (n_{core} - n_{outer\text{-}cladding})/\lambda_p$), where k_{max} (k_{min}) is the largest (smallest) wave vector of any pump mode. The "coherence length" of the pump light in different modes is only of order of 1 mm, which is small compared to the Raman interaction length. While there are likely to be pairs of pump modes with longer beat length, the power carried by any two modes can be expected to be small compared to the total power, and as different modes will beat with different beat lengths, no beat effect is expected in total, when all modes are considered, for typical values of $k_{max} - k_{min}$. There could be beating between signal modes. This then modifies the signal power distribution, which could modify the rate at which different pump modes are absorbed. Typically, however, either the beat length will be sufficiently small for this to be negligible, or the power will be predominantly in a single mode. There is also pump mode coupling due to perturbations (see section 2.2.1). For simplicity, this can be reduced to the two extreme cases: weak (or non-existing) and strong mode coupling [15]. In the absence of mode coupling, the pump modes are depleted at different rates. On the other hand, when strong mode mixing is present over a fibre length where the SRS gain is small, the pump power becomes averaged over the number of modes and all the modes are depleted at the same rate.

My work on FRLs pumped directly by the LDs only considers the average behaviour of MM Raman fibre. Even though the rate of mode coupling is expected to be relatively low, the fibres are sufficiently long for the modes to couple strongly. Therefore, it is reasonable to assume that the pump is evenly distributed across the fibre transverse cross section. Thus only by adjusting the pump distributed effective area A_{eff}, it is possible to use the coupled equations and expressions, already established, for the SRS gain (Eq. (2.11)) and for the threshold of a laser (Eq. (2. 14)) to diodes directly pumped MMF. In this case of DCRF, the effective area for SRS from the pump in the inner-cladding to the 1st Stokes in the core is equal to the inner-cladding area A_{cl}.

In my work, to achieve high Raman gain and good pump coupling efficiency, Raman fibre with high Ge concentration is required. It is possible to calculate the Raman gain corresponding to the pump brightness as shown in Figure 2.2 in the case of scrambled pump and Stokes states of polarisation (SOP). Here the fibre parameters are defined the same as the MM OFS 62.5/125 graded-index (GRIN) fibre which will be

used in the Chapter 5. The fibre *NA* is 0.275. The background losses at pump and signal wavelengths are 1.7 dB/km and 1.5 dB/km respectively, the Raman gain coefficient is estimated to be 2.38×10^{-13} m/W with 18.6% (mol) Ge concentration [16, 17]. For the pump brightness, state-of-the-art pump diodes provide around 0.1 W/(sr·μm^2) while 100 W/(sr·μm^2) may be a typical value for a fibre laser. The different fibre lengths are considered.

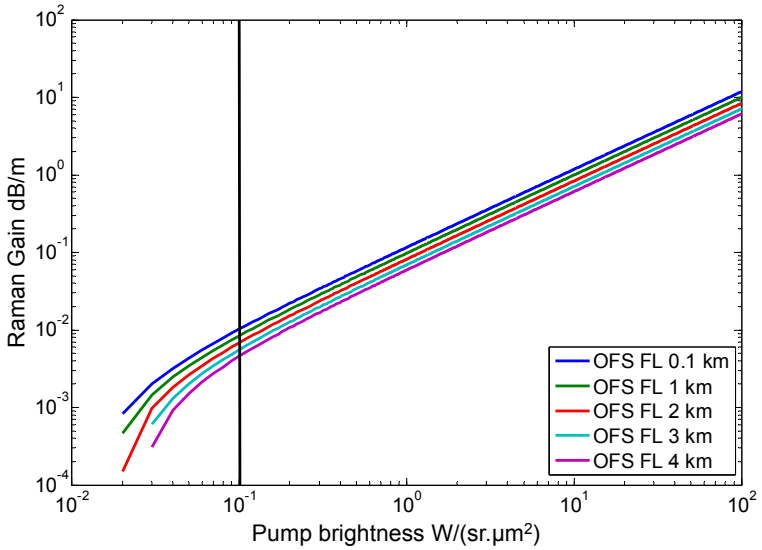

Figure 2.2 Raman signal gain vs pump brightness for MM Raman fibre used in the FRL (black line: brightness of the IPG MM diode).

Therefore, a much lower pump brightness compared to fibre-laser-pumping is a key restriction for Raman amplification pumped by diode. When pumped by a MM diode, such as a broadstripe diode, even in a high *NA* fibre with high Raman gain coefficient, only 0.01 dB/m Raman gain can be reached. Although the gain per unit length is slightly higher in short fibres length as shown in Figure 2.3, such short fibre suffer from a high pump threshold. In my work, to reach higher power density, one option is to operate in the quasi-cw regime with ns duration and kHz frequency which will be introduced in Chapter 4. In addition, another possibility demonstrated in Chapter 5: Chapter 5 is beam combination of the beams from multiple pump diodes through a Volume Bragg grating (VBG) while maintaining the beam quality of a single diode. This method will enhance the pump brightness and therefore improve the Raman gain.

The background loss can be very critical for Raman gain as well. However, the selection of the diode wavelength in my work tends to short wavelength below 1 μm

where the background loss becomes quite high. Therefore, the fibre length needs to be optimised to allow for sufficiently low total propagation loss. This will be further discussed in the Chapter 5.

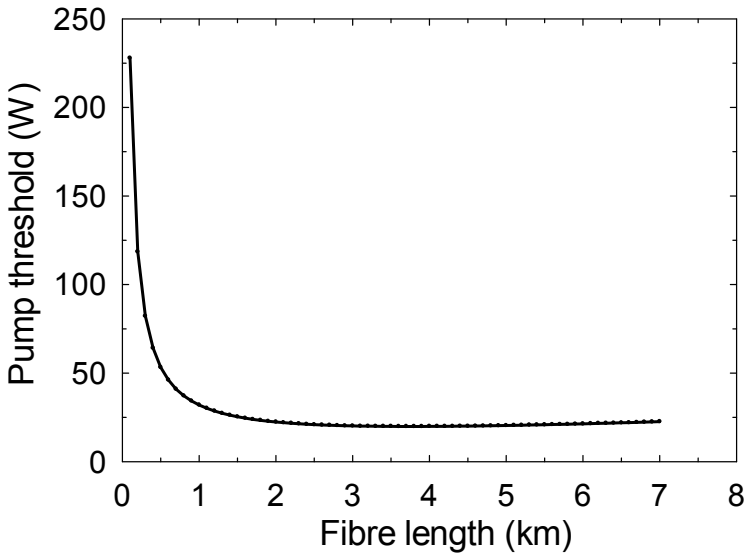

Figure 2.3 Pump threshold dependence with the fibre length.

To ensure a relatively low threshold, the proper fibre length can be chosen on the basis of the laser threshold expression as Eq. (2. 14). By applying the same fibre parameter as above, Figure 2.3 presents the calculated threshold power of FRL linear cavity formed by mirrors with R_1=4% and R_2=90%. The pump diode emits at 975 nm while the first Stokes is at around 1019 nm.

Following the results of calculations, the threshold is smallest for fibres between 3 and 4.4 km long. If the pumping is sufficient to overcome the threshold, the requirement on the fibre length can be relaxed. As the slope efficiency limited by the total propagation loss, it can then be improved. To balance the pump threshold and slope efficiency, the optimised fibre length is of interest and will be discussed in the following chapter. At the chosen lengths of 1.5 km and 3 km applied in the experiments, the threshold power is calculated to 19 W and 16 W.

2.3 Amplifications in ytterbium doped fibre

Among all the RE dopants emitting in a wide range of different wavelengths as candidates for the development of high-power fibre amplifiers, Yb is now the most

outstanding dopant due to several attractive features, including low thermal load [18]. Nevertheless, the power of YDFLs and YDFAs has been rapidly scaled and already reaches the level where the thermal effects play a detrimental role. This spurred interest in high brightness pumping with longer wavelength due to outstanding advantages for high power operation. Thus, another part of my work concentrates on tandem-pumped YDFAs with low QD, which allow for less heat generation.

2.3.1 Spectroscopic properties of ytterbium ions in a glass host

The RE elements or lanthanide series ions are typically trivalent with the same electron configuration in the outer O-shell. The radiative transitions take place within the progressively filled 4*f* subshell. This is an inner shell and is therefore shielded from outside influence, although the energy-levels are still Stark-split. Some intra-4f-transitions between Stark-split Yb-levels are shown in Figure 2.4. The energy level in terms of the electronic layers is classified by the *l*, *s* and J triplet ($^{2s+1}l_J$), which represent the orbital angular momentum, the spin angular momentum and the total angular momentum, respectively. The blue and red arrows correspond to some of stimulated absorption and emission transitions.

The spectroscopic properties of Yb ions are very simple compared to those of other RE ions. As shown in Figure 2.4, the 4*f* energy level structure consists of only two manifolds; the ground manifold $^2F_{7/2}$ with four sublevels and the excited manifold $^2F_{5/2}$ with three sublevels. Thanks to the simple structure, there is no need to worry about excited state absorption (ESA), which would lower the efficiency. Although there are excited levels that correspond to different 5d-configurations, these are in the ultraviolet and are therefore of no direct consequence for infrared lasers. Thus the pump quantum efficiency (QE) can be assumed to equal unity. This is defined as the fraction of absorbed pump photons that excites a Yb-ion. The slope efficiency of the amplified signal also relates to the pump QE by considering additional propagation loss as well as the quantum defect. The lack of parasitic energy levels also protects against concentration quenching. Therefore, it is possible to achieve high gain in high doping levels within a very short length, and in particular pump absorption levels required for high power CP operation.

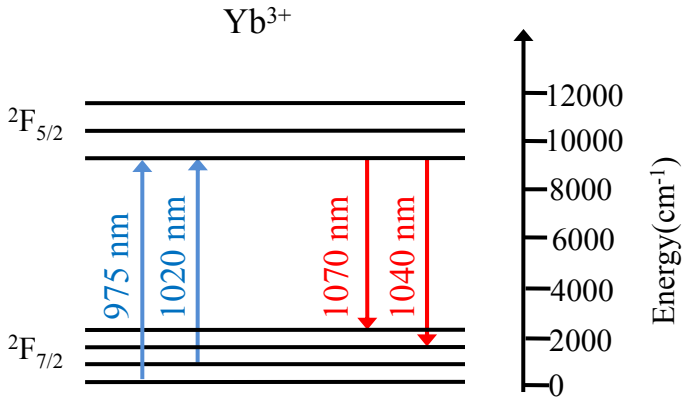

Figure 2.4 Energy level structure of Yb^{3+} in silica.

The absorption and emission cross-section spectra vary with the temperature, and host glass types and compositions [19]. Figure 2.5 shows the room temperature emission and absorption cross sections of Yb in aluminosilicate (Al) and phosphosilicate (P) glasses respectively, which are widely used for high-power RE-doped fibres. The RE ions are larger than typical glass formers. In particular in silica glass with its rigid SiO_2 tetrahedral network, it is therefore necessary to use high levels of passive co-dopants such as Al or P to improve the incorporation of RE ions. Otherwise detrimental clustering or even phase separation can occur, even at modest RE concentration. In addition, the co-dopants are also used for controlling the refractive index.

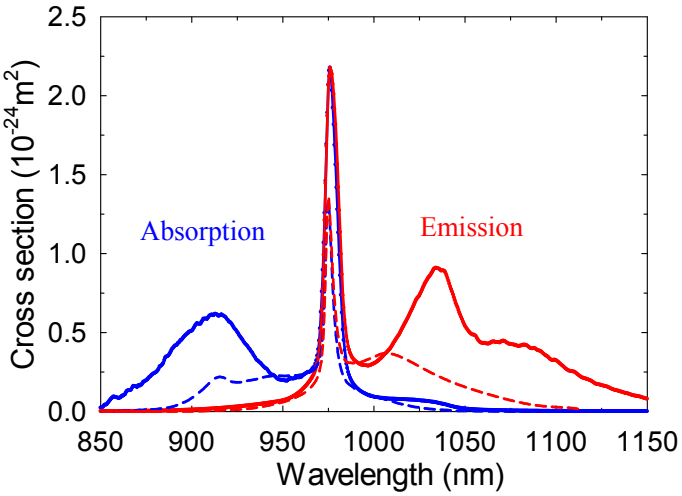

Figure 2.5 Absorption (blue colour) and emission (red colour) cross sections of YDF in Al (solid lines) and P (dashed lines) hosts at room temperature.

Compared to a crystal host, the cross-sections indicate that amplification is possible over a wide spectral range from 975 nm up to 1180 nm at room temperature. This broad gain bandwidth is of great interest for tandem pumping, while also advantageous for wavelength-division-multiplexing (WDM) systems, ultra-short pulse generation, and widely tuneable lasers. The amplification and gain is attained when the populations of the energy levels involved (upper and lower laser level) is inverted, or more precisely, when there are enough ions in the upper laser level to overcome the absorption of the ions that remain in the lower laser level, as well as other losses. The excited state lifetime of Yb ions in silica based fibres is typically around 0.8 to 1.5 ms [20]. Such a relatively long, "meta-stable", lifetime helps in obtaining a population inversion of the system and thus providing amplification through stimulated emission.

2.3.2 Amplification modelling

Modelling of the amplification in RE-doped fibres has been the topic of many papers and books with the growing interest in EDFAs for telecom applications [21 - 23]. Here I would like to summarize the basic properties of amplification and the gain equation in YDFs. In this thesis, I am principally interested in tandem pumped amplification of signals in the 1040-1080 nm wavelength range where the Yb system has nearly no ground-state absorption. As previously described, interactions between ions and ESA can be neglected [20], and the pump QE is assumed to equal unity. Furthermore, thermalisation of the Stark sub-level populations within each manifold is so fast that it can be assumed instantaneous. Therefore, the three- or four-level structure can be simplified into a two-level system with an excited level and a ground level [20, 24]. In practice, the reason why I have to treat it as being two levels is that the sub-levels are in thermal equilibrium within a manifold.

For the two-level system, the population densities N_i are defined as the number of ions in the i^{th} level per unit volume while the total number of Yb ions is expressed as N_0. Rate equations describe the effects of absorption, stimulated emission, and spontaneous emission on the populations of the ground and metastable states.

$$\frac{dN_2}{dt} = -\frac{dN_1}{dt} = R_{12}N_1 + W_{12}N_1 - R_{21}N_2 - W_{21}N_2 - N_2/\tau_l \qquad (2.\ 15)$$

where τ_l is the fluorescence lifetime and the radiation rates are expressed as

$$R_{12}=\frac{\sigma_{ap}I_p}{h\nu_p},R_{21}=\frac{\sigma_{ep}I_p}{h\nu_p},W_{12}=\frac{\sigma_{as}I_s}{h\nu_s},W_{21}=\frac{\sigma_{es}I_s}{h\nu_s} \quad (2.16)$$

where I_i , v_i , and σ_{ji} are the optical intensity, frequency and cross sections in Figure 2.5, respectively, with $i = s, p$ denoting the signal and pump wave, $j = a, e$ denoting the absorption and emission cross sections, h is Planck's constant. In Eq. (2.15), $R_{12}N_1$ represents the pump absorption, $W_{12}N_1$ the signal absorption, $W_{21}N_2$ the stimulated emission by the signal, $R_{21}N_2$ the stimulated emission by the pump, and N_2/τ_l the spontaneous emission, respectively.

Considering the steady state regime, one can obtain

$$N_2=N_0-N_1=N_0\frac{(R_{12}+W_{12})\tau_l}{1+(R_{12}+R_{21}+W_{12}+W_{21})\tau_l} \quad (2.17)$$

The remaining equations describe the evolution of the signal and pump power through the fibre propagation in the absence of amplified spontaneous emission (ASE)

$$\frac{dP_s}{dz}=\Gamma_s\left(\sigma_{es}N_2-\sigma_{as}N_1\right)P_s-\alpha_sP_s \quad (2.18)$$

$$\frac{dP_p}{dz}=-\Gamma_p\left(\sigma_{ap}N_1-\sigma_{ep}N_2\right)P_p-\alpha_pP_p \quad (2.19)$$

where Γ_s, Γ_p are the transverse modes overlap coefficients for signal and pump respectively, which is to account for the fact that some fraction of the power propagates in the un-doped area of the fibre. The set of differential equations with the corresponding boundary conditions can be numerically integrated over the fibre length using well-established methods such as Runge-Kutta. Note the ASE effect can be strong in the case of high peak gain reaching about 30-40 dB. The propagation equations Eq. (2. 18) and (2. 19) can be numerically solved with an effective ASE bandwidth to account for the ASE.

It is possible to calculate the small-signal gain (or absorption for pump) in decibels and the net cross section at wavelength λ along the fibre according to [24, 25]

$$G(\lambda)=4.343N_0\Gamma(\lambda)L\left(\left(\sigma_a(\lambda)+\sigma_e(\lambda)\right)\overline{n_2}-\sigma_a(\lambda)\right) \quad (2.20)$$

$$\sigma_{net}(\lambda) = \left(\sigma_a(\lambda) + \sigma_e(\lambda)\right)\overline{n_2} - \sigma_a(\lambda) \tag{2. 21}$$

where Γ is the ratio of effective areas at wavelength λ and the pump wavelength, $\overline{n_2}$ is the fraction of excited ions as appropriately averaged transversally and longitudinally over the fibre. Note that the fraction of excited Yb-ions $\overline{n_2}$ is the only free parameter for a given fiber in Eq. (2. 20). In the case of purely homogeneously broadened gain, the value of $\overline{n_2}$ is wavelength-independent and Eq. (2. 20) determines the whole gain spectrum uniquely for a given fiber at a given temperature, for all operating conditions that result in that average excitation level.

The above YDFs modelling and analysis rely on the assumption of a homogeneously broadened spectrum which depends on several factors [21]. To proceed, all Yb ions must have identical spectral properties, as described by the absorption and emission cross section spectra. This implies that their local environments are similar and effects due to a spatially varying temperature are negligible. Furthermore, each individual Yb ion must exhibit homogenously broadened spectral properties, so that its effective gain spectrum can be described as a superposition of cross section spectra. This means that the transition rates between the levels must be small compared to the transition rates within the levels, i.e., between the Stark sub-levels. These reach thermal equilibrium on the picosecond scale [26, 27]. An optical power density roughly of the order of 100 kW/μm^2 is needed to drive the inter-band laser transition at a similar rate. Such power densities cannot be reached in the cw regime. Nonlinear scattering would be severe, even if damage is avoided, and it is far from clear that they can be reached in the pulsed regime either, in pulses sufficiently long to appreciably distort the population distribution.

Though a higher value is expected at higher power densities, measurements on YDFs have shown only small inhomogeneous effects (in particular spectral hole-burning) at low powers in SMF [24]. Any wavelength-dependence of the power distribution can also lead to inhomogeneous effects [28, 29], since the average excitation level as seen by different wavelengths will vary inhomogeneously. Such wavelength-dependence can be larger in MM waveguides, e.g., in a double-cladding fibre, than in single-mode ones. Polarisation hole-burning can also be a factor for polarised waves, although this effect is small in measurements at low powers [29].

The net cross sections with average excitation fraction varying from 0 to 16% are shown in Figure 2.6. The net cross sections determine the shape of gain spectra under these excitation levels. In the case of long pump wavelength, the fraction of the excited ions would be much lower than that with 975 nm pump wavelength.

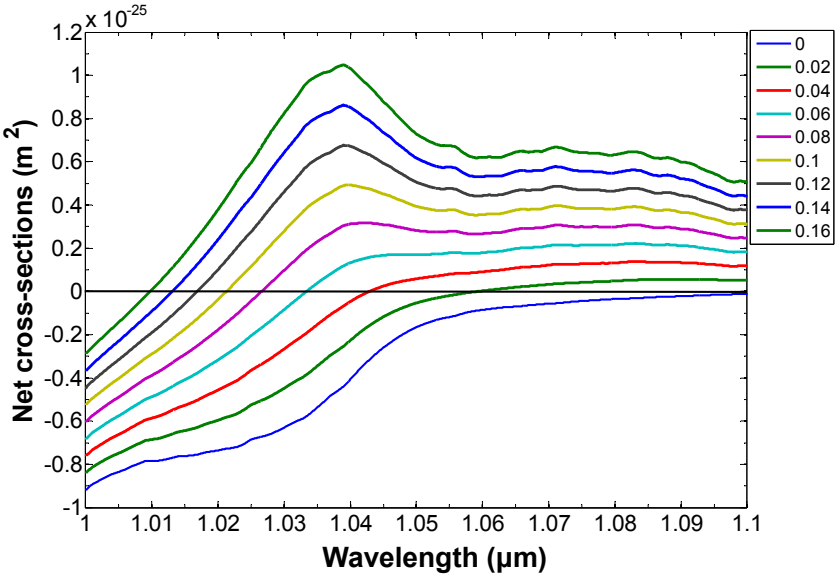

Figure 2.6 Net cross sections with 0 to 16% excitation levels, based on the absorption and emission cross sections of Al/Yb doped fibre at room temperature.

The temperature dependence of the absorption and emission cross sections, and their impact in the performance of the laser sources, which are normally operated at shorter wavelength than 1150 nm, can be found in the reference [19, 30, 31]. For instance, a temperature increase induces a shift to longer wavelengths with subsequent reduction of the peak gain and in turn leads to a reduced efficiency. For tandem pumped YDFAs, one of the main targets is to obtain a lower thermal load caused by the QD, and in turn reduced thermal and nonlinear degradation. In the next section, I will discuss the expression of QD and the thermal distribution, which result in the thermal effects directly.

2.4 Quantum defect and fibre temperature distribution

Among the performance benefits of fibre lasers are high optical-optical and wall-plug efficiencies, single-transverse-mode output, low noise output, and wide tunability [32]. There is now a great deal of interest in further scaling the average output power by another order of magnitude over the kilowatt level. In this regime, bulk crystalline lasers

encounter difficult thermal management issues, and fibre lasers would, therefore, offer substantial advantages because of more favourable surface-to-volume ratios. This has been experimentally and theoretically tested and validated in the kilowatt power domain where thermal effects already play an important role in the average power scaling of fibre lasers [33 - 35].

One limit consists of thermally induced material fracture that is commonly observable in bulk solid-state lasers and is even more pronounced in weaker silica based fibres. In addition, although it has not been observed experimentally, a large change in core temperature may result in significant change of refractive index which could affect the waveguiding properties and eventually degrade the laser efficiency [36, 37]. Furthermore, in some cases with very high thermal load, the core temperature may reach extreme values leading to the catastrophic melting of the core itself. Besides, the temperature dependence of the fibre spectroscopy can give rise to wavelength-dependent output power reduction [30, 31]. All in all, the thermal distribution and the low QD operation continue to catch attention.

2.4.1 Quantum defect

High efficiency and heat load are two linked but still different factors of critical importance for high-power lasers. Several factors can decrease the efficiency and increase the heat load, but arguably the QD is the most fundamental one. Here we define the (relative) QD as the relative difference between the pump and laser output photon energy,

$$QD = \frac{\nu_p - \nu_s}{\nu_p} = 1 - \frac{\lambda_p}{\lambda_s} \tag{2.22}$$

where λ_p and λ_s are the pump and laser wavelengths. Note that while the QD is conventionally and more naturally defined in absolute terms, it is more convenient to consider the relative QD, which is what I do throughout this thesis.

Heat dissipation in fibre has been comprehensively analysed in the literature [33 - 38]. It is mainly generated by the following processes: first, the QD already expressed in Eq. (2.22), yielding 24% for the 1060 nm transition of Nd when pumped at 807 nm. In contrast, the 1071 nm transition of Yb yields only 8.9% heat dissipation when pumped

at 975 nm. According to the definition, the QD can be reduced by a small energy difference between pump and signal, as well as by a shorter pump wavelength. Second, the fibre attenuation during the propagation also leads to some heating. In addition, if ESA or the non-radiative decay rate W_{NR} from the lasing level is nonzero, this will also convert a fraction of the pump power into heat. W_{NR} consists of a number of contributions, including multi-phonon decay and ion-ion energy transfer effects like concentration quenching and cross-relaxation.

2.4.2 Temperature distribution

There have been published analyses on temperature distribution in the radial and tangential directions. The heat generated in the laser may be removed by cooling the fibre through conduction, forced convection or natural convection. Heating and cooling together, in the steady state, lead to a non-uniform temperature distribution across the fibre and a corresponding temperature gradient between the fibre core and the external reservoir. In this section I will present the simulation results of the thermal distribution in terms of different pump wavelengths, such as 975 nm and 1030 nm.

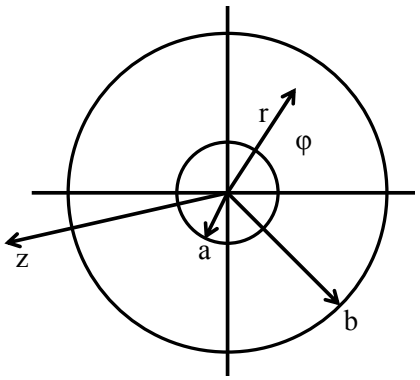

Figure 2.7 Scheme of the cross-section of the fibre light guide. *b* is the glass radius, *a* is the core radius activated by Yb ions.

In the case of Yb doped silica fibre, to calculate the thermal distribution, the heat is assumed to be deposited only in the doped core. The fibre geometry is shown in Figure 2.7. The radial coordinate is r and φ is the tangential angle, the longitudinal coordinate is z, a and b are the core and cladding radius, respectively. Generally, the temperature distribution in the cylindrical symmetry structure, such as optical fibre, can be obtained by the steady-state heat equation expressed as [39]

$$\nabla \cdot \nabla \left(T(r,z) \right) = -\frac{Q(r,z)}{\kappa} \tag{2. 23}$$

where κ is the thermal conductivity, Q is the heat deposition density, and T is the temperature. Here we have ignored any azimuthal variations. The fibre length is invariably much larger than its diameter, and thus, the longitudinal heat transfer is negligible compared to the radial heat transfer.

The solution of Eq. (2.23), subject to the boundary conditions, can result in the following expressions for the temperature in core and inner-cladding regions [33],

$$T_{co}(r) = T_0 \frac{Qr^2}{4\kappa_{co}} \tag{2. 24}$$

$$T_{cl}(r) = T_0 - \frac{Qa^2}{4\kappa_{co}} - \frac{Qa^2}{2\kappa_{cl}} \ln(\frac{r}{a}) \tag{2. 25}$$

where T_0 is the centre temperature and Q is assumed constant across the core. It can be related to the coolant temperature T_c and convective heat transfer coefficient h', and by use of [33]

$$T_0 = T_c + \frac{Qa^2}{2h'c} + \frac{Qa^2}{4\kappa_{co}} + \frac{Qa^2}{2\kappa_{cl}} \ln(\frac{b}{a}) \tag{2. 26}$$

Since my work focuses on the tandem pumped YDFA with high brightness, I will simulate the thermal distribution by the rate equations discussed in the section 2.3, at 975 nm and 1030 nm pump wavelengths for comparison. To simplify the model, the heat source is assumed to be uniform over the cross-section of the fibre core, i.e., it does not depend on the radial coordinate r. In addition, the influences of the ESA and non-radiative decay are assumed to be negligible. The temperature dependence of the cross section and the thermal conductivity is ignored as well. Then, the expression of the thermal density Q of the core is given by [40]

$$Q = \frac{(\alpha_s P_s + \alpha_p P_p) + \frac{QD}{1-QD} P_s (N_2 \sigma_{es} - N_1 \sigma_{as})}{A_{co}} \tag{2. 27}$$

I concentrated in this work on Al co-doped YDFs like those used in the recently demonstrated tandem-pumped YDFA [41]. I, thus, assume a YDF with a 30 μm diameter core with $0.83\times10^{-26}m^{-3}$ Yb-concentration. The core is surrounded by a circular inner cladding with a diameter of 100 μm. The geometry used in the modelling is shown in Figure 2.7. As mentioned previously in this section, to simplify the analysis, I assume that the core and cladding regions are circular and concentric, and that they have the same thermal properties. The fibre length is assumed to be 12 m. To achieve sufficient amplification in the amplifier, at the signal wavelength (1071 nm) a strong remaining seed signal of 200 W after propagation through the fibre is necessary to saturate the amplifier, while the signal power and pump power are defined to be 400 W and 4 kW respectively. In the case of 975 nm wavelength pumping, the same power levels for both pump and signal are applied with a reduced fibre length to 2 m. Table 2.1 shows the rest of parameters required for the calculation. The coolant temperature is assumed to be 298 K and the thermal conductivity is taken as a constant of 1.38 W/(m·K) in both core and inner-cladding area. The convective heat transfer coefficient h' strongly relies on the cooling condition, and may be as low as 10 W/(m^{2}K) for passive cooling and as high as 1000 W/(m^{2}K) for forced air flow or 10000 W/(m^{2}K) for forced liquid flow cooling [35]. Here I take the maximum value of 10000 W/(m^{2}K).

Table 2.1. Parameters used in the fibre thermal distribution analysis

(Al host)

Parameter	Values
Thermal conductivity of glass, $\kappa_{co} = \kappa_{cl}$, W/(m·K)	1.38
Convective heat transfer coefficient, h', W/(m^{2}K)	10000
Coolant temperature of ambient air, T_c, K	298
Lifetime of the excited level, τ_l, ms	0.83
Emission cross section at 975 nm, σ_{ep}, pm^2	207
Absorption cross section at 975 nm, σ_{ap}, pm^2	207
Emission cross section at 1030 nm, σ_{ep}, pm^2	84.6
Absorption cross section at 1030 nm, σ_{ap}, pm^2	6.31
Emission cross section at 1071 nm, σ_{es}, pm^2	44.69
Absorption cross section at 1071 nm, σ_{as}, pm^2	0.55
Background loss at 975 nm, α_p, /m	2×10^{-3}
Background loss at 1030 nm, α_p, /m	1.6×10^{-3}
Background loss at 1071 nm, α_s, /m	1.2×10^{-4}

The simulated thermal distributions for the two pump wavelengths are presented in Figure 2.8. The maximum heat generation occurs at the point where the signal increase is highest, in agreement with Eq. (2.27). The temperature reaches 1200 K in

case of 975 nm pumping. This value approaches the silica melting temperature of 1983 K [35] and would be unrealistic in real life. Thus, a lower Yb-concentration and a longer fibre would be needed. With 1030-nm pumping, the longer fibre and the smaller QD reduces the peak temperature to a wholly realistic 316 K.

The calculated maximum temperature shown in Figure 2.8 is conservative, since the outer-cladding region of fibres, which has not been considered here, tends to be polymeric materials with a thermal conductivity lower than that of glass by a factor of ten. Besides, most fibres are surrounded by plastic outer sheaths that will further increase the thermal resistance and thus the centre temperature. Both of these factors can significantly increase the fibre centre temperature well beyond the levels shown in Figure 2.8. In addition, it is found the temperature increase is much larger in the counter-pumped case due to the large gain near the output end of the fibre.

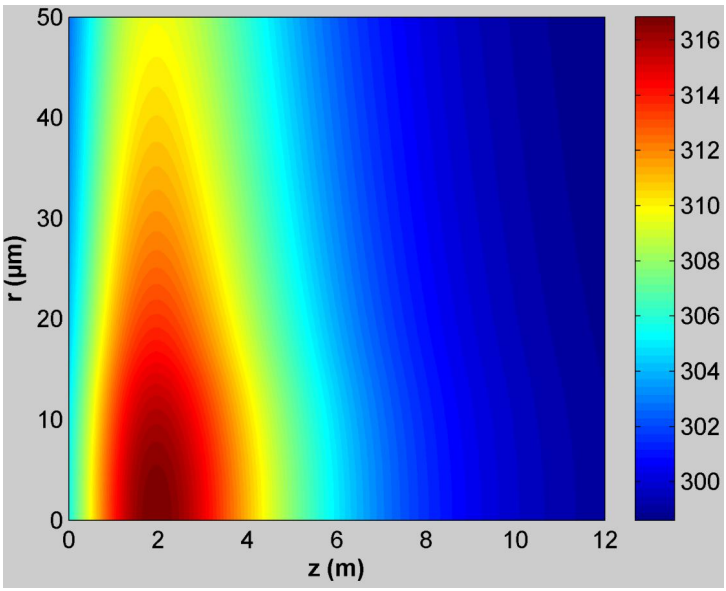

(a)

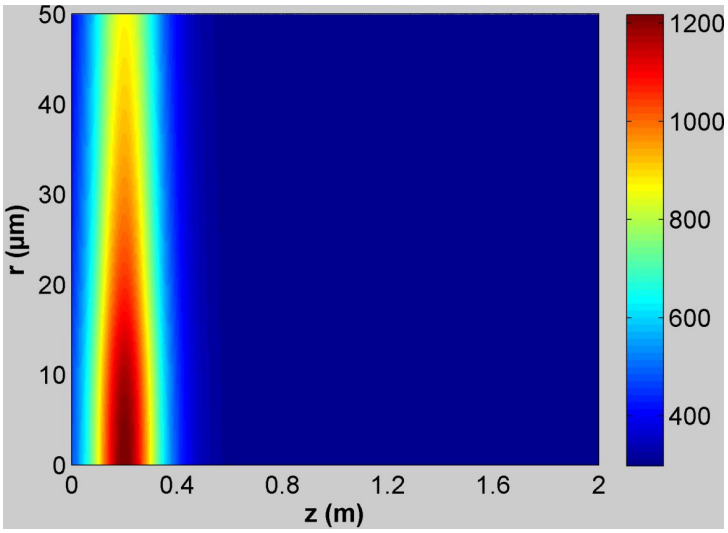

(b)

Figure 2.8 Temperature distribution along the radial and longitudinal coordinates pumped at (a) 1030 nm and (b) 975 nm.

2.5 Summary

In this chapter, I have introduced the background theory related to the work in the thesis, including beam quality and brightness enhancement. I also present the SRS process both in SMF and in MMF in the cw and quasi-cw regimes. Especially for directly LD-pumped Raman fibre, the dependence of Stokes gain and pump threshold on the pump brightness and fibre length is discussed based on the power evolution equations. In addition, the rate equations of Yb-ions in optical fibre are given to model the gain and absorption in YDFs. The thermal effects and heat dissipations in high-power Yb doped laser sources are presented. Simulation results of the thermal distribution indicate that the QD plays a significant role for the thermal generation. Tandem pumping is shown to be a good way to approach the minimum QD in YDFs, while the pump LDs at short wavelength can also contribute for Raman fibre. I will further discuss the details of tandem pumped YDFAs in the next chapter.

2.6 References

1 A. E. Siegman, “How to (maybe) measure laser beam quality,” in Diode Pumped Solid State Lasers: Applications and Issues, M. W. Dowley, Ed. : Optical Society of America, 1998, vol. 17, OSA Trends in Optics and Photonics Series, 184-199.

2 ISO Standard 11146, “Lasers and laser-related equipment — Test methods for laser beam widths, divergence angles and beam propagation ratios,” (2005).

3 O. Svelto, Principles of Lasers, (4th Ed., Springer, (trans. David Hanna), 1998).

4 J. Ji, C. A. Codemard, J. K. Sahu, and J. Nilsson, “Design, performance and limitations of fibers for cladding-pumped Raman lasers,” Opt. Fiber Technol., 16(6), 428-441, (2010).

5 T. H. Russell, S. M. Willis, M. B. Crookston and W. B. Roh, "Stimulated Raman scattering in multimode fibers and its application to beam cleanup and combining," J. Nonlinear Opt. Phys. Mater., 11, 303-316, (2002).

6 J. Nilsson, J. K. Sahu, J. N. Jang, R. Selvas, D. C. Hanna, and A. B. Grudinin, “Cladding-pumped Raman fiber amplifier,” in Proc. of Optical Amplifiers and Their Applications (OAA 2002), paper PD2-1/2/3, Vancouver, Canada 2002.

7 C. V. Raman and K. S. Krishnan, “A new type of secondary radiation,” Nature, 121(3048), 501-502, (1928).

8 R. H. Stolen and E. P. Ippen, “Raman gain in glass optical waveguides,” Appl. Phys. Lett., 22(6), 276-278, (1973).

9 F. L. Galeener and G. Lucovsky, “Longitudinal optical vibrations in glasses: GeO_2 and SiO_2,” Phys. Rev. Lett., 37(22), 1474-1478, (1976).

10 R. H. Stolen, J. P. Gordon, W. J. Tomlinson, and H. A. Haus, “Raman response function of silica-core fibers,” J. Opt. Soc. Am. B., 6(6), 1159-1166 (1989).

11 G. P. Agrawal, Nonlinear Fiber Optics, (4th Ed., Academic Press Inc., San Diego CA, 2007).

12 R. H. Stolen, “Polarization effects in fiber Raman and Brillouin lasers,” IEEE J. Quantum Electron., 15, 1157-1160, (1979).

13 R. G. Smith, “Optical power handling capacity of low-loss optical fibers as determined by stimulated Raman and Brillouin scattering,” Appl. Optics, 11(11), 2489-2494, (1972).

14 S. I. Kablukov, E. I. Dontsova, E. A. Zlobina, I. N. Nemov, A. A. Vlasov, and S. A. Babin, “An LD-pumped Raman fiber laser operating below 1 μm,” Laser Phys. Lett., 10, 085103, (2013).

15 F. Capasso and P. Di Porto, “Coupled-mode theory of Raman amplification in lossless optical fibres,” J. Appl. Phys., 47(4), 1472-1476, (1976).

16 S. T. Davey, D. L. Williams, B. J. Ainslie, W. J. M. Rothwell, and B. Wakefield, “Optical gain spectrum of GeO_2-SiO_2 Raman fiber amplifiers,” Proc. Inst. Elect. Eng., 136(6), 301-306, (1989).

17 J. Bromage, K. Rottwitt, and M. E. Lines, “A Method to predict the Raman gain Spectra of germanosilicate fibers with arbitrary index profiles,” IEEE Photon. Technol. Lett., 14(1), 24-26, (2002).

18 Y. Jeong, J. K. Sahu, S. Baek, C.Alegria, D. B. S. Soh, C. Codemard, V. Philippov, D. J. Richardson, D. N.Payne, and J. Nilsson, “Ytterbium-doped double-clad large-core fibre lasers with kW-level continuous-wave output power,” in Proc. of CLEO, San Francisco, US, 2004.

19 D. E. McCumber "Einstein relations connecting broadband emission and absorption spectra", Phys. Rev., 136(4A), A954-A957, (1964)

20 R. Paschotta, J. Nilsson, A. C. Tropper, and D. C. Hanna, “Ytterbium-doped fiber amplifiers,” IEEE J. Quantum Electron., 33(7), 1049-1056, (1997).

21 E. Desurvire, Erbium-Doped Fiber Amplifiers, (1st Ed., Wiley-Interscience, 1995).

22 A. A. M. Saleh, R. M. Jopson, J. D. Evankow and J. Aspell, “Modeling of gain in erbium-doped fiber amplifiers”, IEEE Photon. Technol. Lett., 2(10), 714-717, (1990).

23 C. R. Giles and E. Desurvire, “Modeling erbium-doped fiber amplifiers,” J. Lightw. Technol., 9(2), 271-283, (1991).

24 H. M. Pask, R. J. Carman, D. C. Hanna, A. C. Tropper, C. J. Mackechnie, P. R. Barber and J. M. Dawes, “Ytterbium-doped silica fiber lasers: Versatile sources for the 1–1.2 μm region,” IEEE J. Sel. Topics in Quantum Electron., 1(1), 2-13, (1995).

25 C. Codemard, J. K. Sahu, and J. Nilsson, “Tandem cladding-pumping for control of excess gain in ytterbium-doped fiber amplifiers,” IEEE J. Quantum Electron., 46(12), 1860-1869, (2010).

26 K. Lu and N. K. Dutta, “Spectroscopic properties of Yb-doped silica glass,” J. App. Phys., 91(2), 576-581, (2002).

27 William F. Krupke, “Ytterbium solid-state lasers—the first decade,” IEEE J. Sel. Topics in Quantum Electron., 6(6), 1287-1296, (2000).

28 D. W. Hall, R. A. Haas, W. F. Krupke and M. J. Weber, “Spectral and polarization hole burning in neodymium glass lasers,” IEEE J. Quantum Electron., 19(11), 1704-1717, (1983).

29 E. Desurvire, J. L. Zyskind and J. R. Simpson, “Spectral gain hole-burning at 1.53 μm in erbium-doped fiber amplifiers,” IEEE Photon. Technol. Lett., 2(4), 246-248, (1990).

30 L. A. Vazquez-Zuniga, S. Chung, and Y. Jeong, “Temperature dependence of a high-power ytterbium-doped fiber amplifier operating at 1060 nm and 1080 nm,” in Proc. of OECC, Hongkong, China, 2009.

31 S. J. Lee, L. A. Vazquez-Zuniga, H. Kim, and Y. Jeong, “Thermal characteristics of Ytterbium-doped phosphosilicate fiber amplifiers,” Proc. of OECC, Busan,Korea, 2012.

32 D. J. Richardson, J. Nilsson, and W. A. Clarkson, “High power fiber lasers: current status and future perspectives,” J. Opt. Soc. Am. B, 27, B63–B92, (2010).

33 D. C. Brown and H. J. Hoffman, “Thermal, Stress, and Thermo-Optic Effects in High Average Power Double-Clad Silica Fiber Lasers,” IEEE J. Quantum Electron., 37(2), 207-217, (2001).

34 Y. Wang, C. Q. Xu, and H. Po, “Thermal effects in kilowatt fiber lasers,” IEEE Photon. Technol. Lett., 16(1), 63-65, (2004).

35 J. W. Dawson, M. J. Messerly, R. J. Beach, M. Y. Shverdin, E. A. Stappaerts, A. K. Sridharan, P. H. Pax, J. E. Heebner, C. W. Siders, and C. P. J. Barty, “Analysis of the scalability of diffraction-limited fiber lasers and amplifiers to high average power,” Opt. Express, 16(17), 13240–13266, (2008).

36 F. Jansen, F. Stutzki, H.-J. Otto, T. Eidam, A. Liem, C. Jauregui, J. Limpert, and A. Tünnermann, “Thermally induced waveguide changes in active fibers,” Opt. Express, 20(4), 3997-4008, (2012).

37 M. S. Kuznetsov, O. L. Antipov, A. A. Fotiadi, and P. Mégret, “Electronic and thermal refractive index changes in Ytterbium-doped fiber amplifiers,” Opt. Express, 21(19), 22374-22388, (2013).

38 J. Li, K. Duan, Y. Wang, X. Cao, W. Zhao, Y. Guo, and X. Lin, “Theoretical analysis of the heat dissipation mechanism in Yb3+-doped double-clad fiber lasers,” J. Mod. Opt., 55, 459-471, (2008).

39 M. E. Innocenzi, H. T. Yura, C. L. Fincher, and R. A. Fields, “Thermal modeling of continuous-wave end-pumped solid-state lasers,” Appl. Phys. Lett., 56(19), 1831-1833, (1990).

40 K. R. Hansen, T. T. Alkeskjold, J. Broeng, and J. Lægsgaard, “Thermo-optical effects in high-power ytterbium-doped fiber amplifiers,” Opt. Express, 19(24), 23965-23980, (2011).

41 C. Wirth, O. Schmidt, A. Kliner, T. Schreiber, R. Eberhardt, and A. Tünnermann, “High-power tandem pumped fiber amplifier with an output power of 2.9 kW,” Opt. Lett., 36(16), 3061-3063, (2011).

Chapter 3: Tandem-pumped ytterbium doped fibre amplifiers with low quantum defect

This chapter treats tandem-pumped YDFA in the cw regime with reduced QD and thus thermal load. In section 3.1, I theoretically analyse the minimum QD based on a model of efficient tandem-pumped YDFA based on the use of longer pump wavelength and shorter signal wavelength than normal. Among the several factors, a high pump brightness is a key one for tandem pumping. Section 3.2 presents cw tandem pumped YDFA with single-mode tuneable pump and seed sources. Then the output characteristics are shown and discussed. Additionally, PD measurement under tandem pumping is performed and shown in section 3.3. Finally, section 3.5 summarises the results and findings of this chapter, followed by a discussion of low QD operation.

3.1 Theoretical approach of lowest quantum defect heating

According to the previous chapter, with the caveat of homogeneously broadened spectra, the magnitude of the gain as given by Eq. (2. 20) can be scaled to an arbitrary value by changing the fiber length, the Yb-concentration, or the overlap. They all change the gain in the same way when scaled and need not be considered separately, although the overlap can be quite different for pump and signal and cannot exceed unity. Figure 3.1 shows theoretical gain spectra of an Al YDF, based on Eq. (2. 20), for two different values of $\overline{n_2}$. Negative gain corresponds to absorption. This absorption, i.e., the operating absorption, depends on the excitation level with $\overline{n_2} = 0$ corresponding to the un-pumped small-signal absorption. For both curves in Figure 3.1, the peak gain is scaled to 30 dB, which we take to be the highest gain that can be readily managed in an YDF. The figure further shows the shortest signal wavelengths that result in 25 dB and 10 dB gain, as well as the longest pump wavelengths that result in 10 and 40 dB operating absorption, for an excitation level of 7%.

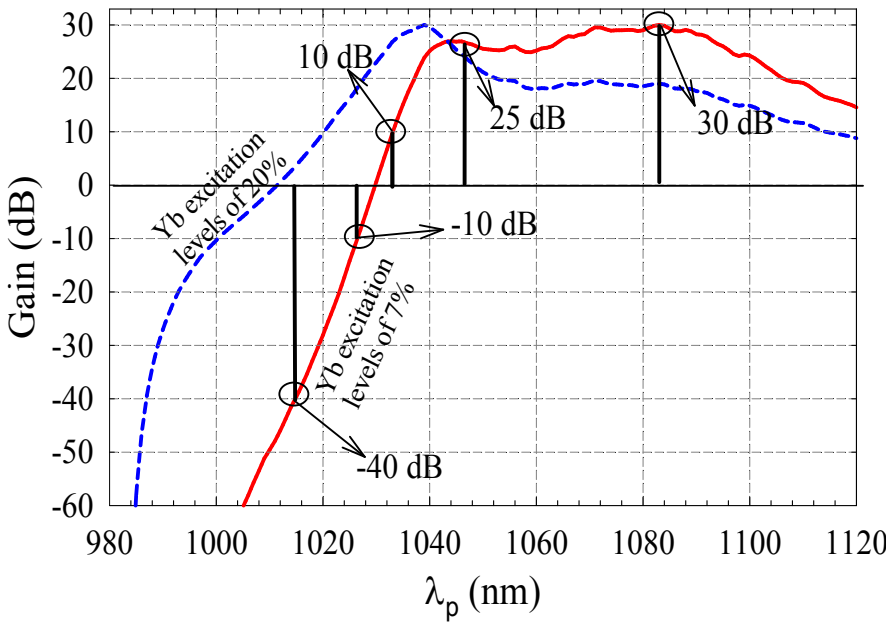

Figure 3.1 YDF gain spectra scaled to 30 dB peak for Yb excitation level 7% (red solid curve) and 20% (blue dashed curve) at room temperature.

Since the QD is given by the wavelength separation between the signal and the pump, it can be decreased with smaller signal gain or smaller pump absorption. A pump absorption of 10 dB (i.e., 90%) may be considered minimum for efficient operation whereas 40 dB is excessive. However, Figure 3.1 does not consider the possibility of variations in the overlap, which can be significant. With cladding-pumping, the pump overlap and thus absorption decreases in inverse proportion to the inner-cladding-to-core area ratio as a first approximation. Thus, if the curves in Figure 3.1 correspond to light guided in the core with $\Gamma = 1$, then the 40 dB absorption in Figure 3.1 would allow for an absorption of 10 dB for light in an inner cladding with an area ratio of four ($\Gamma = 0.25$).

3.1.1 Limitation of the excitation level and area ratio

I repeated the calculations corresponding to Figure 3.1 for different excitation levels, and determined the wavelengths that correspond to different levels of signal gain and pump absorption for light propagating through a fibre. In all cases the gain and absorption values are for light propagating in the core. One can find the operating signal and pump wavelengths with a certain excited fraction. The results are shown in Figure 3.2, for signal gain between 5 and 30 dB and pump absorptions between 10 and 1000

dB, which are independent with each other. We assume that the pump and signal overlaps are equal, and to be specific we assume it is for light propagating in the core with $\Gamma = 1$. While the decrease in pump absorption that results from cladding-pumping can be somewhat larger than a simple area-ratio scaling suggests, an operating absorption of 1000 dB in the core at the pump wavelength allows for an area ratio of up to 100 for a pump absorption of ~10 dB. This area ratio is a typical value for a conventional diode-pumped YDF. The QD for all operating conditions corresponding to a specific average excitation level $\overline{n_2}$ is then given by the difference between signal and pump wavelengths in Figure 3.2, for selected combinations of core absorption and gain. In case of core-pumping, pumping around 1020 nm looks attractive, although up to 1040 nm seems good, too, at least for up to 15 dB of gain.

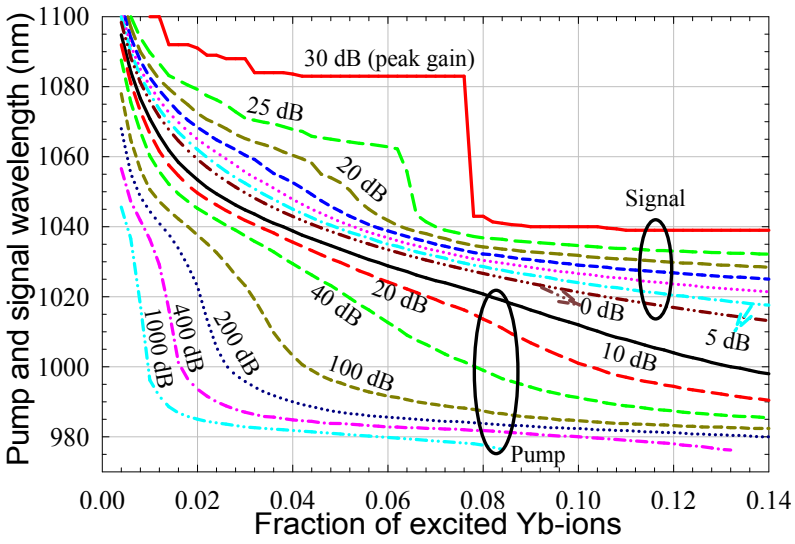

Figure 3.2 Longest possible pump wavelength and shortest possible laser wavelength for an YDF at room temperature. Signal gains are, from bottom to top, 5, 10, 15, 20, 25, and 30 dB (peak gain). Core pump absorption ranges from 10 dB to 1000 dB. The wavelength for which there is neither gain nor absorption is also plotted (0 dB).

It is clear from this analysis that a smaller pump area (which requires higher pump brightness) and / or a larger core (i.e., smaller area ratio), lower pump absorption, and lower signal gain can allow for a smaller QD. Furthermore, at fixed excitation level, the slope of the gain around 0 dB is proportional to the peak gain (or equivalently to the concentration and the fibre length according to the gain equation). Therefore, also a higher peak gain allows for a lower QD by allowing for a longer pump wavelength and a shorter signal wavelength (away from the gain peak), at fixed levels of signal and

pump absorption. However the maximum gain is limited by unwanted effects such as ASE and spurious lasing.

Figure 3.2 can be reworked to explicitly show the lowest attainable relative QD *vs.* excitation level. This amounts to calculating the difference between the signal and pump wavelengths shown in Figure 3.2, and then calculating the relative QD according to its definition. Figure 3.3 shows the results, for signal gains from 10 to 30 dB. I have also reworked the pump absorption in the core to the area ratio that allows for 10 dB absorption with cladding-pumping, under the assumption that the pump absorption is inversely proportional to the area ratio. Thus, the core absorption levels of 10 - 1000 dB in Figure 3.2 corresponds to area ratios from 1 to 100 in Figure 3.3. For a fixed core size, this change in area ratio effectively means different inner-cladding sizes and pump beam quality requirements. The QD reaches below 1% with core pumping (unity area ratio) for 10 dB signal gain, for fractions of excited Yb ions of around 5%.

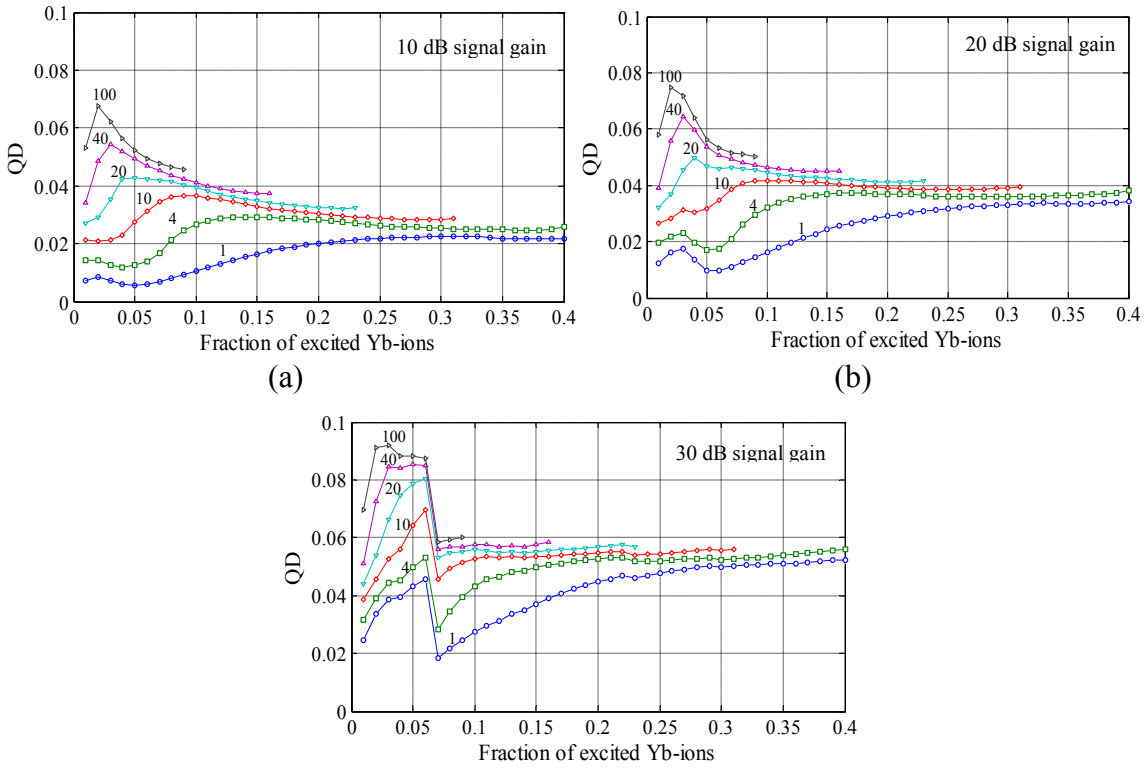

Figure 3.3 Smallest attainable relative QD *vs* Yb excitation level for (a) 10 dB, (b) 20 dB, and (c) 30 dB signal gain.

3.1.2 Limitation of the pump wavelength

The data can be further manipulated to find the dependence of the QD on pump wavelength, which is a more directly available parameter than the average excitation level is. This is shown in Figure 3.4 for a signal gain of 10 dB. For each pump wavelength, this calculation amounts to finding the excitation level and fibre length that yield the smallest possible QD. This fibre length is also shown in Figure 3.4, under the assumption of a Yb-ion concentration of 2×10^{26} m^{-3}. It is clear that the QD depends more on the area ratio (i.e., effectively the pump brightness) than on the pump wavelength. However, some combinations of pump wavelength and area ratio lead to impractical fibre lengths. According to Figure 3.4, the optimum pump wavelength for high-brightness tandem pumping of Yb is around 1030 nm, corresponding to fibre lengths of 2 m or more, at the concentration we assume. For cladding pumping with large inner-cladding-to-core area ratio, the QD is higher, and, for a fixed pump wavelength, the fibre is longer.

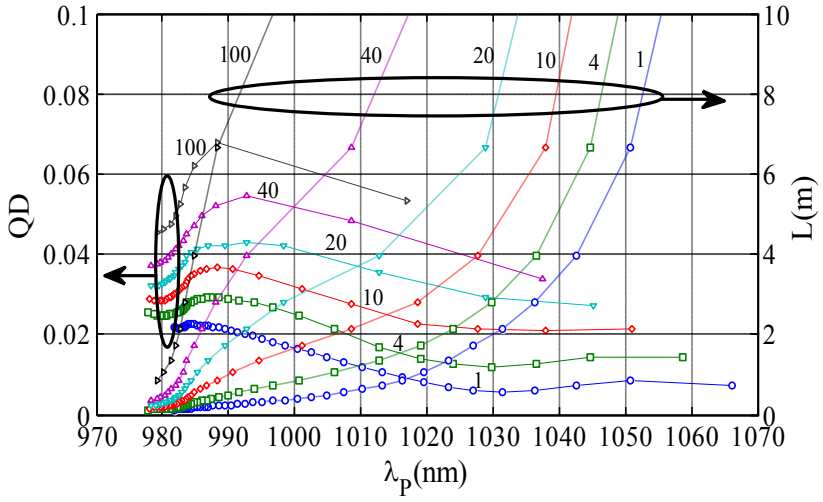

Figure 3.4 Smallest attainable relative QD (solid curves) & corresponding fibre length (dashed curves) *vs* pump wavelength for 10 dB signal gain.

With this model, I find that the QD depends strikingly strongly on the inner-cladding / core area ratio, and its lowest value of only 0.6% is reached in a fibre with unity area ratio, i.e., with core-pumping. This is an order-of-magnitude improvement over YDFs using conventional direct-diode CP technology. The pump wavelength is less critical, but for smallest QD the pump and the signal linewidths need to be small compared to the wavelength difference between the pump and signal, which can be as

small as 6 nm. Fortuitously, the best pump wavelength (found to be around 1020 or 1030 nm) and required linewidths can be reached by YDF-based pump lasers. Such pump sources, providing high brightness and high beam quality outputs, can be directly coupled into the core or in a small inner cladding, which opens up for percent-level QD even at high power level, in theory at least. By contrast, while 1020 nm can be reached with diodes, as well, which can in principle be used for core-pumping, the power would be limited since high-power narrow-line diodes are still far from the brightness levels required for core-pumping. Our calculations and conclusions are only valid to the extent that the gain equation describes the gain accurately, and the validity as well as its limits need to be determined experimentally.

3.2 Experiments and discussion

The potential for percent-level QD needs experimental confirmation. For this, there are several advantages of the narrow-band tuneable pump and seed sources. One of them is to investigate the closest pump and seed wavelength which still allow for sufficient amplification. Secondly, flexible pump and seed wavelengths enable the pump absorption and signal gain to be varied without changing the lengths of the tested YDFs. Besides the small wavelength differences between the pump and seed, the pump wavelength should lie in the range from 1020 nm to 1030 nm according to the simulation results. What's more, as discussed in the previous section, it is also necessary to use a high pump brightness. For this reason, and for simplicity and measurement accuracy, core pumping is preferred for tandem pumping.

3.2.1 CW tuneable pump laser source

The experimental setup of the tuneable pump source is shown in Figure 3.5. For high-power high-brightness operation, it is necessary to use a double clad active fibre. The laser consisted of a double clad large core YDF (OFS YB125). The inner cladding is flower-shape in order to increase the pump absorption. The inner-cladding diameter is 130 μm. The core diameter is 6 μm with a NA of 0.13. The core absorption was measured to be 323 dB/m at 915 nm. Finally, the fibre is coated with a low refractive index polymer which provides the outer cladding for the DC structure with an NA of 0.45. The fibre has a pump absorption of about 1.6 dB/m at the pump wavelength of 974

nm and the total fibre length is about 1 m. The unabsorbed pump in the cladding was stripped out by the index matching gel.

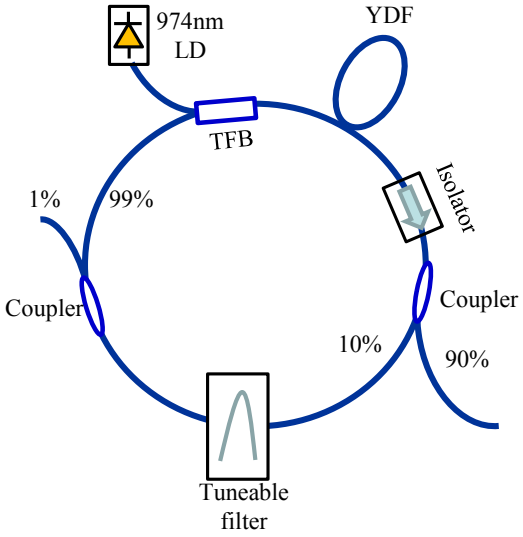

Figure 3.5 Experiment configuration of the pump source.

The output of a 60 W LD (IPG Photonics) pump diode was coupled into the inner cladding through a tapered fibre bundle (TFB) (Sifam) and an isolator (AFR) so that the laser was co-pumped with respect to the laser output. The free-running ring cavity was formed by the coupler (Opto-Link) with ratios 90%-10%. Another coupler (LighTel) with ratio of 99%-1% was used to monitor the power. The wavelength was set with a tuneable filter (Agiltron FOTF-026122131) 0.2 nm linewidth. The incorporation of a tuneable filter in the laser cavity provided a wavelength selective feedback into the cavity, thus restricting the laser operation to the tuning range of the filter. All passive fibres were HI-l060 ensuring the single-mode selection of the output. All fibres were fusion-spliced together.

The output power in terms of wavelength at various pump powers is shown in Figure 3.6 (a). The output power peaked at 1040 nm, at 16% slope efficiency and 3.8 W of power when pumped at 25 W, while it was 2.8 W output at 1020 nm at the same pump power. Although I could further raise the output power over that by increasing the pump power, in principle, the larger amount of heat dissipated at the cladding-mode stripper because of the higher pump leakage becomes increasingly serious. Therefore I restricted pumping to 25 W. Another limitation is the power tolerance of the fibre components, such as isolator and filter, applied in the cavity. All in all, this output

power level is enough to investigate the tandem pumped YDFA with minimised QD in the case of single-mode pumping.

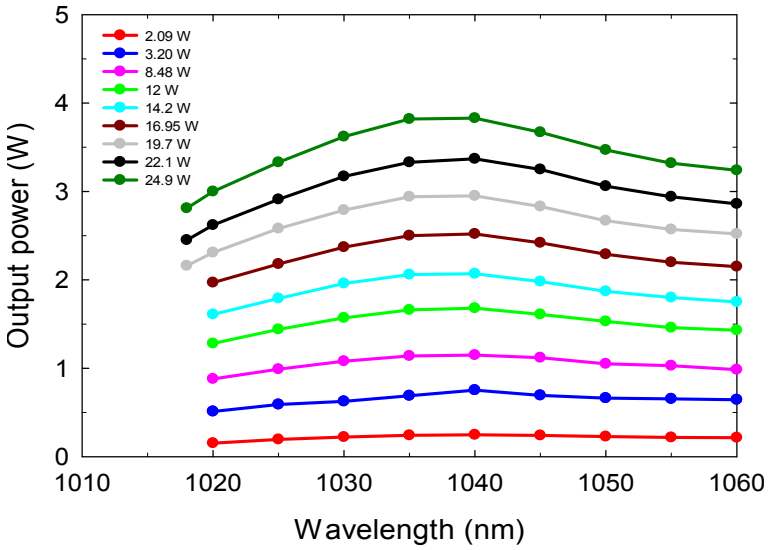

Figure 3.6 Output power *vs* wavelength at various pump powers.

The tuning range from 1020 nm to 1060 nm covers the wavelengths that are expected to be best for tandem pumping, including 1020 nm and 1030 nm which have been used in the past [1, 2]. Figure 3.7 shows laser spectra for the different filter wavelengths at an output power of around 2 W, measured using an OSA (ANDO AQ6317B) with a resolution bandwidth of 2 nm. The spectra are clean and free from ASE.

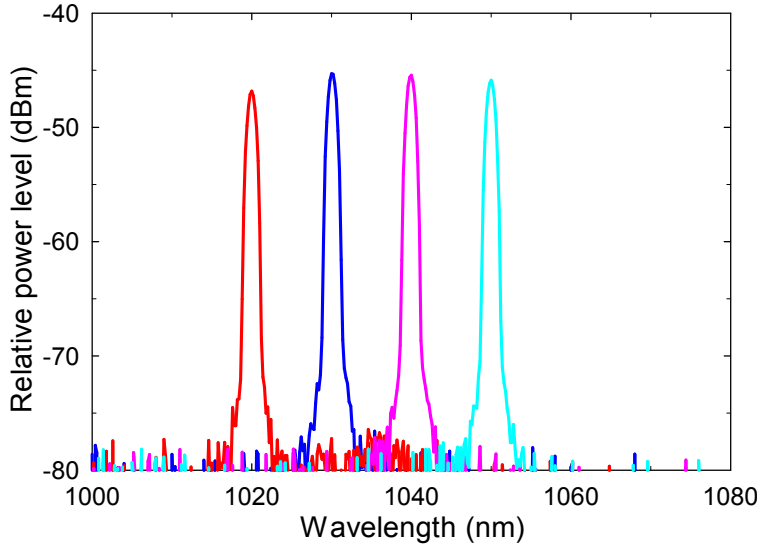

Figure 3.7 Spectra of the tuneable YDFL for different filtering wavelengths.

3.2.2 CW tuneable seed laser source

As shown in Figure 3.8, a setup similar to that of the pump (Figure 3.5) was constructed as the seed source for tandem pumped YDFAs. It uses a 10 m long Yb-doped GT-wave fibre with a phosphosilicate core of 25 μm diameter with NA of 0.22, twisted with a pure silica dummy fibre. The GT-wave fibre is coated with a low refractive index polymer that provides a pump dummy fibre NA of 0.48. In this case the fibre has a small-signal inner-cladding absorption of ~ 2.5 dB/m at the pump wavelength of 975 nm. The pump-LD (Apollo) provides up to 10 W of output power. The laser output was taken from the 70% port of the output coupler (AFW). An isolator (Shinkosha) was installed to ensure uni-directional signal propagation. All passive fibres were HI-l060.

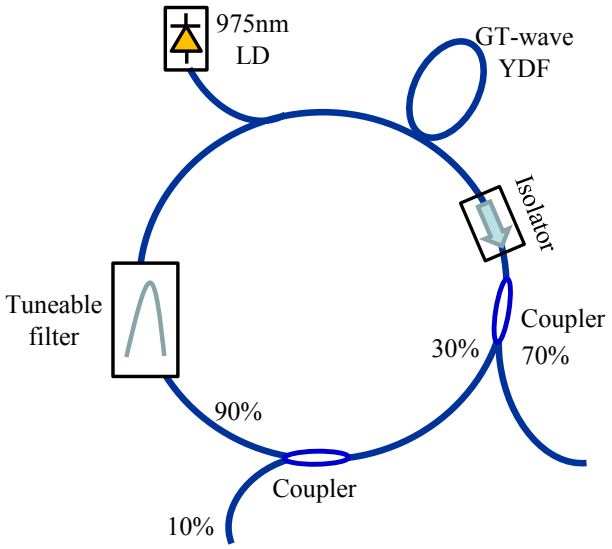

Figure 3.8 Experiment configuration of the seed source.

The laser could be tuned from 1040 to 1098 nm, as shown in Figure 3.9. At 1070 nm, I reached a peak output power of 600 mW. At shorter wavelengths such as 1050 nm and 1060 nm, the output power became about 450 mW and 500 mW respectively.

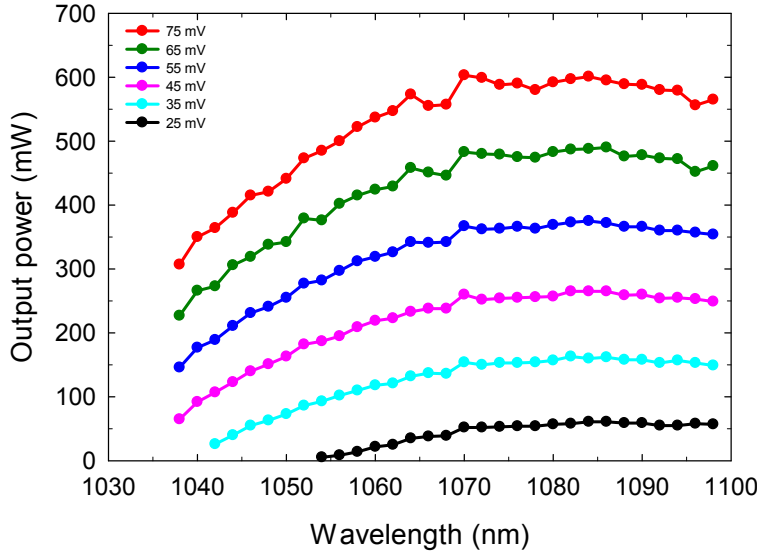

(a)

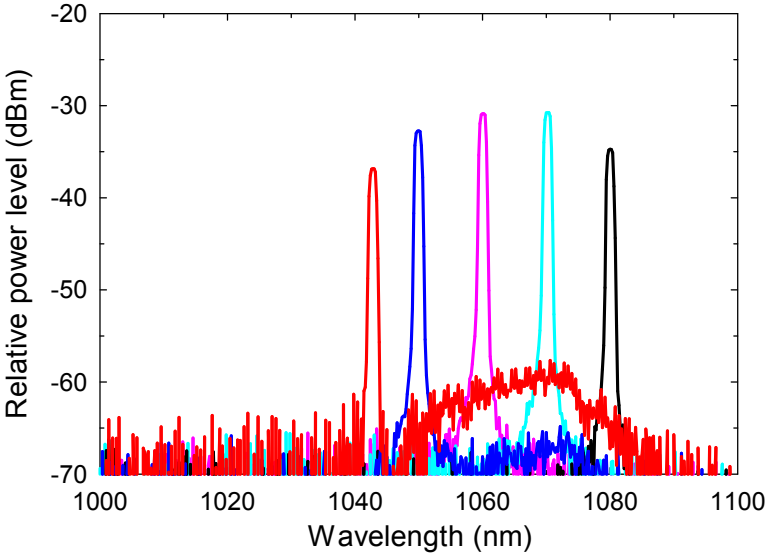

(b)

Figure 3.9 (a) seed output power *vs* wavelength for different pump powers as designated by a calibration voltage; (b) output spectra at different lasing wavelengths.

Short-wavelength tuning was limited to 1040 nm by the reduction in the Yb gain at shorter wavelengths [3, 4]. For shorter tuning wavelengths, the Yb excitation level required for lasing is so high that the gain at the gain peak becomes excessive, to the point where ASE at the gain peak starts to dominate the emission and the laser becomes unstable and prone to self-pulsing. This can damage the laser. Figure 3.9 (b) shows that already at 1040 nm the ASE build-up is quite significant. Furthermore, as the input seed for tandem pumping, the unwanted ASE could reach significant power by subsequent amplification, which would distort the measurements. Thus, in practice, 1050 nm was

the shortest seed wavelength. Furthermore, the upper tuning limit of 1098 nm was set by the tuning range of the filter. Otherwise, as for short-wavelength tuning, a low gain relative to the peak gain would ultimately limit the long-wavelength tuning if the filter tuning limit were removed. In any case, the laser tuning range with clean spectra of 50 nm is sufficient for tandem-pumping, and tuning beyond 1098 nm is not needed.

3.2.3 Fibre characteristics

Here I list four YDFs achieving low QD and high efficiency in experiments. As shown in Figure 3.10, the refractive index profiles (RIPs) of the fibre core are well matched with the HI-1060 fibre (6.5 μm core diameter and 0.14 NA) such that the pump power and brightness can be maintained. All the investigated YDFs are fabricated in-house by Prof. J. K. Sahu. Their structures are double-clad formed by the low refractive index polymer coating, with approximately single-mode core, 120 μm inner-cladding and about 250 μm fibre diameters. The RIPs of A0276-L10186 and T0285-L30184 also show the waveguiding raised-index pedestal surrounding the core but since the pump and signals are launched (mostly) into the core the influence of the pedestal is small. Finally, the background loss must be kept low. Our fibres had background loss of about 200 dB/km at 1280 nm.

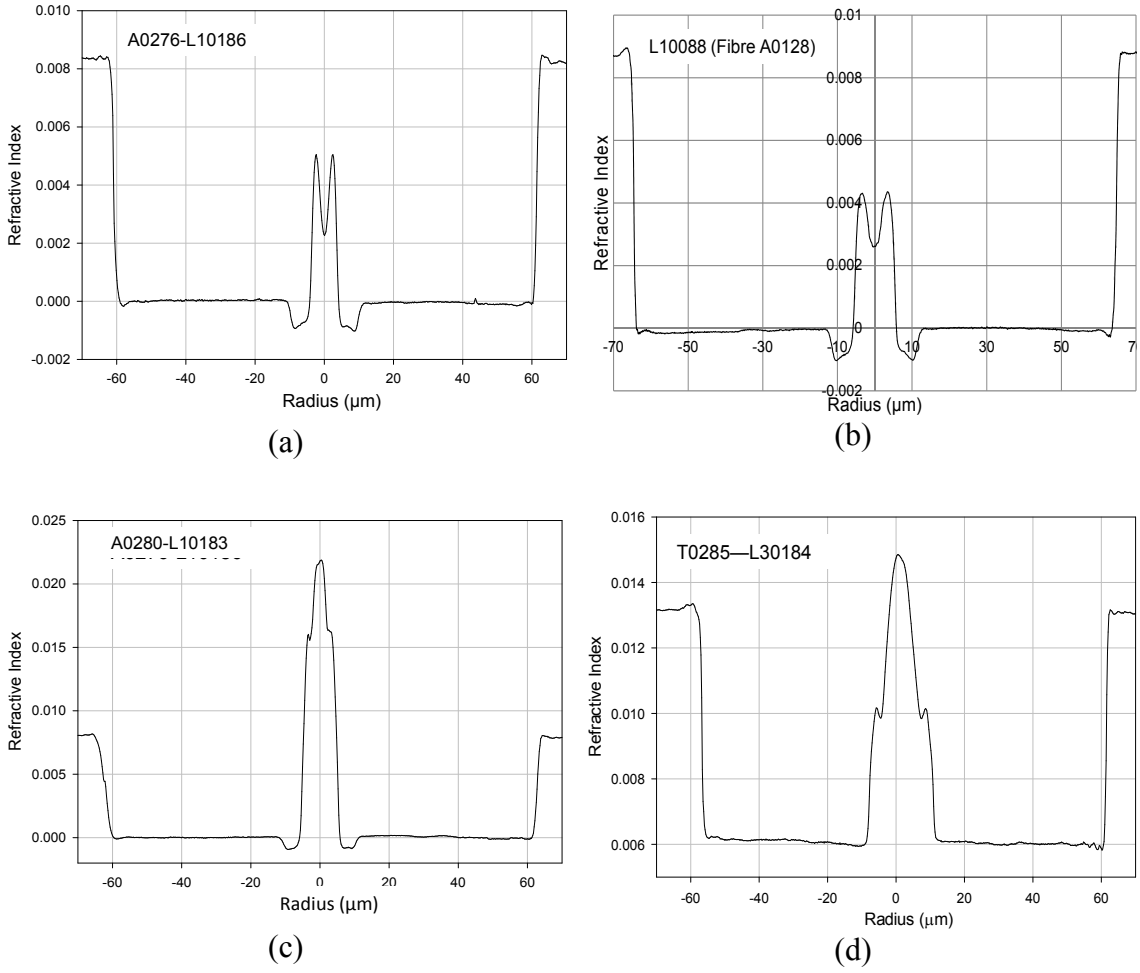

Figure 3.10 Measured RIPs of the YDFs tested in the tandem pumped YDFAs.

The concentration and absorption, as well as other characteristics of the YDFs investigated by the tandem pumped YDFA in this chapter, are given in Table 3.1. The Yb concentrations of those YDFs under test need to be high enough to efficiently absorb the pump power at the longer wavelength with relatively small absorption cross section. To determine the concentration of Yb ions in the fibres used, cutback measurements of the absorption spectra were performed using a white light source (WLS) with low incident power. Note here I used the value of absorption cross section of Yb in pure Al host to calculate all the fibres, including those with Al and P co-dopant. This under-estimates the concentration of those YDFs.

Table 3.1 List of fibres under test in the low QD YDFA

Fibre designation	Core Diameter (μm)	YDF core absorption (dB/m)	Estimated Yb Concentration (m^{-3})	Fibre length (m)	Composition
A0276-L10186	**7**	207@915nm 861@975nm	0.8×10^{26}	4	Al/P/Yb
A0128-L10088	~13	274@915nm	1.0×10^{26}	2.4	Al/P/Yb
A0280-L10183	~5	470@927nm	$>2.3 \times 10^{26}$	0.6	Al/P/Yb (note: may be fluorine)
T0285-L30184	10	2334@975nm	2.6×10^{26}	1.5	Al/Yb

3.2.4 Tandem pumped YDFA

For experimental investigations of the achievable QD we used a simple YDF amplifier configuration, in which a piece of YDF is core-pumped by the pump-YDFL (tuneable from ~1020 nm to 1060 nm) nm and seeded by seed-YDFL (tuneable from 1040 nm to 1098 nm). The pump and seed waves were combined in a 1020/1060 nm WDM and then launched together into a 1% tap coupler for monitoring, and finally, via the 99% port into the core of YDF. See Figure 3.11. To avoid unwanted back-reflections, a fibre end cap with cleaved at an angle of 7 degrees was splices to the end of the YDF under test. Measurement of splicing losses at two ends of YDFs was carried out indicating those losses were negligible.

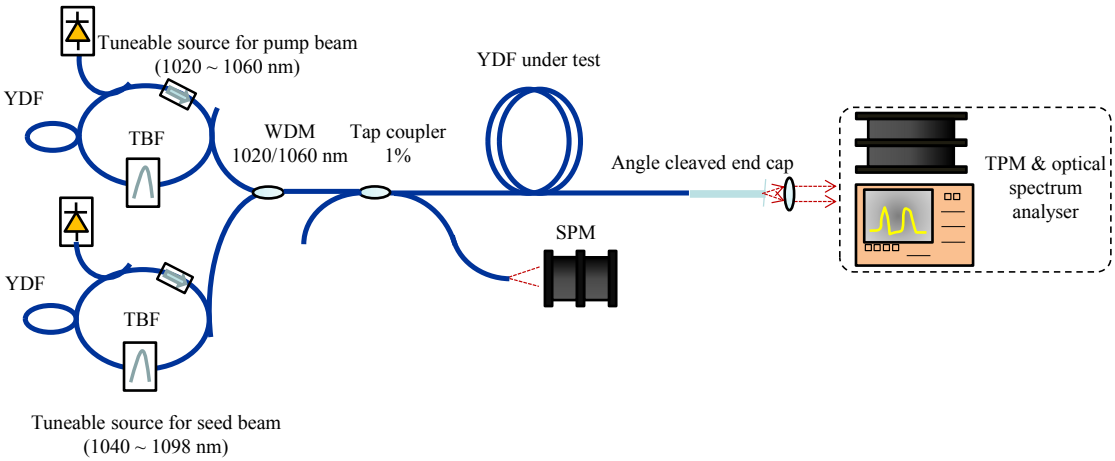

Figure 3.11 Experimental setup of the tandem-pumped YDFA.

As for the output power measurement, it is difficult to rely on a dichroic mirror (DM) to separate the amplified signal beam and the leaked pump beam due to the small wavelength difference. Instead, the fraction of the signal and pump power was calculated from the measured output spectrum.

For the tandem-pumped YDFA, the conversion efficiency and the slope efficiency with respect to absorbed pump power should be measured to demonstrate low QD operation with low heat generation. This calls for high measurement accuracy. However even though the setup has been designed with this in mind, I estimate the uncertainty to 5%, which is significant. More careful measurements are needed in order to confirm slope efficiencies in excess of 90%.

3.2.5 Laser characteristics

I have discussed and emphasised the importance of sufficient pump absorption and signal gain in conjunction with low QD operation. According to the theoretical analysis, a fibre of appropriate length will be able to reach adequate pump absorption without compromising the QD significantly. The length depends on the pump wavelength. To reach the minimum QD, I have investigated different YDFs with various Yb ions concentrations, compositions and fibre lengths, as mentioned above. Various seed wavelengths from 1050 nm to 1070 nm have also been investigated. Here I only present the results at 1050 nm, the shortest seed wavelength with lowest QD.

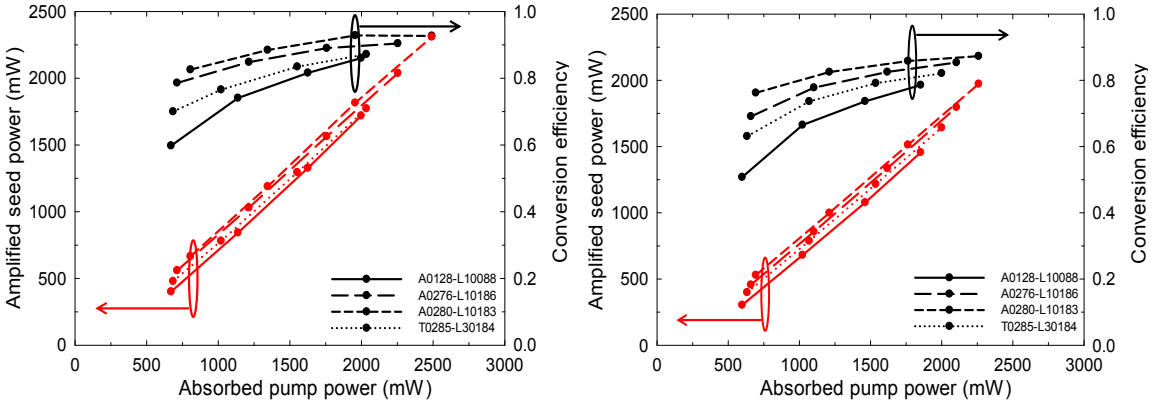

Figure 3.12 Output power (red curves) of YDFA tandem-pumped (a) at 1030 nm and (b) at 1020 nm, seeded at 1050 nm. Left axis shows the conversion efficiency (black curves).

By investigating different pairs of pump and seed wavelengths, the longest pump wavelength, 1030 nm, was found to work best and allowed for efficient amplification by 8 – 10 dB at seed wavelengths down to 1050 nm (Figure 3.12). The QD is then as low as 2%. Furthermore the obtained pump leakage was less than 10%, corresponding to over ~10 dB absorption. Slope efficiencies between 95% and 96% were recorded with these wavelengths, with respect to absorbed pump power. These are very high efficiencies, and no similar values have been reported in the literature. The maximum conversion efficiencies at the highest pump power reached over 87% for all the YDFs.

Although the pump wavelength is less important according to the theoretical analysis (as long as pump absorption is sufficient), the slope efficiencies with 1020-nm pumping dropped to around 91% to 92%, while the peak conversion efficiencies

varying from 79% to 87%. Except of the larger QD of ~ 3%, the pump power was slightly lower at 1020 nm. However the pump absorption increased to 12 dB or more. A slightly shorter fibre of with ~ 10 dB pump absorption may regain the QD and efficiency of 1030-nm pumping. Generally, this and the ability to operate efficiently at 1030 nm pump wavelength suggesting the fibres are over the optimum length in the case of 1020 nm pumping. Then a higher ASE can be expected which would lead to the reduction of efficiency. Thus a better performance can be expected with shorter pieces of fibres when pumped at 1020 nm. Figure 3.13 shows the output spectra of A0280-L10183 at highest pump power.

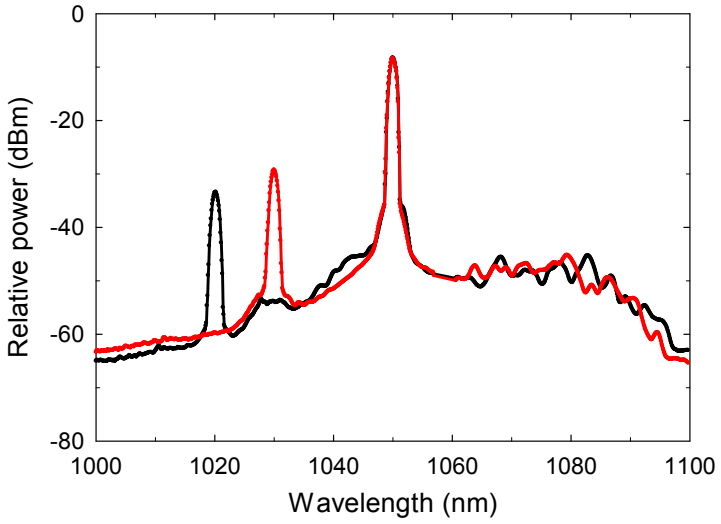

Figure 3.13 Output spectra of tandem pumped YDFA pumped at 1030 nm (red line) and 1020 nm (black line), seeded at 1050 nm for A0280-L10183.

The output power and conversion efficiency depend on the fibres as well, when other conditions are the same. Among the four tested YDFs, the best results were achieved with A0280-L10183, which has the highest concentration and shortest fibre length. A conversion efficiency of 93% was obtained.

A QD of 2% in principle allows for an ultralow thermal load. However, there are also other potential sources of heating, e.g., resulting from impurities or PD. Given the uncertainty in the slope efficiency measurement, the total heat load may well be closer to 10% than 2%. More precise optical measurements, or direct calorimetric measurements at higher power level, are needed to determine the thermal load at the percent level.

In the other aspect, the ratio of total output and input power including both pump and seed is much easier to be measured precisely. Those quantities are shown in Figure 3.14.

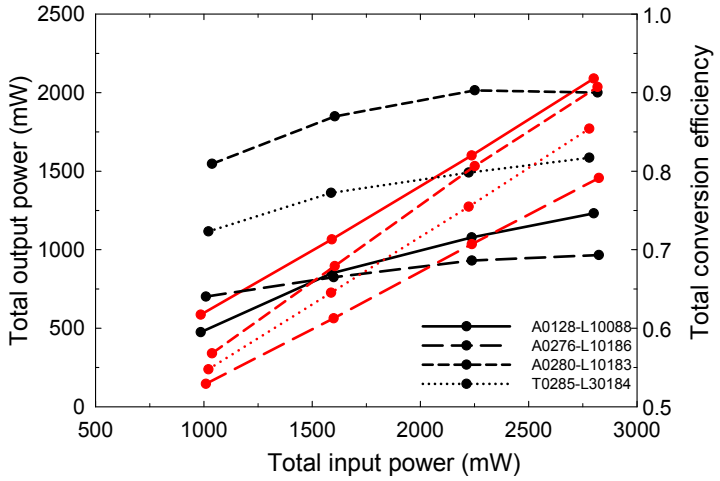

(a)

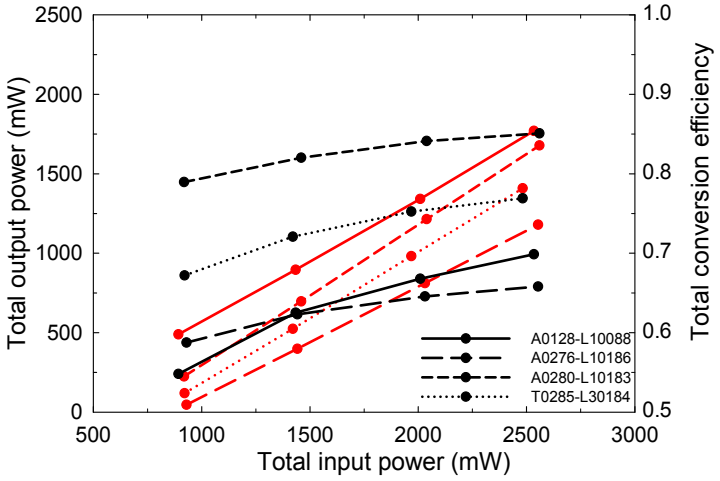

(b)

Figure 3.14 Total output power (red lines, left axis) and total conversion efficiency (black lines, right axis) *vs* total input power of YDFA pumped at (a) 1030 nm and (b) 1020 nm, both seeded at 1050 nm for different YDFs.

3.3 Photodarkening

High-power YDFLs benefit from high Yb-concentrations. However, accompanied with the continuous increase in output power, this can lead to a permanent optical excess loss with low-energy absorption tail that reaches the 0.9 - 1.1μm operation band. This is called photodarkening. The excess loss, which increases with the excitation level and

depends on the composition, can build up over minute-scale times but also slowly over hours or even years. Studies on PD suppression have focused on evaluating the kinetics involved in the PD, such as the inversion level, colour centre and chemical configuration [5, 6]. For example, Al and especially P co-doping is known to reduce PD, and is commonly used in Yb-doped fibres.

Tandem pumping of YDFL sources by longer pump wavelength represents another possible solution to reducing the PD, thanks to the lower Yb inversion level. In this section, I will mainly present the experimental investigation of PD in YDFs of different compositions (mainly Al and P codopant). The combination of Al and P in equal concentration in the host material was proved to give the optimised amplification in Yb doped fibre laser sources, while compromising the coordination of Yb ions, refractive index adjustment and PD suppression [7, 8].

Here I will present an investigation of PD-induced excess loss in our tandem pumped YDFAs. I only present the experimental results with the 1030 nm pump and 1050 nm seed wavelengths. Further study on PD should also include the other pump wavelength, such as 9xx nm, for comparison.

3.3.1 Measurement setup

Measurement of PD, in most cases, relies on monitoring the transmitted power of a probe beam located far away from the Yb absorption band during pump irradiation [5]. The loss in the Yb band can be scaled from the loss at the probe wavelength owing to the similar spectral shape of the induced loss in a wide range of YDFs.

I used a 650 nm fibre-coupled single-mode LD coupled to the input of the YDFA through a WDM coupler and existing 1% tap coupler as a probe. The probe beam propagated in the same direction as the pump and signal beams. A pair of DMs was placed after the test YDF output end to isolate the probe beam. The probe beam was modulated by an arbitrary function generator (AFG 3252) and the output power of the probe beam was detected by photodiode (PDA100A) and lock-in amplifier after passing through the DMs. See Figure 3.15.

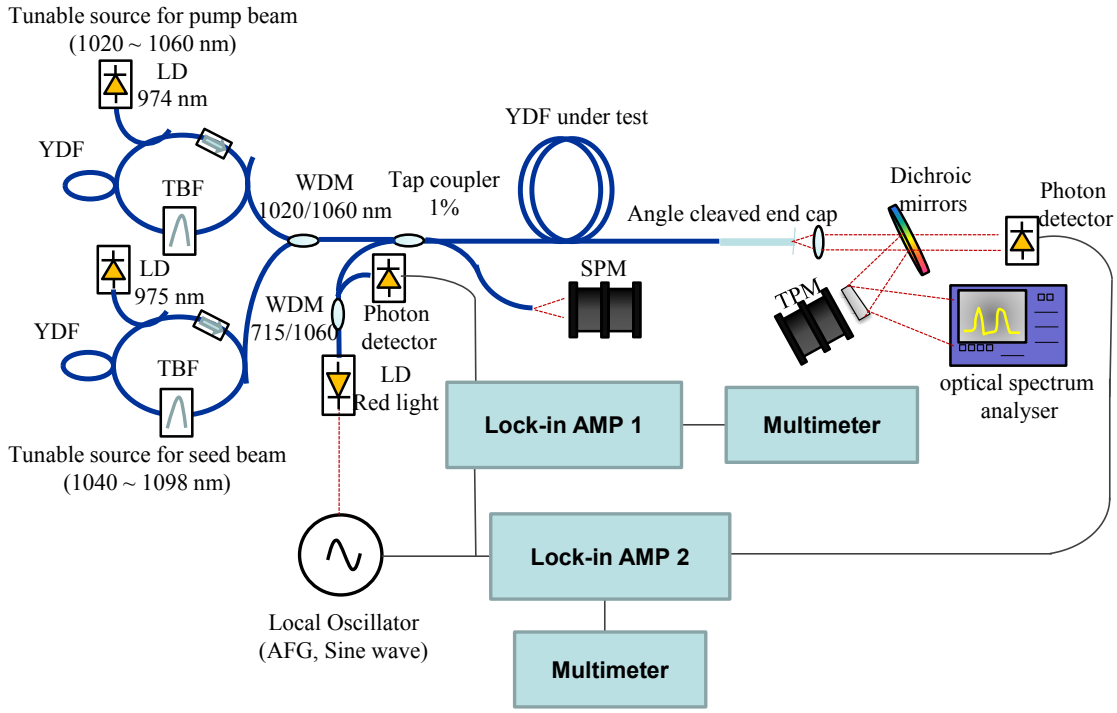

Figure 3.15 Experimental configuration for evaluating the PD-induced loss in tandem-pumped YDFA.

PD-induced loss was measured while the amplifier was running with constant pump and signal power. I used input pump at 1030 nm and seed power at 1050 nm at about half of the maximum output which was about 1.7 W and 250 mW, respectively. This input power level is enough for signal gain with 2% QD and low thermal load.

3.3.2 Result and discussion

The temporal characteristics of the transmitted probe power are presented in Figure 3.16. The degradation lines of four fibres were obtained before reaching a new equilibrium state after approximately 3 hours. The results are qualitatively similar to those reported with 9xx nm pumping. Firstly, lower Yb concentration and longer fibre length reduced the PD-induced loss due to lower density of excited Yb-ions. In addition, pure Al composition allow for low excess loss when the concentration is high. While we could be encouraged to use pure Al composition with high concentration, Al/P co-dopant shows potential advantage on lower refractive index which is significant for LMA fibre.

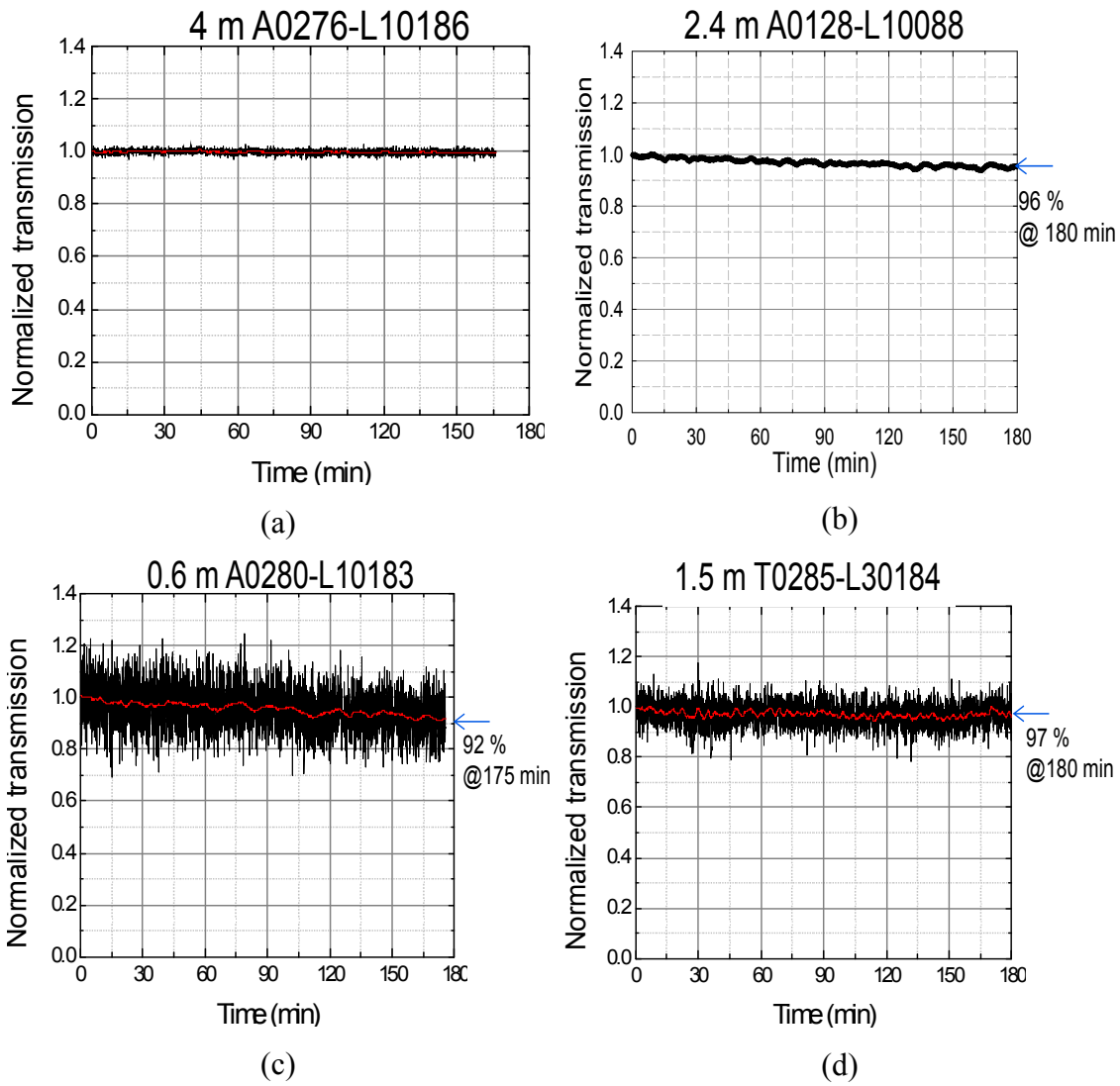

Figure 3.16 Temporal evolution of the PD loss at 650 nm in the tandem pumped YDFA with different YDFs.

Figure 3.17 shows the result of the PD measurement of YDF A0128-L10088 after reaching its final equilibrium state, together with the laser slope efficiency after long-term testing. The temporal degradation of the PD loss at 650 nm during tandem-pumping at 1030 nm pump and 1050 signal wavelength can be fitted by stretched exponentials [9]. Although a decay was observed, the influence of the PD was shown to not influence low-QD operation very much. Comparisons to 9xx-nm pumping would be useful to clarify the significance of these results.

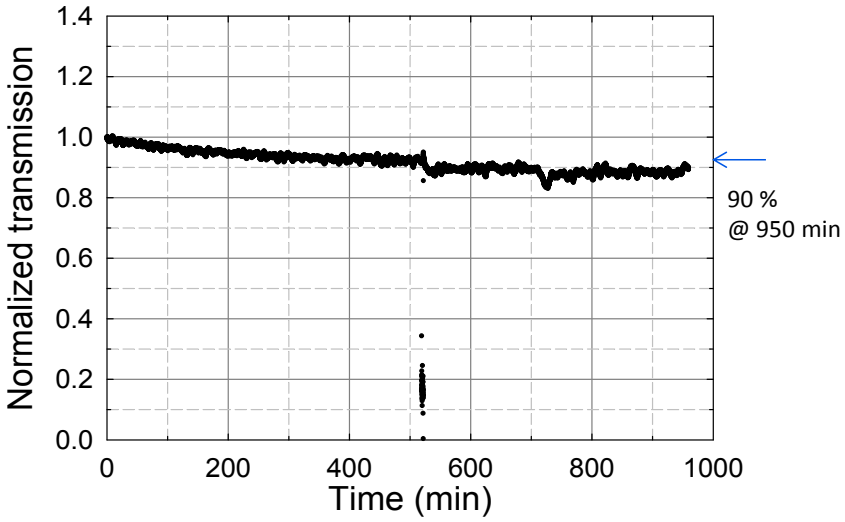

Figure 3.17 Temporal evolution of the PD loss at 650 nm in the tandem pumped YDFA

3.4 Other limitations on low quantum defect

The thermal issues that a low QD can mitigate occur primarily at high powers, so a low QD is particularly relevant in that regime. As mentioned in Chapter 2, inhomogeneities such as spectral hole-burning [10, 11] are more likely to occur at high power-densities, and can then reduce the pump absorption and the gain at high power densities. This would increase the QD required for a specific combination of signal gain and pump absorption.

Furthermore nonlinear gain, due, e.g., to SRS, can add to the gain at high power and thus necessitate the use of peak Yb-gain lower than 30 dB. The Raman gain increases with the wavelength separation to the pump until it peaks around 50 nm away from the Raman pump wave for signal wavelengths in the 1 - 1.1 μm range in silica fibres. Note here that both our Yb pump and signal act as Raman pumps. On the other hand SRS helps to transfer power from our primary Yb-pump to the signal, which is beneficial. However a preliminary analysis suggests that when SRS is important, the attainable QD will be larger.

Furthermore the temperature rise occurring at high power changes the absorption and emission cross-section spectra, conceivably so that the attainable QD increases [12]. However, while our analysis uses cross-sections at 10°C, preliminary calculations

indicate that a similarly low QD is possible also at uniformly elevated core temperatures, and the results are near-identical at room temperature. Still, it is possible that the QD increases if the temperature varies along the fibre (variations across the core are negligible). Thus, although preliminary, non-optimised, experiments do show QD of 2%, these were obtained at low power levels. At higher powers, the attainable QD may well be larger.

On the other hand we expect that both the use of spectral filters to reduce the gain at the peak and narrower transition linewidths, as are possible in crystals, can allow for lower QD. While thermodynamics also sets a lower limit on the heat generation in an optically pumped laser, the reduction in entropy of the output beam relative to that of the pump beam allows for a heat generation that is several orders of magnitude lower than 1% [13]. This can be neglected.

The added complexity and relative immaturity of tandem-pumping (especially with high pump brightness) are practical drawbacks of our approach, and any use of filters and non-standard host materials would present additional challenges. The laser threshold is another issue to consider. For this to be low, the total number of excited ions at threshold should be low. For a given fibre, this is determined by the excited fraction of ions that is required. The threshold in terms of absorbed pump photons per unit time is equal to the total decay rate (e.g., from spontaneous emission) of all excited ions at threshold, and is therefore independent of the pumping approach. On the other hand, operating off the gain peak will increase the required number of excited ions, so this does increase the threshold. However the threshold of a high-power fibre laser is generally negligible. ASE may be a bigger source of power loss. This can also increase the threshold, especially in case of MM core-pumping due to the increased number of modes with high overlap with the gain medium. ASE can build up in each of these modes. However the power lost to ASE can still be low at 30 dB peak gain.

Finally, it is interesting to consider the possibility of fluorescence-cooling and radiation-balanced lasers [14]. This has primarily been considered in “bulk” (i.e., non-waveguiding, lasers. While the spontaneous emission from the excited gain medium adds to the thermal load in most lasers due to the QD, the opposite occurs when the pump wavelength is longer than the average fluorescence wavelength. This is around 990 nm in Yb:aluminosilicate. The QD is then negative. This fluorescence-cooling

increases for longer pump wavelengths, as the energy difference to the average fluorescence photon increases. However, the lower absorption cross-sections at longer wavelengths lead to requirements on the concentration - length product that are difficult to achieve in bulk lasers. Still, improved results with a 120 mm long Yb-doped YAG crystal pumped at 1030 nm have been reported recently [15, 16].

By contrast, the concentration - length product can be much larger in fibres, and may allow for pumping up to, say, 1050 nm. Combined with a QD of 1%, this means that one fluorescence-photon used for cooling can compensate for approximately six signal photons. However, the beam confinement in a typical fibre leads to a high gain efficiency and a laser threshold of only a few watts, which in this context is a disadvantage for power-scaling. Although the threshold power is all lost to fluorescence in the absence of excess loss mechanisms, the heat carried away by the fluorescence is only a few percent of this, so much less than 1 W. Therefore, fluorescence-cooling will not be a significant effect in a conventional high-power fibre laser operating high above threshold, but can be in fibres with very large core areas, e.g., in leakage channel fibres, large pitch fibres, and multi-trench fibres or fibres using a ‘Y’-bridge cladding [17 - 20].

3.5 Summary

This chapter has described how pumping of YDFs with high beam quality allows for a reduction of the QD down to the percent level. This theoretical result, which relies on core-pumping and amplification on the short-wavelength side of the gain peak, is a substantial reduction from the 10% level typical for directly diode-pumped high-power YDFLs. Experimentally I reached a QD of 2% with 1030 nm pump wavelength when seeded at 1050 nm. PD measurement under the YDFA has been performed, which still requires further investigation. Fortuitously, the pump wavelength of around 1030 nm is reachable with high-power YDFLs, which suggests that tandem-pumping is a viable architecture for this regime of operation. High-brightness cladding pumping would be even more attractive for power scaling and heat measurement, and can perhaps become possible in the long term.

3.6 References

1 Bill Shiner, “High power fiber laser technology,” presentation on Annual Department of Energy Laser Safety Officer (DOE LSO) Workshop, September 10, (2013).

2 C. Wirth, O. Schmidt, A. Kliner, T. Schreiber, R. Eberhardt, and A. Tünnermann, “High-power tandem pumped fiber amplifier with an output power of 2.9 kW,” Opt. Lett., 36(16), 3061-3063, (2011).

3 O. G. Okhotnikov, L. Gomes, N. Xiang, T. Jouhti, A. B. Grudinin, “Mode-locked ytterbium fiber laser tunable in the 980-1070-nm spectral range,” Opt. Lett., 28(17), 1522-1524, (2003).

4 D. Y. Shen, J. K. Sahu, and W. A. Clarkson, “Highly efficient Er, Yb-doped fiber laser with 188 W free-running and >100 W tunable output power,” Opt. Express, 13(13), 4916-4921, (2005).

5 S. Yoo, A. J. Boyland, R. J. Standish, and J. K. Sahu, “Measurement of photodarkening in Yb-doped aluminosilicate fibres at elevated temperature,” Electron. Lett. 46(3), 233-244 (2010).

6 K. E. Mattsson, “The three-electron bond =Si<O2:·Yb absorption center of pre-darkened ytterbium-doped silica,” Opt. Express, 21(10), 12849-12864, (2013).

7 S. Unger, A. Schwuchow, S. Jetschke, V. Reichel, M. Leich, A. Scheffel, and J. Kirchhof, “Influence of aluminum-phosphorus codoping on optical properties of ytterbium-doped laser fibers,” Proc. SPIE7212, 72121B1 (2009).

8 J. Kirchhof, S. Unger, S. Jetschke, A. Schwuchow, M. Leich, and V. Reichel, “Yb-doped silica-based laser fibers: correlation of photodarkening kinetics and related optical properties with the glass composition,” Proc. SPIE7195, 71950S, (2009).

9 S. Jetschke, S. Unger, A. Schwuchow, M. Leich, J. Kirchhof, “Efficient Yb laser fibers with low photodarkening by optimization of the core composition,” Opt. Express 16, 15540-15545 (2008).

10 H. M. Pask, R. J. Carman, D. C. Hanna, A. C. Tropper, C. J. Mackechnie, P. R. Barber and J. M. Dawes, "Ytterbium-doped silica fiber lasers: Versatile sources for the 1–1.2 μm region," IEEE J. Sel. Topics in Quantum Electron., 1(1), 2-13, (1995).

11 R. Paschotta, J. Nilsson, A. C. Tropper, and D. C. Hanna, "Ytterbium-doped fiber amplifiers," IEEE J. Quantum Electron., 33(7), 1049-1056, (1997).

12 L. A. Vazquez-Zuniga, S. Chung, and Y. Jeong, "Temperature dependence of a high-power ytterbium-doped fiber amplifier operating at 1060 nm and 1080 nm," in Proc. of OECC, Hongkong, China, 2009.

13 Th. Graf, J. E. Balmer, H. P. Weber, "Entropy balance of optically pumped cw lasers," Opt. Commun., 148 (4-6), 256-260, (1998).

14 Steven R. Bowman, "Lasers without internal heat generation," IEEE J. Quantum Electron., 35(1), 115-122, (1999).

15 Steven R. Bowman, Shawn P. O'Connor, Subrat Biswal, Nicholas J. Condon, and Armand Rosenberg, "Minimizing heat generation in solid-state lasers," IEEE J. Quantum Electron., 46(7), 1076-1085, (2010).

16 S. R. Bowman, S. O'Connor, S. Biswal and N. J. Condon, "Demonstration and analysis of a high power radiation balanced laser," in Proc. of CLEO, CMH4, Baltimore, US, 2011.

17 K. Saitoh, Y. Tsuchida, L. Rosa, M. Koshiba, F. Poli, A. Cucinotta, S. Selleri, M. Pal, M. Paul, D. Ghosh and S. Bhadra, "Design of all-solid leakage channel fibers with large mode area and low bending loss," Opt. Express, 17(6), 4913-4919, (2009).

18 F. Stutzki, F. Jansen, T. Eidam, A. Steinmetz, C. Jauregui, J. Limpert and A. Tünnermann, "High average power large-pitch fiber amplifier with robust single-mode operation," Opt. Lett., 36(5), 689 -691, (2011).

19 D. Jain, C. Baskiotis, and J. K. Sahu, "Mode area scaling with multi-trench rod-type fibers," Opt. Express, 21(2), 1448-1455, (2013).

20 A. Docherty, L. Poladian, A. Argyros, M. C. J. Large, J. Poulin and R. Kashyap, “Increasing the numerical aperture of large-core microstructured polymer optical fibers using a ‘Y’-bridge cladding,” J. Lightwave Technol., 27(11), 1610-1616, (2009).

Chapter 4: Pulsed laser diodes directly pumped fibre Raman lasers

This chapter describes stimulated Raman scattering in a multi-mode fibre which is then applied to the particular case of diodes direct pumping. Section 4.1 introduces and reviews the potential of direct MM-diode-pumping of FRLs for low QD. Section 4.2 presents the characteristics of the HNLF with high Ge concentration applied as the Raman fibre used in the experimental study presented in this chapter. Then, section 4.3 presents the experimental realisation and study of co-directionally diode pumped fibre Raman laser explicitly targeted a high efficiency. Subsequently, the properties of these lasers are discussed in section 4.4. Section 4.5 presents possible improvements to increase the output power and enhance the laser efficiency. Finally, section 4.6 summarises the findings of this chapter.

4.1 Introduction

For the RE-doped fibres, lasers and amplifiers are based on emission in fixed spectral bands and require that the pump wavelength falls in an absorption band. In those cases, the minimisation of the QD discussed in Chapter 3 focuses on high-brightness pumping at long pump wavelengths.. However, some applications call for higher photon energy than what is available from high-power RE-doped fibres. Then, diode pumped FRLs possess the potential for both short wavelength (comparable to the pump wavelength) and low QD [1]. The nature of Raman gain eliminates the need for an intermediate conversion stage for low QD, and furthermore benefits from the short wavelengths available from pump diodes. Other unique properties of Raman fibre that can overcome limitations of RE-doped fibres have already been introduced in Chapter 1.

Until now, despite those attractions, diode-pumped FRLs have been held back by the high pump densities and low fibre propagation losses that are needed to reach laser threshold, since SRS is a weak process. For a long time, diode pumping has been restricted to single-mode devices operating at around 1.5 μm [2]. These benefit from the high brightness of single-mode laser diodes and low fibre loss. However shorter wavelengths allow for lower QD. In addition, the power of single-mode diode is limited to the watt-level or less, and MM diodes at 1.4 – 1.5 μm lack in brightness and are much

lower in power than what is possible at shorter wavelengths. By contrast, the advanced high power semiconductor diodes around 800 nm can maintain a good beam qualityand look attractive for direct diode-pumping of FRLs [3]. With a pump wavelength at 806 nm, the first Stokes is as close as at 835 nm [4] for a QD of only 3.5%. All in all, the availability of high-brightness commercial diodes at short wavelengths makes it possible to achieve low-QD SRS. In the pulsed regime with 50-100 ns duration and 200-300 kHz frequency, commercially available MM LD can reach as high as 30 W peak power with high brightness.

In this chapter, a HNLF was utilised in the experiments. The high Raman gain coefficient and small area enhance the SRS process. However, the relatively high fibre loss at short wavelengths means that the required pump brightness could only be reached in pulsed mode, which restricts the average power. Generally, a long piece of fibre leads to a low pump threshold, while the relatively high propagation loss limits the conversion efficiency. Special attention is paid to the polarisation dependent Raman gain. By controlling the polarisation state at the launch of the pump and signal feedback in the ring cavity, higher Raman gain can be expected in the beginning of the HNLF.

4.2 Characteristics of the highly nonlinear fibre

4.2.1 RIP of the highly nonlinear fibre

The HNLF, fabricated by Sumitomo Electric Industries, Ltd (Part number: HNRAC-2), has enhanced nonlinearity with a heavily Ge-doped small core. A careful investigation of the fibre properties is needed to understand how it works as a Raman fibre converter with direct diode-pumping. Next I will describe the details of this fibre.

The approximated RIP of this fibre is shown in Figure 4.1. This SI fibre comprises a pure-silica cladding and germanium-doped silica core. They are circularly shaped and concentric. The effective core diameter of the HNLF is 3.6 μm, the corresponding core area about 10 μm^2, and the NA 0.34. Thus, the V-value becomes 5.1 at the signal wavelength and the fibre supports around nine modes at the pump and signal wavelengths, disregarding polarisation multiplicity.

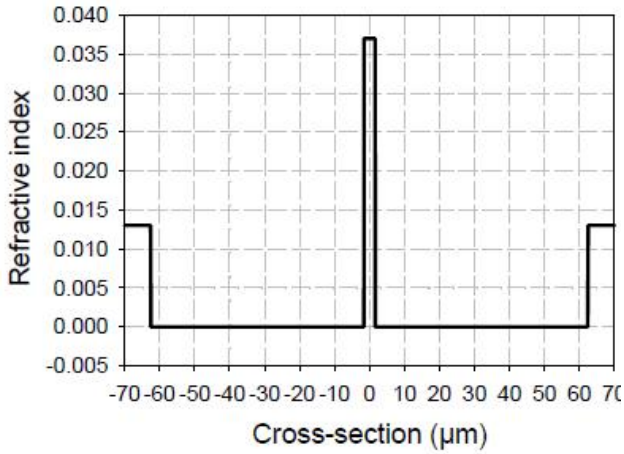

Figure 4.1 Approximate refractive index profile of the HNFL.

4.2.2 Background loss

A short piece of fibre (SMF-28), serving as a standard-fibre pigtail was spliced to the HNLF during the experiment. Splicing directly to the HNLF is difficult, and the pigtail helps to overcome this. It serves no purpose in the setup, but since the splice was factory-optimised I left it in place. While there is still some splice loss which introduces an uncertainty and reduces the performance, the effects are deemed acceptable.

The background loss of a 600 m long piece of this fibre was characterised with a conventional cutback measurement that employed a WLS that overfilled the core and an OSA (ANDO AQ6317B). The curve of the loss spectrum after averaging is shown in Figure 4.2. The background propagation loss of the HNLF are about 4.4 dB/km and 2.7 dB/km at the pump and Stokes wavelengths, respectively. The reported background loss in 30% (mol) Ge doped fibre is around 1.33 dB/km at 1550 nm [5]. The background loss measured in our fibre is very close to the reported value at that wavelength. The loss of the splice to the piece of SMF-28 is estimated to 1.3 dB, by comparing the measured total propagation loss in fibre assemblies with 944 m and 600 m long HNLF as experienced by pump light in the actual FRL setup at power below the threshold.

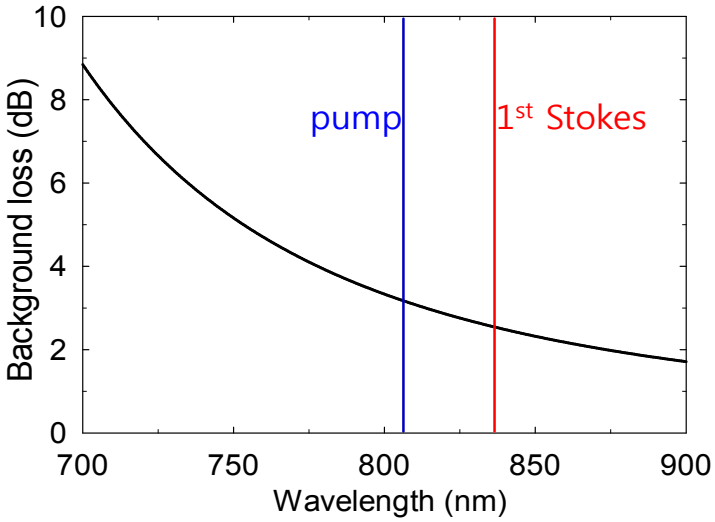

Figure 4.2 Background loss spectrum in the core of 600 m HNLF.

Two different fibre lengths were used, approximately 944 m and 600 m, chosen to provide a good balance between the requirements for high Raman gain to allow for low threshold, and low background loss to allow for high slope efficiency. The effective lengths become 598 m and 451 m, respectively.

4.2.3 Raman gain coefficient

Based on the RIP of this fibre, the HNLF has a Ge content of ~26% (mol) at the highest point. It is possible to calculate the Raman gain coefficient from the Ge dopant concentration. If the pump and signal are co-polarised, the Raman gain coefficient is estimated to 4.0×10^{-13} m/W at 806 nm [6]. For comparison, a standard single-mode fibre has a Ge-concentration of around 3% and a Raman gain coefficient of $\sim1.3\times10^{-13}$ m/W at 806 nm and of $\sim1.0\times10^{-13}$ m/W at 1060 nm for co-polarised light.

Multi-order Stokes generation resulted in HNLF longer than 1.5 km. With synchronous pumping scheme, a Raman laser cavity was formed by a perpendicularly cleaved, 4% reflecting, facet at both fibre ends. The output spectrum at the far end of the fibre is shown in Figure 4.3, which was operated at peak pump power of 30 W. In shorter fibres, e.g., 944 m and 600 m long, higher conversion efficiency of the 1st Stokes should be possible due to the reduced loss and suppression of higher-order SRS.

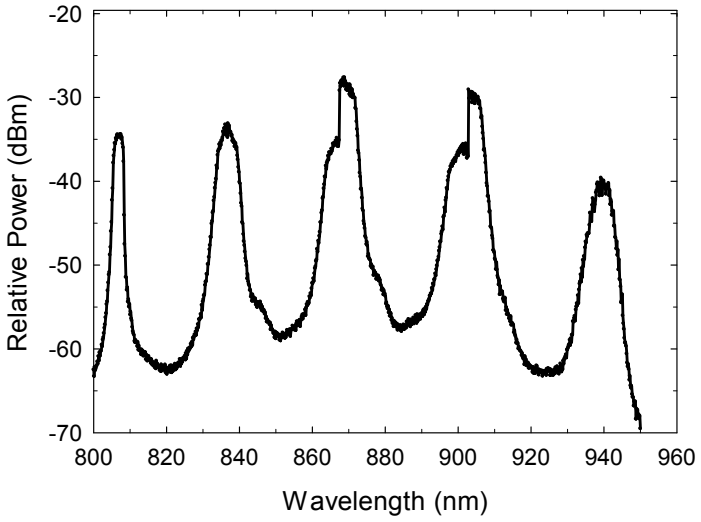

Figure 4.3 Multi order Stokes generation with 1.5 km long HNLF pulse-pumped by 30 W LD.

4.2.4 Dispersion

Dispersion can be significant over km-length fibres. If the group velocity of different modes could reach the limiting values corresponding to the refractive indices of the core and the cladding, the intermodal group velocity dispersion would reach 100 ns/km. However, measurements of the dispersion of the pump in the 944 m long fibre (with SMF-28 spliced at the output) showed broadening from 50 ns to 59 ns. From this one concludes that intermodal dispersion starts to become negligible for pulse durations above 50 ns. Intra-modal dispersion between pump and signal wavelength could also be a problem. However, material dispersion is only of the order of 1 ns/km between the pump and signal wavelengths, and the intra-modal waveguide dispersion is expected to be of a similar order or smaller. Thus, walk-off caused by the difference in wavelength between pump and signal is much smaller than the intermodal broadening, and can be disregarded.

4.3 Experiments

4.3.1 Experimental set-up

As discussed in Chapter 2, for Raman amplification with pulses, the pump and Stokes pulses must temporally coincide in the fibre to achieve the maximum energy transfer,

because the SRS gain is only available to the Stokes wave during the pump pulse. This is referred to as synchronous pumping. The gain disappears as soon as the pump pulse has passed. In comparison, in a RE-doped fibre, the pump energy is transferred to the gain medium, and the gain remains as long as the gain medium remains excited. The gain created in a Raman amplifier by a pump pulse automatically forms its own short time-gate, which negates the effects of spurious feedback and ASE build-up. There is no ASE generated between the pulses. Moreover, the SRS gain becomes biased co-directionally with the pump propagation because forward- and backward-propagating signal light have different temporal overlap with the pump. The gain is higher in the forward direction (for light temporally synchronised with the pump pulses).

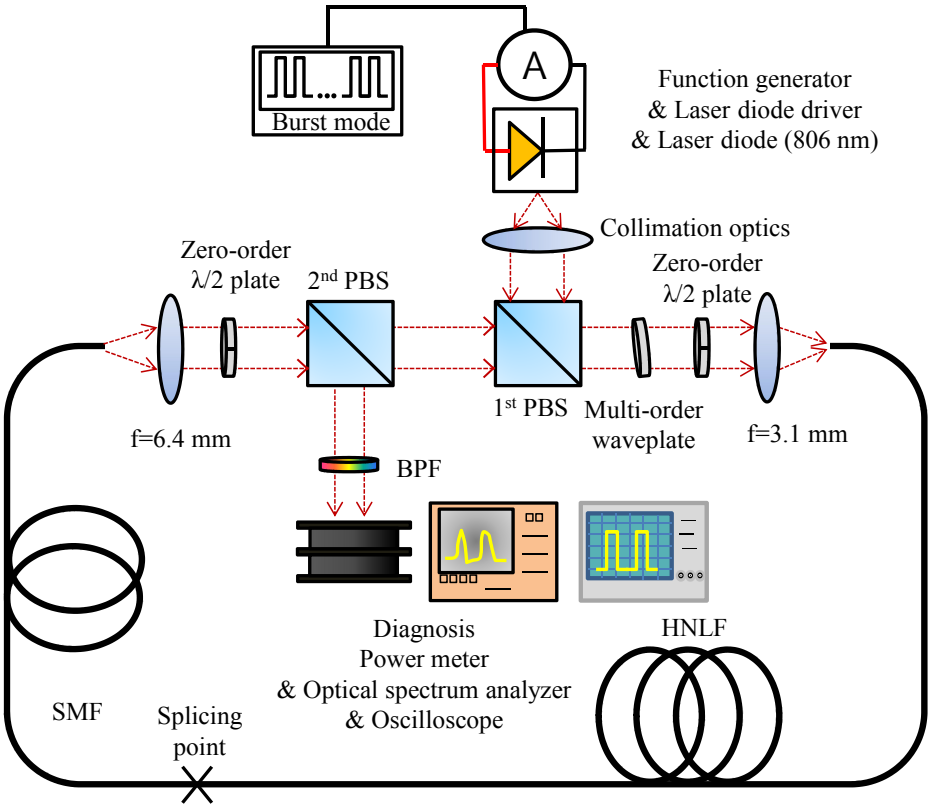

Figure 4.4 Laser cavity of diode pumped FRL with HNLF.

Based on the analysis above, the FRL is set up in a synchronously pumped ring configuration comprising a pulsed broadstripe LD pump source at 806 nm (Ferdinand Braun Institute) and the HNLF. See Figure 4.4. The pump LD has a 90 μm stripe width and is capable of producing 30 W of peak output power. It was driven by pulses of up to 30 A from a diode driver (Picolas LDP-V 50-100 V3) at the roundtrip frequency of the Stokes wave. A function generator set the pump pulse frequency. The cavity round trip

frequencies were determined to be 208.52 kHz and 322.87 kHz with our fibre lengths, and the diode driver was adjusted to match. However, the driver was unable to generate the average current required for a continuous train of pulses, so we resorted to bursts of 50 (50 ns pulse duration) and 20 pulses (100 ns durations) at a total duty cycle of 0.1% and 0.08%, respectively. Figure 4.5 shows the pump pulse shape in burst mode with 50 ns and 100 ns duration. We used an oscilloscope with bandwidths up to 500 MHz, which was sufficient for detailed characterisation of the temporal pulse shapes. The amplitudes of the pump pulses fluctuate due to the sampling of the digital oscilloscope. The pump light is predominantly linearly polarised in the vertical direction.

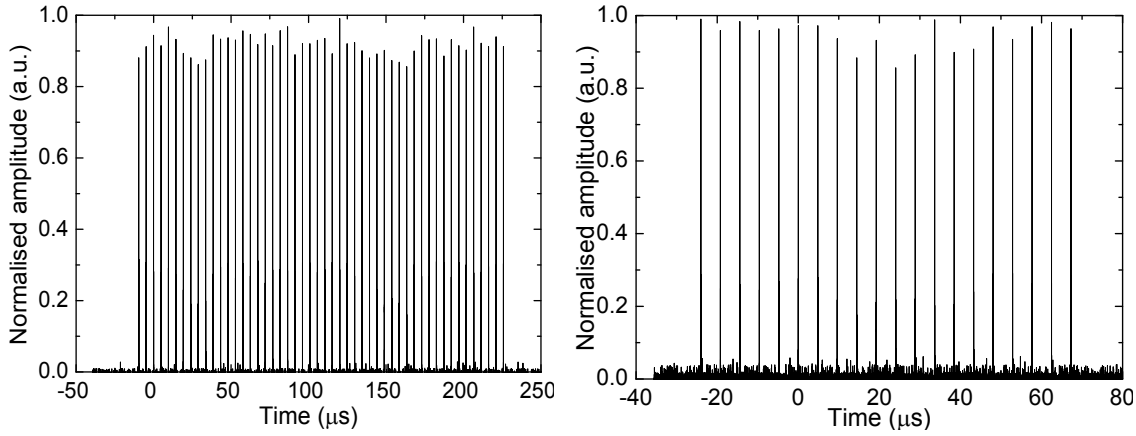

(a) (b)

Figure 4.5 Bursts of pump input with (a) 50 pump pulses of 50 ns duration; (b) 20 pump pulses of 100 ns duration;

As typical for a broadstripe diode, the beam quality (M^2) of the fast (vertical) and slow (horizontal) axis are quite different, 1.6 and 10.6 respectively, measured with a continuous train of 50 ns pulses with 1% duty cycle at about 5 W peak power. The beam quality is expected to depend on the operating parameters of the diode, but this was not investigated. The slow-axis beam quality is insufficient for the fibre we used, so the launch efficiency was limited to 11% when measured through a short length of the HNLF at a peak power of 30 W in bursts of 50 ns long pulses. The low launch efficiency restricted the output power could reach. Theoretically, with our fibre and our beam quality (though measured at 5 W peak power), one could conceivably reach up to twice as high launch efficiency. The shortfall may, for example, be caused by imperfect

compensation of the astigmatism that is typical for broadstripe diodes [7]. The highest pump peak power we could launch was ~ 4 W.

4.3.2 Beam path in the ring cavity

As shown in Figure 4.4, the pump light was launched into the Raman fibre via a first polarising beam splitter (PBS), a multi-order waveplate, a zero-order halfwave-plate, and a focusing lens. The purpose of the PBS is to combine the pump and Stokes waves, and the purpose of the waveplates is to allow for partial polarisation control. A fraction of the launched pump pulse is then Raman-scattered in the HNLF to a Stokes pulse at 835 nm. The pulses exited the HNLF via the SMF-28 pigtail and a collimating lens. Both ends of the fibre assembly were perpendicularly cleaved.

The pump and Stokes pulses that exited the fibre assembly were partly outcoupled from the cavity via a second PBS. The outcoupled pump and Stokes could be separated by a bandpass filter (BPF, Thorlabs FB 840-10) and characterised by a power meter (HP 8153A), an OSA (ANDO 6317B), and the same oscilloscope as the pump traces measurement. A zero-order halfwave-plate was placed between the output lens and the 2nd PBS. One could find that the fraction of outcoupled Stokes power changes if this was rotated. This also changed the fraction of outcoupled pump power. The fraction remained stable over several hours. The polarisation axes of the 1st and 2nd PBS were parallel for the results I report here, so there was no outcoupling in the 1st PBS. The remaining Stokes and weak pump pulses were thus transmitted through the 1st PBS, where they were combined with the next pump pulse, timed to coincide with the Stokes pulse. The pulses were then launched into the HNLF again, after passing through the two launch-end waveplates.

4.3.3 Polarisation dependent Raman gain

Polarisation is important for SRS and needs to be considered. At the output of the 1st PBS, which combines the pump and Stokes, the pump and Stokes were orthogonally polarised, which hampers SRS [4, 8]. The subsequent multi-order waveplate addresses this by changing the SOP of the pump relative to the Stokes. Figure 4.6 shows the spectral transmission behaviour of the multi-order waveplate, inserted between two parallel polarisers. The rapid variation in the resulting spectrum implies that the

waveplate provides multiple orders of retardation. The spectral periodicity is in the range 30 - 35 nm, which is close to the wavelength separation between the pump and Stokes. Since these are orthogonally polarised on the input of the multi-order waveplate, they will have similar SOPs on the output, if the birefringence axis is set at 45° to the pump and Stokes polarisation axes. The resulting SOPs are elliptical, insofar as the retardance is not a multiple of $\lambda/4$. The zero-order halfwave-plate at the launch-end can then be used to further adjust the SOP of the light launched into the HNLF in order to maximize the SRS. Since it is a zero-order waveplate with little difference in the retardation between pump and Stokes, their SOPs will remain similar.

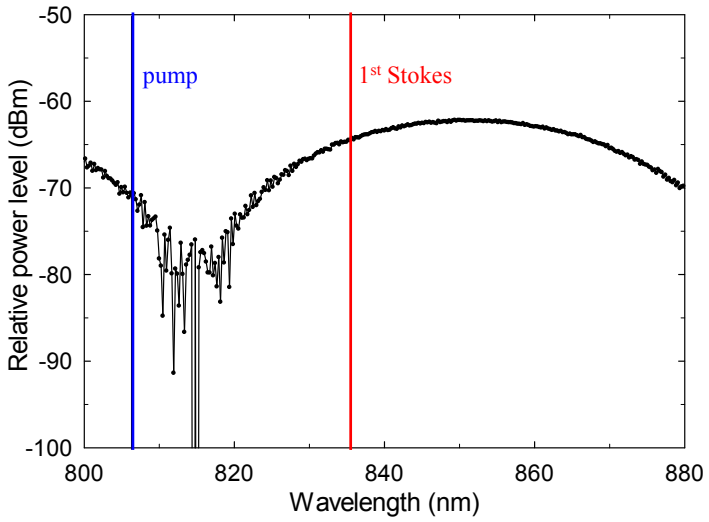

Figure 4.6 Transmission spectrum of multi-order waveplate when placed before the fibre launching end (resolution 2 nm).

While having similar SOP for pump and Stokes waves is a reasonable choice, it is not necessarily the best one. The evolution of the SOPs in the fibre, as well as the Raman gain as integrated along the fibre, can reveal several different regimes, and can be quite complex, in particular in a few-moded fibre. For example, sometimes polarisation mode dispersion (PMD) is used to characterise a fibre. This is appropriate when the SOP varies randomly, as can be the case in a fibre that is much longer than the so-called diffusion length. For sufficient lengths and PMD, the Raman gain can then become polarisation-independent [9, 10]. The PMD of the HNLF was measured by the manufacturer to 0.07 ps/km$^{0.5}$ at 1550 nm, from which we can estimate the diffusion length to 160 m [9]. This is shorter than our fibre lengths, but not by a sufficient amount to guarantee polarisation-independent gain. This is especially so since the pump-to-

Stokes power transfer can effectively occur over a relatively small fraction of the fibre length. Indeed, the outcoupled fraction does depend on the setting of the waveplate at the fibre output, and it is stable, so it is clear that the total Raman gain of the fibre does actually depend on polarisation. Ideally, the launched Stokes and pump SOPs as well as the output coupling ratio, as controlled by the waveplate on the output, should then be jointly optimised for optimum Raman conversion and output coupling. However our cavity did not allow for independent control of pump and Stokes SOPs, and even if it did a full optimisation would be difficult in practice. Within those limitations we used the following simple procedure to partially optimise the cavity. The multi-order waveplate was set at 45°, and the pump current was set to the maximum value to be used for a measurement. The halfwave-plates on the input and output were then rotated to find the maximum output power. Around these setting, one could then tweak all three waveplates in order to further increase the output power. It was found that the maximum output power occurred for an output coupling of 70%, which was the highest output coupling ratio I could reach. The settings were then kept constant as the current was reduced. The output coupling ratio was reduced to 60% near threshold.

I did not investigate the effect of the input-end halfwave-plate in detail. I expect that the outcoupling would change, i.e., drop from the 70% maximum value, but that it could then be recovered to a similar value by rotating the second halfwave-plate. Simultaneous optimisation of both waveplate positions did show that the overall efficiency was different for different positions of the input-end halfwave-plate, but I did not quantify this.

While the output polarisation is in general elliptical, it can be expected to drift and can be modified by the settings of the waveplates on the fibre input. This suggests that at least when the polarisation has drifted to particular states, it should be possible to reach output coupling of more than 70%, if the degree of polarisation is high. The SOP or the degree of polarisation was not measured, but the output may be partly depolarised, e.g., as a result of multimode propagation or the wavelength dependence of the SOP combined with the finite Stokes linewidth. This was typically around 5 nm. Given the length of the fibre, some depolarisation may well be expected, even if it is not complete. Also note that for a multimode fibre, there are no principal SOPs for which Stokes and pump can remain co-polarised even in the absence of birefringence [9, 11]. Depolarisation may then limit the output coupling attainable with our configuration.

It is possible that a higher outcoupling ratio would allow for a higher efficiency. A higher outcoupling ratio is possible with a birefringent polarisation-maintaining fibre or with a partially reflecting mirror. In addition it would be possible to couple out light also in the 1st PBS, by rotating the 2nd PBS relative to the 1st one, and thus reach a higher total outcoupling ratio, albeit in two beams.

Polarisation optics and the polarisation dependence of SRS complicate the laser. However SRS also has properties which simplify the cavity, notably the instantaneous gain. Because of this, gain is only present where there is pump light. Outside the pump pulses, there is no gain in the co-propagating direction, and the gain in the counter-propagating direction is quite small, of the order of 1% of the gain in the pulses, as determined by the duty cycle in the pulse train. Therefore, there is no need for an isolator to ensure unidirectional Stokes propagation. In stark contrast to RE-doped fibres, this also means that residual reflections are of little consequence, so there is no need to angle the fibre ends, which simplifies the optical arrangement.

An outcoupling of 70% leads to 5.2 dB of cavity loss. Add to this a Stokes re-launch loss of 10 dB, a splice loss of 1.3 dB, and the background loss of 2.7 dB/km at Stokes wavelength, and we find a total cavity loss of 19.0 dB for the 944 m long fibre and 18.2 dB for the 600 m long fibre.

4.4 Laser characteristics

4.4.1 Transient compensation

There is a transient effect as the Stokes power builds up in the beginning of a burst, as illustrated in Figure 4.7. This effect, which can overestimate the threshold as well as the slope near threshold, relative to what they would be for fully developed pulses in a continuous train, can be significant in short bursts and near threshold. To compensate for this effect and calculate the slope efficiency and threshold in the steady-state section of the burst, where the Stokes pulses are fully developed, the Stokes output powers we present are multiplied by a factor $M > 1$:

$$M = \frac{NP \times P_{average}}{\sum_{i=1}^{NP} P_i} \quad (4.1)$$

where NP is the number of pulses in the burst, $P_{average}$ is the average amplitude of the developed pulses, and P_i the amplitude of the i^{th} pulse. The formula assumes that the Stokes pulse duration was constant throughout the burst, which was approximately the case.

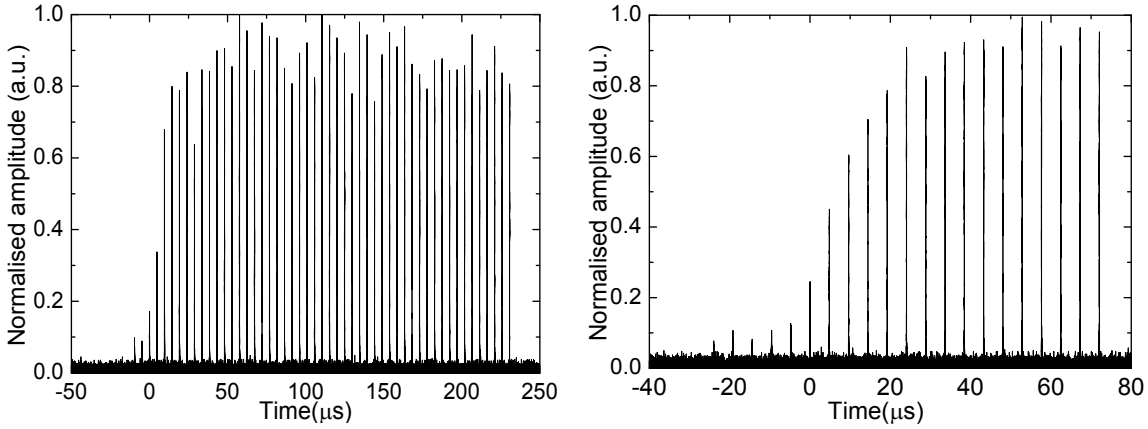

(a) (b)

Figure 4.7 Bursts of laser output pulses close to the lasing threshold. (a) 50 laser output pulses of 50 ns duration; (b) 20 laser output pulses of 100 ns duration.

4.4.2 Output power

The peak laser output power from the 2nd PBS for 50 ns pulse duration is shown in Figure 4.8, including the correction factor M for the power conversion. This is with respect to launched peak power, as determined from the transmitted average pump power (measured in the absence of significant Raman conversion), the background loss, and the splice loss to the SMF-28. The output peak power of the Stokes is determined from the output average Stokes power, measured through the BPF and adjusted to compensate for the 68% Stokes loss in the BPF. Figure 4.8 suggests a threshold of 570 mW for the 944 m long fibre and of 1400 mW for the 600 m long fibre, as extrapolated from the measured power data points. The slope efficiency improves from 29% with 944 m HNLF to 50% with 600 m HNLF.

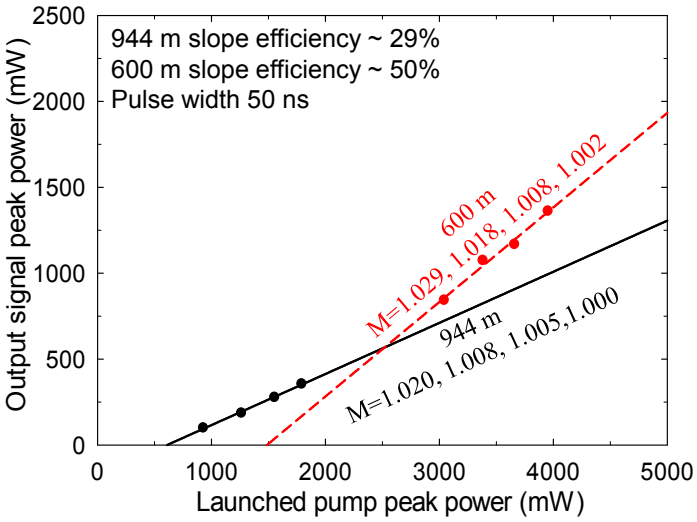

Figure 4.8 Output Stokes peak power *vs.* launched pump peak power for 50 ns pulse duration, 944 m fibre length (black solid line) and 600 m fibre length (red dashed line).

Figure 4.9 compares the results for 50 ns long pulses (as already shown in Figure 4.8) to those for 100 ns long pulses. The 100 ns pulses show a lower threshold (extrapolated), as expected from the reduced impact of dispersion for the longer pulses. The extrapolated peak power threshold is 440 mW for the 944 m long fibre and 610 mW for the 600 m long fibre. As for the 50 ns pulses, the slope is higher for the shorter fibre also for 100 ns pulses, and reaches 65%.

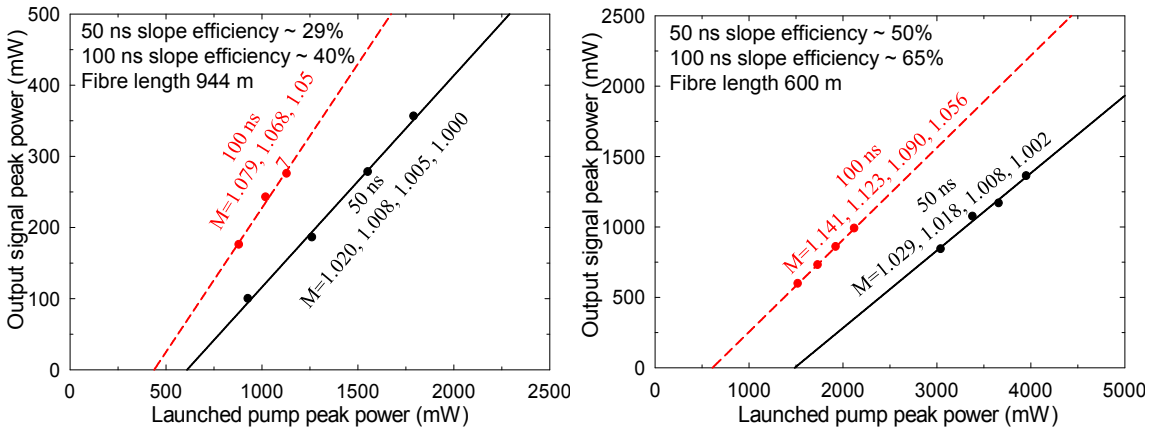

(a) (b)

Figure 4.9 Output laser peak power *vs.* launched pump peak power for (a) 944 m and (b) 600 m fibre length, 50 ns pulse duration (black solid line) and 100 ns pulse durations (red dashed line).

Figure 4.10 shows the output spectrum with highest launched pump power in 944 m HNLF. The linewidth is 4 nm. There is no higher order Raman Stokes generation.

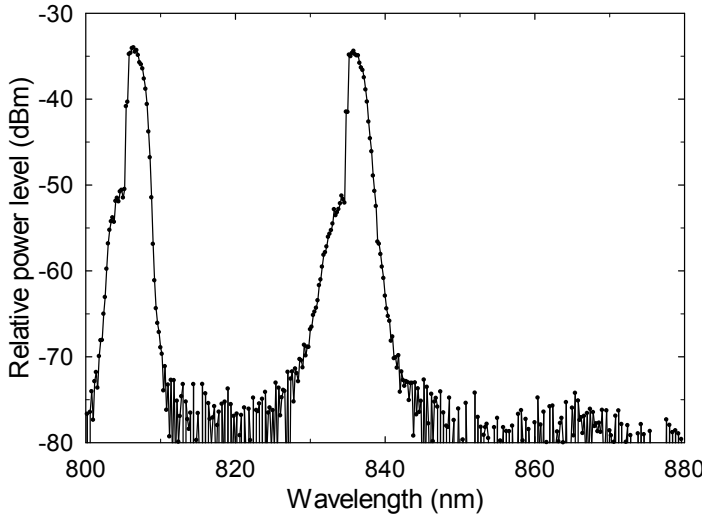

Figure 4.10 Laser output spectrum at highest output power for 100 ns pulse duration with 944 m long HNLF (resolution 2 nm).

I measured the beam quality of the output Stokes and found that the beam quality (M^2) of the fast (vertical) and slow (horizontal) axis at highest power level are 4.9 and 5.1, respectively. This is rather high for a V-value of 5.1, in particular in light of the beam clean-up effect that is common in multimode fibre Raman lasers [12]. The splice at the output end may explain this. It is also possible that the loss of lower-order modes, with lower M^2-values, is higher as a result of the relatively higher Ge concentration in the centre of the core. More sophisticated designs such as a double-clad Raman fibre could be used generate effectively single-mode output [13]. I will demonstrate this in the next chapter.

4.5 Discussion

Figure 4.11 shows theoretical power characteristics for a fibre Raman ring-laser using the parameters of the HNLF. For this I used a simple scalar cw model with spectrally unresolved Raman gain proportional to the pump power and with uni-directional co-propagating pump and Stokes waves. The cavity parameters were chosen to match the experimental ones. Thus, the outcoupling is 70%, while 10% of the light transmitted through the 2nd PBS is launched back into the input end of the fibre. The 1.3 dB splice

loss reduces the outcoupled power directly as well as indirectly, through an increased threshold. I consider both the case when the pump and Stokes waves are co-polarised, with a Raman gain coefficient of 4.0×10^{-13} m/W, and the case when their polarisations are uncorrelated, i.e., effectively unpolarised as it comes to the Raman gain. The Raman gain coefficient is then 2.0×10^{-13} m/W, i.e., half of the value for co-polarised light. The actual effective Raman gain coefficient is unknown, but would lie somewhere between those two limiting cases.

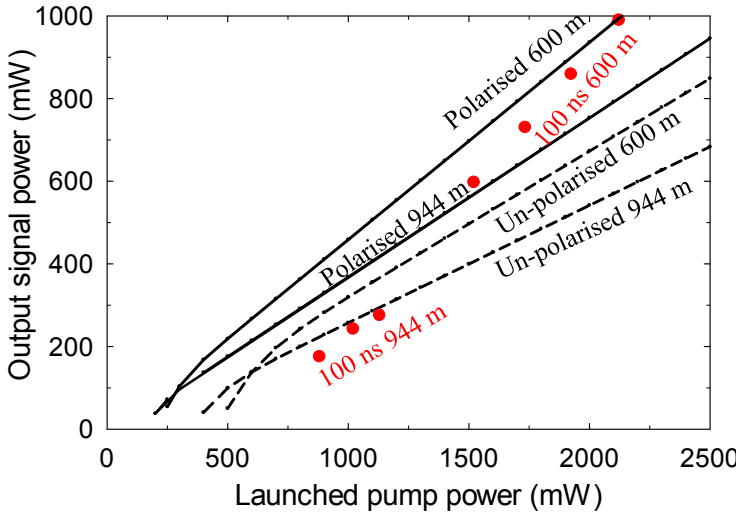

Figure 4.11 Calculated Stokes output power from a cw co-pumped Raman laser in a ring cavity with 944 m and 600 m long HNLF for co-polarised (black solid curves) as well as unpolarised waves (black dashed curves), together with experimental results for 100 ns pulse width.

The calculated thresholds are lower than the experimental 100-ns thresholds. These seem more appropriate to compare to cw calculations than the 50-ns thresholds are, because of the smaller effect of walk-off and pulse broadening. For unpolarised light, the threshold becomes 460 mW (600 m) and 360 mW (944 m), which is ~25% - 30% lower than the experimental values. The experimental slope efficiency, on the other hand, is comparable to, or even higher than, the theoretically calculated values, even with the co-polarised assumption. A multimode partially polarised FRL is quite complicated and difficult to model, so some deviation is not surprising. Several effects warrant attention. For example, the increased pump depletion at higher pump powers can increase the slope efficiency over a limited range of powers near threshold, even beyond the quantum limit. Also the difference in loss between Stokes and pump can

increase the slope efficiency. As the power increases, the pump is converted to Stokes over a shorter distance, which in combination with the lower propagation loss for the Stokes reduces the overall impact of the fibre loss. These effects are only significant over the range of powers for which the change in pump depletion and in effective conversion length is significant.

The pump depletion and difference in pump and Stokes losses are included in the simulations, but polarisation matters, too. Experimentally, the SOPs of pump and Stokes are likely to be better correlated, and SRS therefore more effective, in the beginning of the fibre than in the end. The effect of this increases as the power increases and the conversion accelerates. Similarly, the effect of walk-off between pump and Stokes decreases as the power increases and the effective SRS conversion length becomes shorter, although we believe this to be a small effect for 100 ns long pulses. Nevertheless, these effects were not modelled, but can also result in a higher slope efficiency, experimentally, although again only over a limited range of pump powers.

While changes in SOP may lead to an experimental slope that is higher than those calculated with fixed polarisation, the power should still lie between that calculated for co-polarised and unpolarised waves. This is indeed approximately the case in Figure 4.11. Note that the higher-power, shorter-fibre measurements are closer to the co-polarised case, whereas the lower-power, longer-fibre measurements are closer to the unpolarised case. This is in line with our discussions. Still, several uncertainties remain, including measurement errors, uncertainties in the exact experimental conditions, as well as model limitations. One example is the change of outcoupling as the power increased, which we attribute to changing polarisation properties.

4.6 Summary

I have reported a directly diode-pumped fibre Raman laser emitting at 835 nm, which is the shortest wavelength reported to date. A QD as low as 3.5% is realised by pumping at short wavelength. At this wavelength the background losses are around ten times higher than at 1550 nm, and constitute a major hurdle even in state-of-the-art fibres such as the high-NA HNLF I used. To overcome this, the FRL was synchronously pumped by a high-brightness broadstripe diode laser at 806 nm, which was pulsed to generate multi-watt peak-power pump pulses of 50 - 100 ns duration. I polarisation-combined pump

and Stokes, and used a waveplate at the Stokes output to vary the outcoupling. In addition, partial polarisation control was used to improve the Raman conversion in the HNLF. This way, a slope efficiency of 65% was reached in a 600 m long fibre with watt-level threshold in a ring-cavity. Higher efficiencies are expected in shorter fibres with smaller total background loss. The average output power was limited to 1.4 mW, primarily due to limitations in the pump driver which limited us to burst-mode operation.

Although a FRL can benefit from controlled polarisation, this is difficult in multimode fibres. Therefore, I will discuss higher pump power through wavelength multiplexing, which looks more attractive for further improvements of output power and efficiency. It will also be important to use a fibre that matches the pump beam rather than just captures a fraction of it. For high-power operation, this will require larger-core fibres than I used. Even then it would be possible to use double-clad fibres to improve the beam quality. Also note that the fibre background losses decrease rapidly with increasing wavelength. This makes longer-wavelength operation easier, and the demonstrated cw FRL pumped by a 975 nm diode source will be shown in the next chapter. I expect further rapid increase in output power of short-wavelength diode-pumped FRLs now that the underpinning fibre and diode technology has reached the threshold performance also in this wavelength range.

4.7 References

1 See http://www.rp-photonics.com/quantum_defect.html.

2 S. Namiki and Y. Emori, “Ultrabroad-Band Raman Amplifiers Pumped and Gain-Equalized by Wavelength-Division-Multiplexed High-Power Laser Diodes,” IEEE J. Sel. Top. Quantum Electron. 7, 3-16 (2001).

3 S. I. Kablukov, E. I. Dontsova, E. A. Zlobina, I. N. Nemov, A. A. Vlasov, and S. A. Babin, “An LD-pumped Raman fiber laser operating below 1 μm,” Laser Phys. Lett., 10, 085103, (2013).

4 G. P. Agrawal, Nonlinear Fiber Optics, (4th Ed., Academic Press Inc, San Diego CA, 2007).

5 M. M. Bubnov, S. L. Semjonov, M. E. Likhachev, E. M. Dianov, V. E. Khopin, M. Y. Salganskii, A. N. Guryanov, J. C. Fajardo, D. V. Kuksenkov, J. Koh, and P. Mazumder, "On the origin of excess loss in highly GeO_2-doped single-mode MCVD fibers," IEEE Photon. Technol. Lett., 16(8), 1870-1872, (2004).

6 S. T. Davey, D. L. Williams, B. J. Ainslie, W. J. M. Rothwell, and B. Wakefield, "Optical gain spectrum of GeO_2-SiO_2 Raman fiber amplifiers," Proc. Inst. Elect. Eng., 136(6), 301-306, (1989).

7 W. A. Clarkson and D. C. Hanna, "Two-mirror beam-shaping technique for high-power diode bars," Opt. Lett., 21(6), 375-377, (1996).

8 Q. Lin and G. P. Agrawal, "Vector theory of stimulated Raman scattering and its application to fiber-based Raman amplifiers," J. Opt. Soc. Am. B., 20(8), 1616-1631, (2003).

9 D. Mahgerefteh, H. Yu, D. L. Butler, J. Goldhar, D. Wang, E. Golovchenko, A. N. Phlipetskii, C. R. Menyuk, and L. Joneckis, "Effect of randomly varying birefringence on the Raman gain in optical fibers," in Proc. of CLEO, 11, 447, (1997).

10 S. Popov, E. Vanin, and G. Jacobsen, "Influence of polarization mode dispersion value in dispersion-compensating fibers on the polarization dependence of Raman gain," Opt. Lett., 27(10), 848-850, (2002).

11 M. Fridman, M. Nixon, M. Dubinskii, A. A. Friesem, and N. Davidson, "Principal modes in fiber amplifiers," Opt. Lett. 36(3), 388-390 (2011).

12 K. S. Chiang, "Stimulated Raman scattering in a multimode optical fiber: evolution of modes in Stokes waves," Opt. Lett., 17 (5), 352-354, (1992).

13 J. Nilsson, J. K. Sahu, J. N. Jang, R. Selvas, D. C. Hanna, and A. B. Grudinin, "Cladding-pumped Raman fiber amplifier," in Proc. of Optical Amplifiers and Their Applications (OAA 2002), paper PD2-1/2/3, Vancouver, Canada 2002.

Chapter 5: High-power operation of directly diode-pumped continuous-wave fibre Raman lasers

This chapter covers my work on directly diode-pumped cw fibre Raman laser sources. Section 5.1 reviews the motivations for the study of stimulated Raman scattering for beam quality improvement. The characteristics of the GRIN and double-clad Raman fibres used in the experiment are introduced in section 5.2. Section 5.3 presents experimental results on FRLs in linear cavities pumped by diodes and the potential for brightness enhancement. Then section 5.4 deals with the analytic simulation of SRS in linear laser cavities and further future power scaling. Finally, section 5.5 summarises this chapter.

5.1 Introduction

Power-scaling of FRLs pumped by MM lasers has been the subject of much research, and typically with diode-pumped RE-doped fibre lasers used as pump sources [1, 2]. In the 1990s, Liu shows that MM fibres could efficiently generate SRS [3]. In the same period of time, Chiang experimentally demonstrated the beam clean-up properties of SRS in MM fibre, i.e. brightness enhancement through SRS in a MMF, and envisaged the single-mode operation of such a fibre [4, 5]. The SRS fibre laser was pumped by a high-peak power pulsed dye laser and low order mode operation was achieved by the appropriate modal excitation of the MMF.

An alternative to core-pumped MM fibre is to use double-clad fibre which can be pumped with even lower brightness sources. Brightness enhancement through fibre devices has been the most compelling advance in the high power regime. As an example, YDFLs emitting around 1 μm work particularly well, and have reached 20 kW of output power with excellent beam quality [6]. In term of conventional MM Raman fibre, the transverse pump distribution results in Raman gain which preferentially favours lower-order modes at the Stokes wavelength. Consequently, the output beam quality is improved with respect to the pump beam quality. Still, in a CP fibre the power injected

into the fundamental mode of the Stokes can be controlled more easily than in large MM structures.

As demonstrated in Chapter 4, it is also possible to pump the FRL directly with diodes. However, the high fibre loss at 0.8 μm meant that the required pump brightness could only be reached in pulsed mode, which restricted the average power. For power-scaling of FRLs, lower fibre loss and superior cw brightness and power make 0.9 - 1 μm diodes a better choice, and devices based on MM pumping of MM fibres have recently been demonstrated [7], largely after the work described in this chapter. However these still operated relatively close to threshold, with output power of 3 W and slope efficiency of 35% or less. Furthermore, while some beam quality improvement is possible ("beam clean-up") in MM FRLs, the beam quality was still limited.

In this chapter, I investigate the realisation of Raman laser cavity with GRIN-MM Raman fibre, by an improved diodes pumping system that allows me to operate higher above threshold and with fibres with higher loss. Then encouraged by the achieved record output power, I demonstrate the first FRL cladding-pumped directly by diodes. In both the GRIN-MM Raman fibre and the DCRF, the output brightness was improved. The analytic solution of Raman conversion in the FRL cavity with the Lambert function was also presented. Further optimisation based on the laser and fibre parameters is discussed for potential power scaling.

5.2 Graded index fibre and double clad Raman fibre

In this chapter, two fibres with high Ge-doping are used in FRLs pumped by 975 nm LDs. The GRIN-MM fibre was fabricated by the OFS (model OM-4) while another Raman fibre (A0386-L10284) having the double clad structure was fabricated by Prof. J. K. Sahu through the MCVD process. A careful investigation of the fibre properties is needed to understand how it works as a MM Raman fibre converter. Next I will describe the details of these two fibres.

5.2.1 Graded index fibre

This fibre comprises a Ge-doped silica core with diameter of 62.5 μm and a NA of 0.275. They are circularly shaped and concentric. Outside the cladding, there is a polymer coating to protect the fibre. The coating has a high refractive index so that the

outer cladding does not guide light. Thus the fibre has a so-called all glass structure for guiding light, with neither pump nor Stokes wave in contact with the polymer coating. A normalised RIP of this GRIN-MM fibre is shown in Figure 5.1.

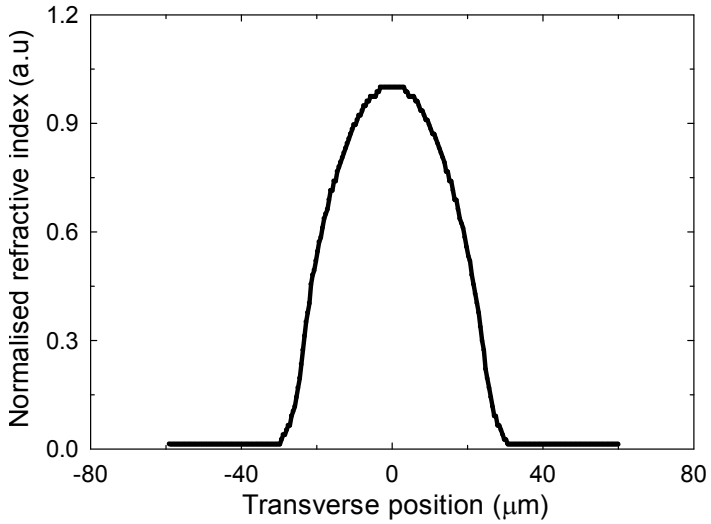

Figure 5.1 Measured refractive index profile of GRIN-MM fibre.

The background loss spectrum of a 1 km long piece of this fibre was characterised with a conventional cutback measurement by employing the WLS. As shown in Figure 5.2, the background loss is measured to 1.7 dB/km at the pump wavelength of 975 nm and 1.5 dB/km at the Stokes wavelength of 1019 nm. I used two different fibre lengths, 3 km and 1.5 km, giving effective lengths of 1.8 km and 1.1 km, respectively.

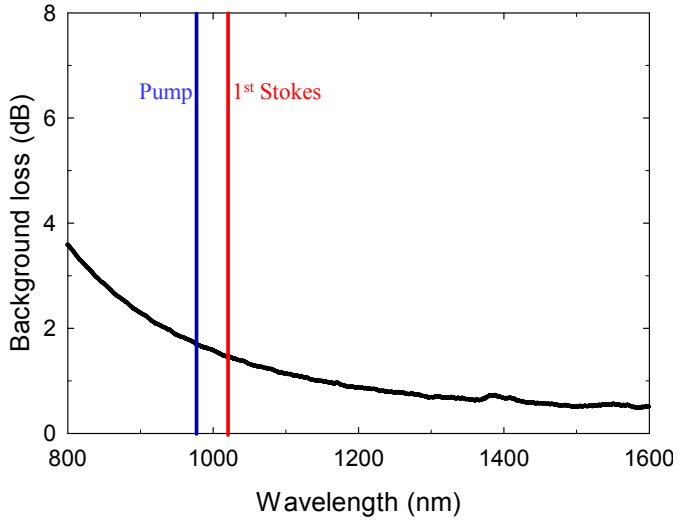

Figure 5.2 Measured background loss spectrum of 1 km long GRIN-MM fibre.

The Raman gain coefficient can be estimated based on the refractive index difference shown in Figure 5.1 between the pure-silica cladding and Ge-doped core [8, 9]. At 975 nm, the Raman gain coefficient is estimated to 2.38×10^{-13} m/W in the core for co-polarised light. For unpolarised light the gain coefficient is half of the value, i.e. 1.19×10^{-13} m/W.

5.2.2 Double clad Raman fibre

The DCRF (A0386-L10284) used in my experiments, is an all-glass fibre formed by a pure-silica outer-cladding and the Ge-doped inner cladding and core. The core is defined as the section with raised refractive index (with respect to the inner-cladding) of the fibre as shown in Figure 5.3. Here, the core is formed by increasing the Ge concentration. The inner cladding has a diameter of 38 μm and an NA of 0.3 with respect to the outer cladding. The core has a diameter of 14.6 μm and an average NA of 0.1 relative to the inner cladding. The cladding-to-core area ratio equals 6.8. This is below eight and therefore small enough to allow for efficient first-Stokes generation in the absence of higher order Stokes [10]. The outer cladding has an outside diameter of 228 μm comparable in size to that of a standard fibre. The fibre is protected by a low-index coating, so also the outer cladding can guide light.

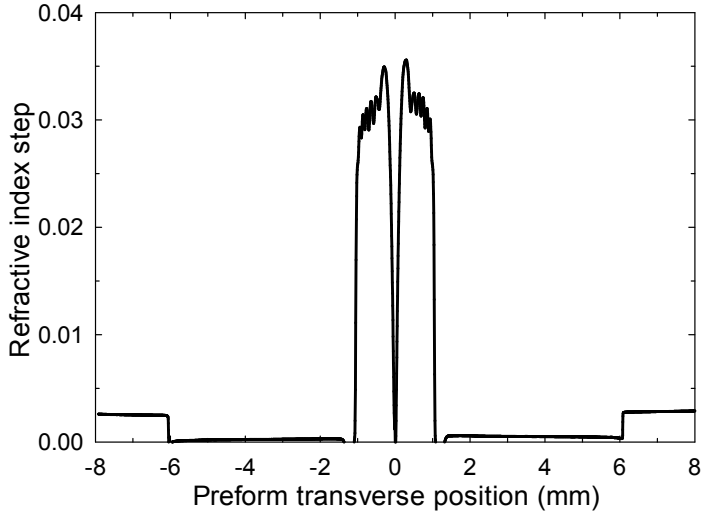

Figure 5.3 Measured RIP of preform A0386-L10284.

The core supports two modes at the Stokes wavelength, LP_{01} and $LP_{11}$with effective refractive indexes of 1.4846 and 1.4838, respectively. A central dip is present in the fibre refractive index profile due to the evaporation of germanium during the

preform collapse. The dip modifies the shape of the fundamental mode at the Stokes wavelength, but it does not affect the working principle of the Raman amplification process.

The high Ge concentration used in the design of A0386-L10284 leads to scattering, which translates into background losses for the pump and Stokes. As shown in Figure 5.4, the fibre background loss at pump wavelength of 975 nm has been measured to be 7.5 dB/km in the inner-cladding whilst this loss was 6.9 dB/km at the Stokes wavelength of 1019 nm.

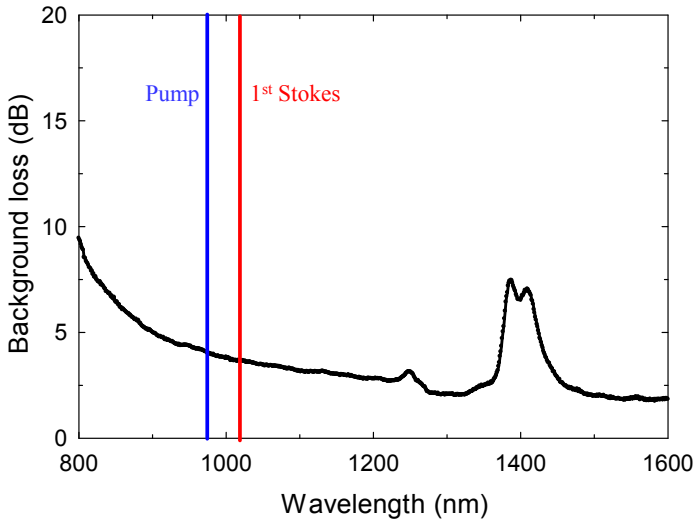

Figure 5.4 Measured background loss spectrum of 0.65 km long DCRF A0386-L10284.

The Raman gain coefficient, in the presence of Ge dopant, can be estimated from the difference of refractive index of the doped region with respect to fused silica. From the empirical formula given in [8] for a wavelength at 975 nm and from the RIP shown in Figure 5.3, the Raman gain coefficient for unpolarised light is expected to be around 1.31×10^{-13} m/W in the inner-cladding whilst in the core it is estimated to be around 1.4×10^{-13} m/W because of the higher Ge concentration.

5.3 Experimental setup and laser characteristics

5.3.1 Spectral beam combination of pump diodes

In these experiments, to ensure high pump brightness, the pump source was realised with spectral combination of two pigtailed MM diode sources (IPG Photonics). The

setup scheme of the beam multiplexing is shown in Figure 5.5. This helps increase pump power without any degradation of the beam quality. In the case of FRL with the GRIN MM fibre, the two pump diodes were wavelength-stabilised. Each source could deliver 45 W of power from a 110 μm diameter core with an NA of 0.12. The diodes were spectrally offset from each other, at 974.6 nm and 975.1 nm, with linewidth of ~ 0.5 nm (full width at half maximum).

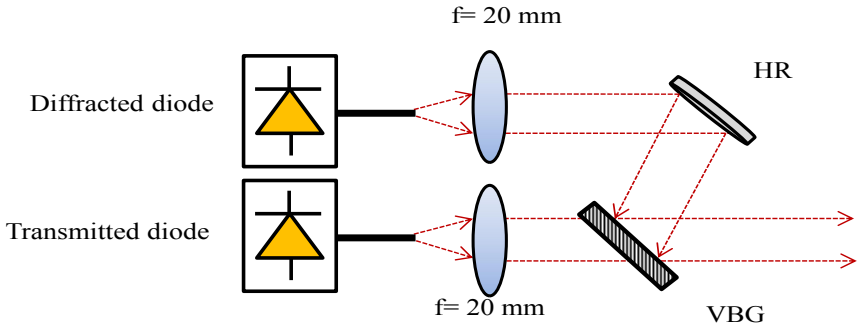

Figure 5.5 Experimental setup schematic of the spectrally beam-combined diode pump source. HR: high reflection mirror.

As shown in Figure 5.5, the output beams from the two diodes were collimated and then combined into a single beam in a tilted narrow-band VBG (Optigrate model C38-48-C1). The VBG had an aperture of 5×2 mm, a thickness of 5 mm, and the full width at half maximum (FWHM) linewidth of 0.43 nm. The diffraction efficiency for the 975.1 nm diode was ~ 70%, and the transmission efficiency of the 974.6 nm diode was ~ 80%. We reached 70 W of combined power, without discernable degradation of the beam quality. See Figure 5.6.

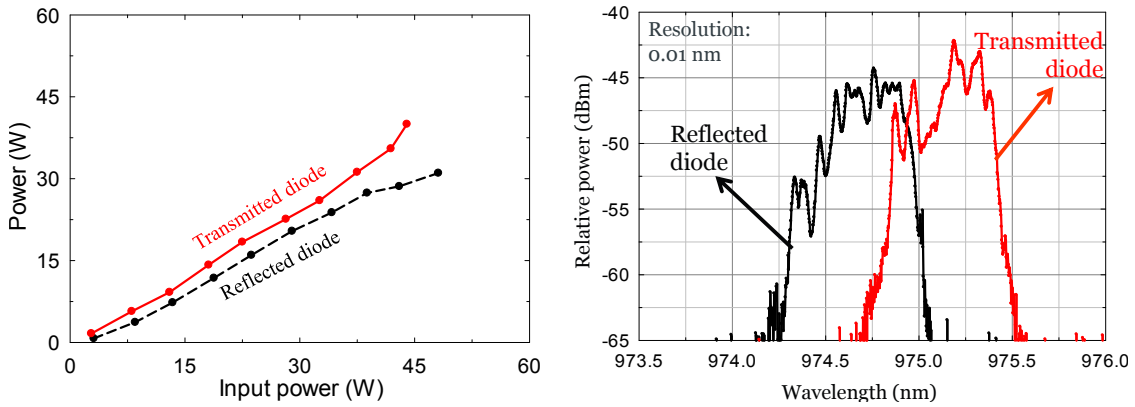

(a) (b)

Figure 5.6 (a) Reflected (black dashed line) and transmitted (red solid line) pump power after VBG with 45-W diodes *vs* power incident on the VBG. (b) Combined spectra of pump sources after VBG.

When it comes to further improvement of the pump source for DCRF, the 45 W diodes was replaced by ones that could provide 60 W of power from a 105 μm diameter core at an NA of 0.13. The new reflected diode source (IPG Photonics) was wavelength-stabilised at 975.6 nm with ~ 0.6 nm linewidth FWHM. The transmitted diode (IPG Photonics), which was not wavelength-stabilised, had a central emission wavelength in the range of 969.4 - 971.2 nm and a linewidth of 4 nm.

The un-stabilised diode had higher transmission through the VBG than the previous stabilised one, and could also be taken to slightly higher power than the rated 60 W. When this diode was used on its own, the power through the VBG reached 54 W. When the reflected diode was used on its own, the power from the VBG reached 35 W, which was comparable to the power with the 45 W diode, due to the larger linewidth and perhaps also increased heating, which could perturb the VBG [11]. As shown in Figure 5.7, the maximum total combined pump power reached nearly 85 W, compared to the previous 70 W. The beam quality degraded from M^2 = 22.2 to M^2 = 23.2. Thus, the pump brightness was improved by 11%.

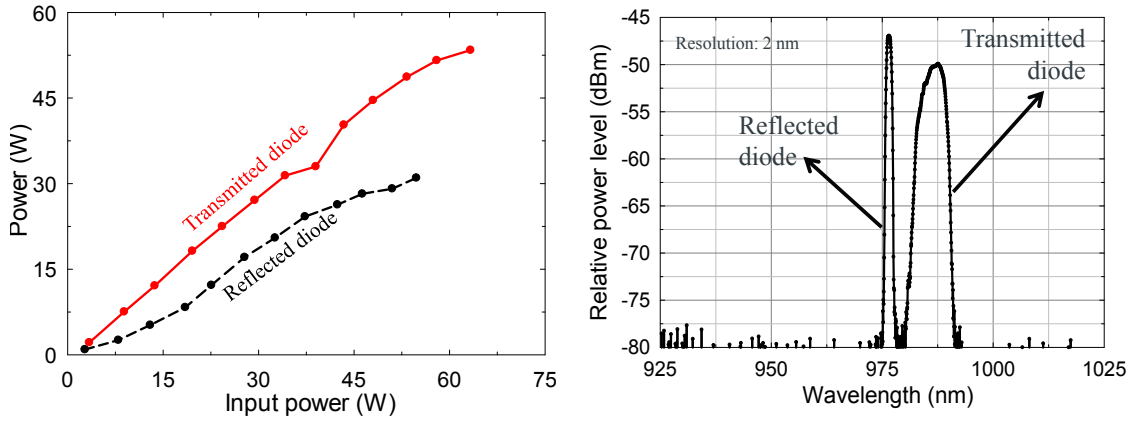

Figure 5.7 Reflected (black dashed line) and transmitted (red solid line) pump power after VBG *vs* input power of each diode.

5.3.2 Laser cavity with graded-index fibre

The wavelength-combined pump light is launched into the GRIN-MM Raman gain fibre via a lens. See Figure 5.8. The launching efficiency is 60%. In the far end of the fibre, a lens-coupled DM with reflectivity over 99% for both of pump and signal, was used to launch escaping light back into the fibre with 80% launch efficiency. The DM has a reduced reflectivity of less than 5% at the wavelength of the 2nd Stokes at around 1064 nm. This helps to prevent SRS to the 2nd Stokes at around 1064 nm, which can degrade the conversion efficiency [10]. The fibre had flat normal cleaves in both ends. Thus, the resulting 4% reflectivity closed the laser cavity in the combined pump launch & outcoupling end of the fibre. There, another DM separated the outcoupled beam from the pump path.

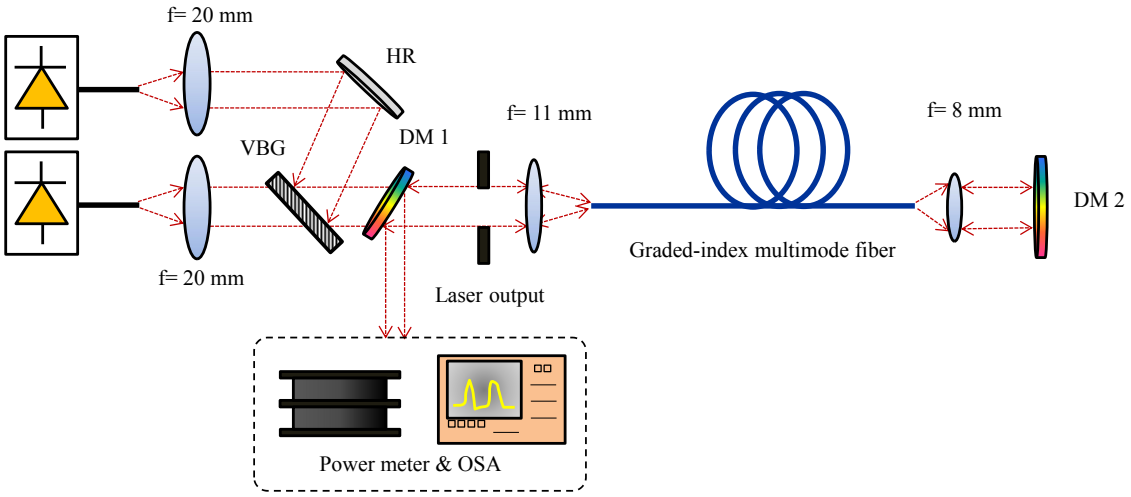

Figure 5.8 Experimental setup of the FRL with GRIN-MM Raman fibre.

Figure 5.9 shows the total output signal power measured from 1.5 km and 3 km long GRIN-MM fibres. The pump threshold powers are about 19 W and 16 W, corresponding to the total roundtrip loss of 19.37 dB and 23.13 dB for two fibre lengths respectively. Those are calculated by assuming 80% pump re-launching efficiency in the far end and the 1809 μm^2 effective SI core area of GRIN-MM fibre matching the pump brightness (110 μm, 0.12 NA) for 0.275 *NA*. Then an additional re-launching efficiency of Stokes can be estimated by the already-known 1.5 dB/km fibre propagation loss and 96% output coupling ratio. In the cases of 1.5 km and 3 km long fibre length, we can get the re-launching loss of 82% efficiency (-0.87 dB) and 97% efficiency (-0.13 dB). Those laser parameters will be used in the next simulation section.

The output power with the 3 km long fibre reaches 15 W with a slope efficiency of 62%. For 1.5 km long fibre, an even higher slope efficiency of up to 80% is achieved, while the highest output power is as high as 20 W. This corresponds to a record optical-optical device efficiency of about 50%.

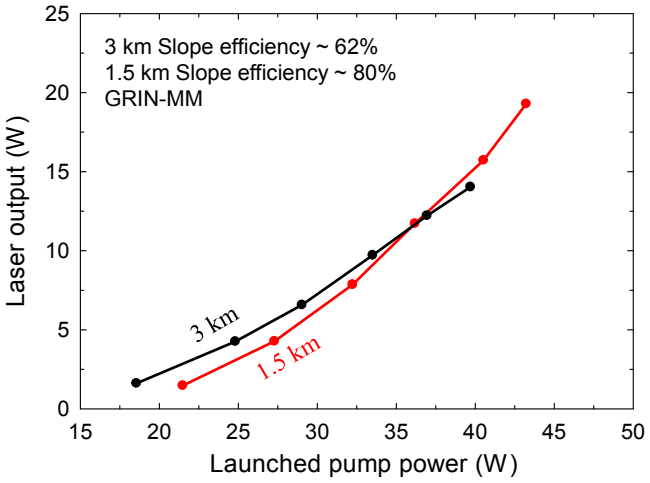

Figure 5.9 Experimental FRL output power with GRIN-MM fibre *vs* input pump power.

The high power and efficiency are attributed to the high pump power and brightness, which allow us to operate relatively high above threshold in a short fibre, and the use of low-loss fibre. Figure 5.11 shows the output spectrum from the 1.5 km fibre at full power. There is no sign of the 2nd Stokes. The emission wavelength is 1019 nm for a QD of only 4.3%.

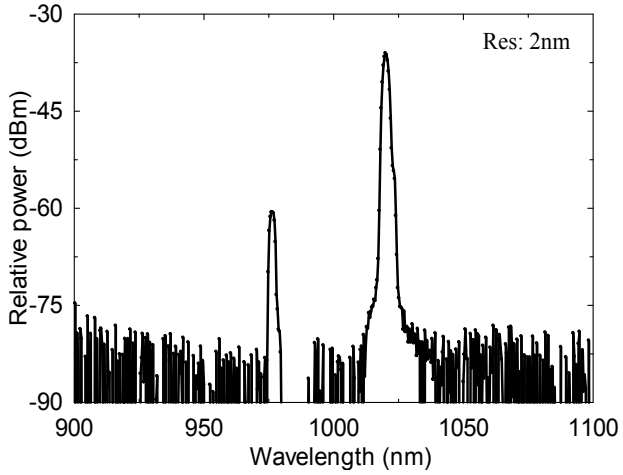

Figure 5.10 Experimental output spectrum of the FRL with 1.5 km GRIN-MM fibre at 20 W maximum power.

5.3.3 Laser cavity with double clad Raman fibre

Figure 5.11 shows the experimental configuration of FRL with DCRF (A0386-L10284). Using the 60 W IPG diodes, the wavelength-combined pump beam was launched into

the inner-cladding of the DCRF through a DM and a lens with a launch efficiency of ~ 76%. A small fraction of the light was actually launched directly into the core, while high-index gel used to strip out any light launched into the outer cladding The Raman laser cavity comprised 0.65 km of the DCRF as the Raman gain medium and the same lens-coupled DM as before, with higher reflectivity for pump and 1st Stokes and with reduced reflectivity at the 2nd Stokes. The fibre was perpendicularly cleaved in both ends. However, because of the higher fibre loss, the resulting 4% feedback in the pump launch end of the cavity was no longer sufficient for lasing to occur. A longer fibre could perhaps help to reduce the threshold, but the 0.48 km effective length is already 82% of the limiting case of an infinitely long fibre. Therefore, we reduced the cavity losses by using an external output coupler. This reflects 60% of the incident power back towards the DCRF via a DM that splits the pump and Stokes beam paths.

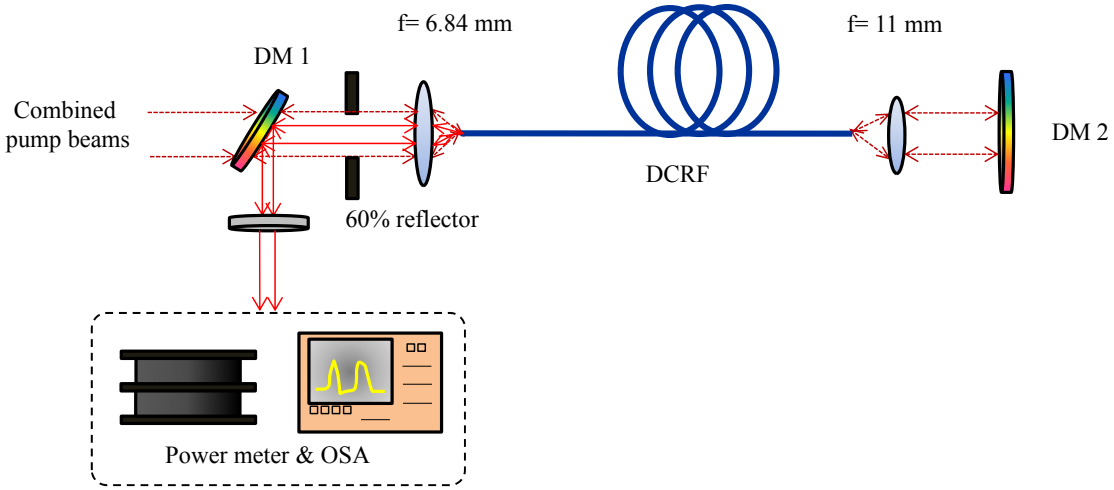

Figure 5.11 Experimental setup of the cw FRL with DCRF (A0386-L10284).

The output power from the Raman laser through the output end are shown in Figure 5.12. The laser threshold is 33 W and we obtain a maximum output power of 6 W for 65 W of launched pump power. The laser slope efficiency is 19%. The output power is limited by the pump power.

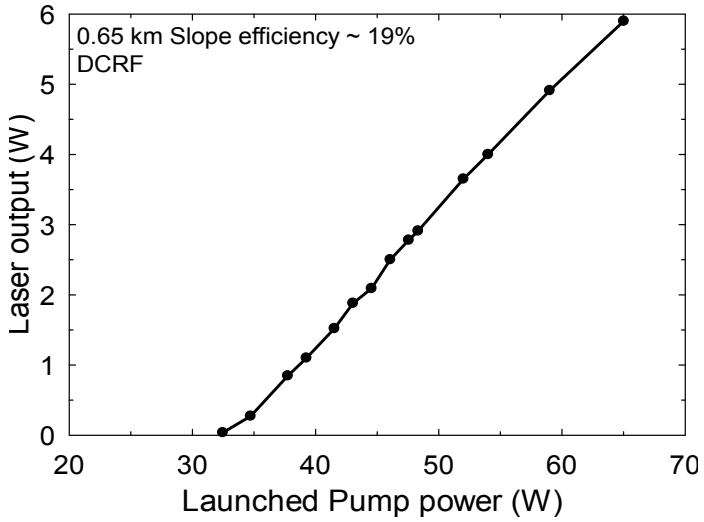

Figure 5.12 Experimental FRL output power with DCRF *vs*. input pump power.

As shown in Figure 5.13, the measured output spectrum is free from higher order Stokes light even at the highest output power, which indicates that further power scaling is possible.

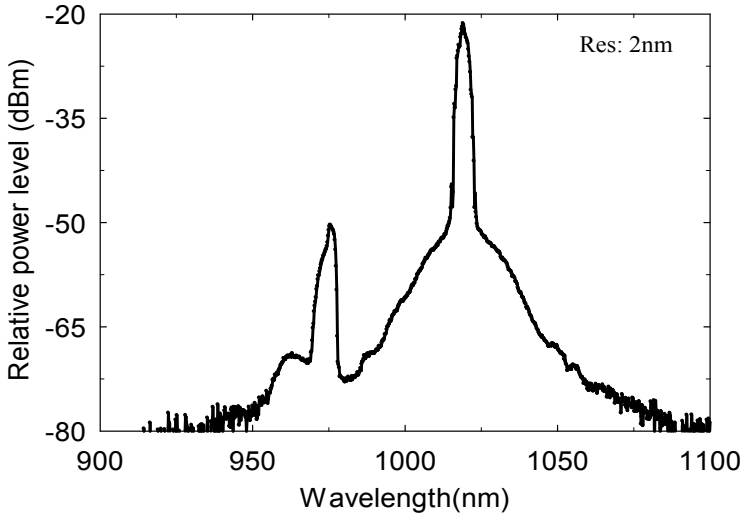

Figure 5.13 Experimental FRL output spectrum at 6 W maximum power with DCRF.

5.3.4 Temporal traces and beam enhancement

With 1.5 km GRIN-MM fibre length, the short-term output power fluctuations as shown in the Figure 5.14 (a) were below 5% rms in a 200 MHz bandwidth. Moreover, I measured the M^2 of the pump incident on the fibre to 22.2, while it became 5.0 for the output signal. Thus, the brightness (radiance) improved from 0.1494 $sr^{-1} \cdot \mu m^{-2}$ to 0.7704

$sr^{-1}\cdot\mu m^{-2}$, i.e., by a factor of 5.157. These measurements were at maximum power (20 W).

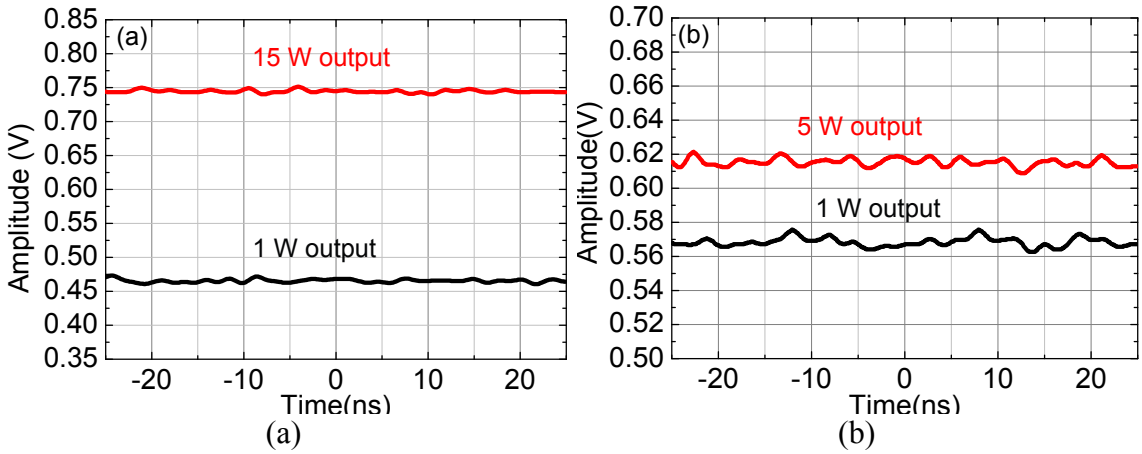

Figure 5.14 Temporal traces at various laser output levels for (a) 1.5 km GRIN-MM fibre and (b) 0.65 km DCRF.

The short-term power stability of the FRLs with DCRF was < 5% rms in a 200 MHz bandwidth at maximum power level (See Figure 5.14 (b)). The output beam quality became M^2 = 1.9 and the radiance 1.601 $sr^{-1}\mu m^{-2}$ at maximum power (6 W). The brightness enhancement in the DCRF case was about 11.5 times over that of the pump beam.

5.4 Discussion and laser cavity optimisation

5.4.1 Analytic solution of Raman coupling equations

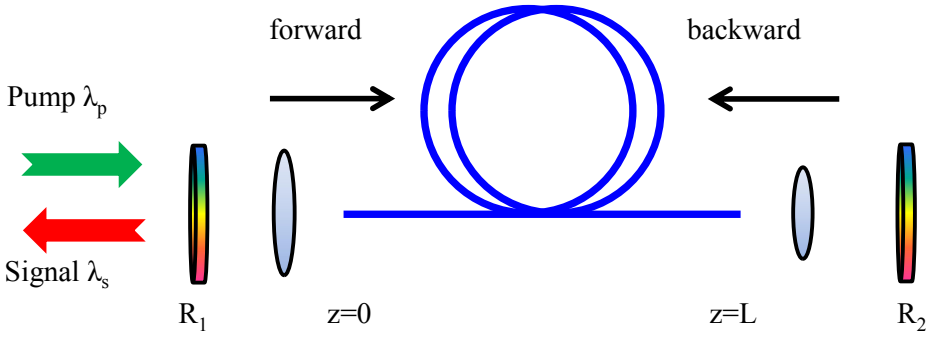

Figure 5.15 Schematic diagram of a single-pass pumping FRL.

Figure 5.15 shows the layout of the FRL as considered in this chapter. The pump beam is coupled into the fibre with a length of L inside a Fabry-Perot resonator at z=0. The

resonator is composed of two mirrors and their reflectivity are R_1 *(z=0)*, and R_2 *(z=L)* at the Stokes wavelength, respectively. For simplicity, in contrast to the experiments, I here only consider the single-pass of the pump. The power evolution of the depolarised pump, forward and backward Stokes waves can be expressed as below as discussed in Chapter 2

$$\frac{dP_s^f}{dz} = \frac{g_R}{A_{eff}} P_p P_s^f - \alpha_s P_s^f \tag{5.1}$$

$$\frac{dP_s^b}{dz} = -\frac{g_R}{A_{eff}} P_p P_s^b + \alpha_s P_s^b \tag{5.2}$$

$$\frac{dP_p}{dz} = -\frac{g_R}{A_{eff}} \frac{\omega_p}{\omega_s} P_p (P_s^f + P_s^b) - \alpha_p P_p \tag{5.3}$$

where the subscripts denote pump (*p*) and Stokes (*s*) wave and the superscripts represent forward (*f*) and backward (*b*) propagation directions. The boundary conditions of the three waves at position *z=0* and *z=L* can be expressed as

$$P_s^f(0) = R_1 \eta_1 P_s^b(0) \tag{5.4}$$

$$P_s^b(L) = R_2 \eta_2 P_s^f(L) \tag{5.5}$$

$$P_p(0) = P_{p0} \tag{5.6}$$

where P_{p0} is the pump power, η_1 and η_2 are the additional re-launching efficiencies at *z=0* and *z=L* respectively. The evolution of the forward and the backward Stokes obey the same physical mechanism, so Eq. (5.1) and (5.2) differ only because of the different propagating directions. Accordingly, we can deduce that

$$P_s^f(z) P_s^b(z) = C \tag{5.7}$$

where *C* is a constant independent of *z*. Using boundary conditions of Eq. (5.4) and Eq. (5.5), it follows directly that

$$\frac{P_s^f(0)}{P_s^f(L)} = \frac{P_s^b(L)}{P_s^b(0)} = \sqrt{R_1 R_2 \eta_1 \eta_2} \tag{5.8}$$

$$C = \frac{\left(P_s^f(0)\right)^2}{\eta_1 R_1} \tag{5.9}$$

Substitute Eq. (5.7) into Eq. (5.3), divide Eq. (5.1) by Eq. (5.3) and then integrate the resulting equation. The following expression are then obtained

$$\begin{aligned} &\exp\left(\frac{g_R}{A_{eff}}P_p + \frac{g_R}{A_{eff}}\frac{\omega_p}{\omega_s}\left(P_s^f - \frac{C}{P_s^f}\right)\right)P_p^{-\alpha_s}P_s^{f\,\alpha_p} = \\ &\exp\left(\frac{g_R}{A_{eff}}P_{p0} + \frac{g_R}{A_{eff}}\frac{\omega_p}{\omega_s}\left(P_s^f(0) - \frac{C}{P_s^f(0)}\right)\right)P_{p0}^{-\alpha_s}P_s^f(0)^{\alpha_p} = D \end{aligned} \tag{5.10}$$

where D is also a constant. This equation is valid at arbitrary z within the fibre. In particular, using the expressions for D at z=0 and z=L and Eq. (5.8), the forward Stokes power at z=0 can be written as

$$P_s^f(0) = \frac{\alpha_s \log\frac{(R_1R_2\eta_1\eta_2)^{\frac{\alpha_p}{\alpha_s}}P_p(L)}{P_p(0)} + \frac{g_R}{A_{eff}}(P_p(0) - P_p(L))}{\frac{g_R}{A_{eff}}\frac{\omega_p}{\omega_s}\left[\frac{1}{\sqrt{R_1R_2\eta_1\eta_2}} - \frac{\sqrt{R_1R_2\eta_1\eta_2}}{R_1\eta_1} + \frac{1}{R_2\eta_2} - 1\right]} \tag{5.11}$$

What's more, by exploiting Lambert W function [12, 13], the pump power described in Eq. (5.10) can be presented as

$$P_p = -\frac{A_{eff}\alpha_s}{g_R}W\left\{-\left[D\left(P_s^f\right)^{-\alpha_p}\left(\frac{A_{eff}\alpha_s}{g_R}\right)^{\alpha_s}\exp\left(-\frac{g_R}{A_{eff}}\frac{\omega_p}{\omega_s}\left(P_s^f - \frac{C}{P_s^f}\right)\right)\right]^{-1/\alpha_s}\right\} \tag{5.12}$$

where W is the Lambert W function. The Lambert W function is an important factor in the simulation and will be further discussed in the following section. Integrating Eq. (5.1) and exploiting Eq. (5.12) result in

$$\int_{P_s^f(0)}^{\frac{1}{\sqrt{R_1R_2\eta_1\eta_2}}P_s^f(0)} \frac{1}{-\left(W(u)+1\right)\alpha_s P_s^f} dP_s^f = L \tag{5.13}$$

where

$$W(u) = W\left\{-\left[D\left(P_s^f\right)^{-\alpha_p}\left(\frac{A_{eff}\alpha_s}{g_R}\right)^{\alpha_s}\exp\left(-\frac{g_R}{A_{eff}}\frac{\omega_p}{\omega_s}\left(P_s^f-\frac{C}{P_s^f}\right)\right)\right]^{-1/\alpha_s}\right\} \tag{5.14}$$

From Eq. (5.10) to (5.14), we can conclude the forward Stokes power at *z=0*, as well as the constants *C* and *D*, can be expressed as a function of the residual pump power. Therefore, the only variable in Eq. (5.11) is the residual pump power if the fibre length is known. This can be solved by Newton–Raphson method or simple search algorithm [14]. Once the residual pump power is obtained, we can easily get the lasing power at *z=0*

$$P_{laser} = (1-R_1)P_s^b(0) = \frac{1-R_1}{R_1\eta_1}P_s^f(0) \tag{5.15}$$

When the partial derivative of Eq. (5.11) with respect to $P_p(L)$ equals to 0, that is the Raman gain at the pump output end equals the signal propagation losses ($P_p(L) = \frac{\alpha_s A_{eff}}{g_R}$), $P_s^f(0)$ will be maximum and can be expressed as [15]

$$P_s^f(0)_{\max} = \frac{\alpha_s \log\frac{(R_1R_2\eta_1\eta_2)^{\frac{\alpha_p}{\alpha_s}}A_{eff}\alpha_s}{P_p(0)g_R} + \frac{g_R}{A_{eff}}P_p(0) - 1}{\frac{g_R}{A_{eff}}\frac{\omega_p}{\omega_s}\left[\frac{1}{\sqrt{R_1R_2\eta_1\eta_2}} - \frac{\sqrt{R_1R_2\eta_1\eta_2}}{R_1\eta_1} + \frac{1}{R_2\eta_2} - 1\right]} \tag{5.16}$$

The corresponding fibre length L_{opt} can be obtained by Eq. (5.13) with the already known residual pump power.

5.4.2 Simulated output power from the FRLs

The Lambert *W* function is the inverse function of $f(W)=We^W$. If *x* is real, *W(x)* will have two real branches for *-1/e<x<0* as shown in Figure 5.16 [12]. The branch satisfying *W(x)>-1* is denoted by $W_0(x)$ and that satisfying *W(x)<=-1* denoted by $W_{-1}(x)$.

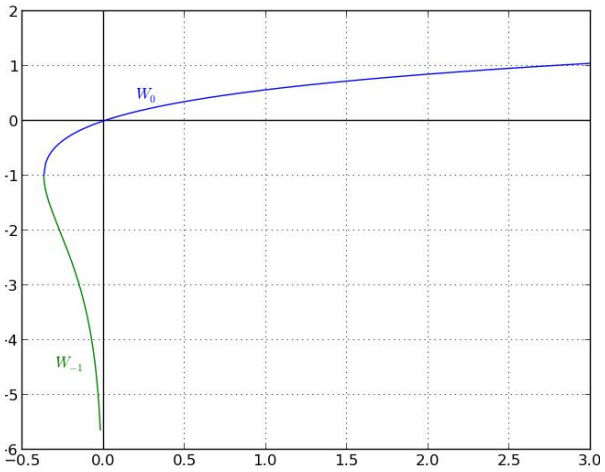

Figure 5.16 The two real branches of Lambert *W* function. The upper branch with $W \geq -1$ is the function W_0, the lower branch with $W \leq -1$ is the function W_{-1} [15].

Figure 5.17 shows the evolution of the power of pump and forward Stokes along *z* for short fibre length (case 1) and long fibre length (case 2), which have to be treated separately. The pump is depleted along the fibre by the Stokes generation in both cases. The forward Stokes keeps increasing in the whole range because the Raman gain is always larger than the background loss in the case 1. Taking into account the relationship between the pump and the Stokes shown in Eq. (5.12) and the properties of Lambert *W* function, $W_0(x)$ should be used. However, in the case 2, there is a turning point where the forward Stokes begins to decrease due to the less generating signal gain compared with the loss. Then one should employ $W_0(x)$ and $W_{-1}(x)$ separately to meet the different evolution trends in case 2. The branches of Lambert *W* function should be properly chosen according to the actual case of the FRLs. To the best of my knowledge, this has not been discussed before.

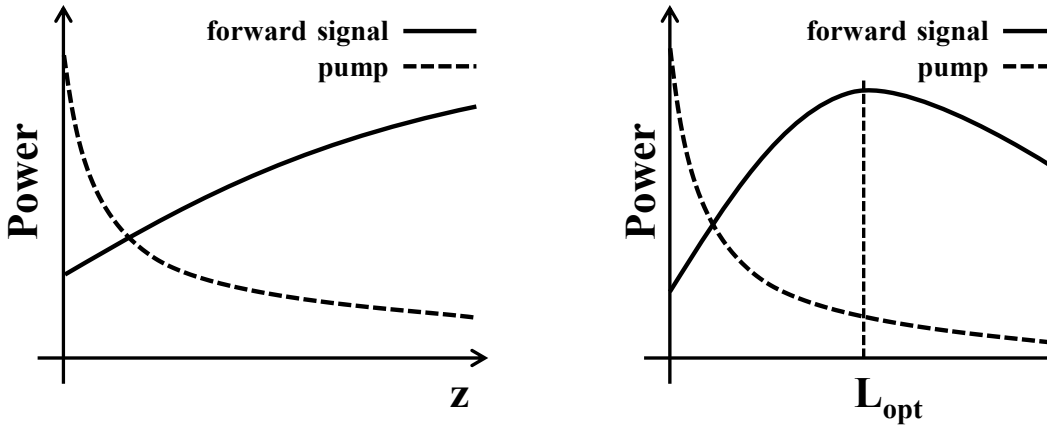

Figure 5.17 Scheme of the power evolution within the (a) short piece and (b) long piece of Raman fibre.

We can conclude for best utilization of the pump, the fibre length should be chosen so that the pump power is just enough to compensate for the signal propagation loss at the pump output end.

To verify the analytic mathematical solution, I compared it to experimental results. Figure 4.16 shows the case of 1.5 km and 3 km long GRIN-MM fibres. The simulated thresholds are 20 W and 26 W respectively, while the slope efficiencies are as high as 71.8% and 90%. Compared with the experimental results, the higher threshold may be caused by the simplifying assumption of single-pass pump. At higher signal powers, the relative pump leakage and therefore the difference between single-pass and double-pass pumping becomes smaller, which may explain why the slope efficiencies are in fair agreement at high power but not at lower power.

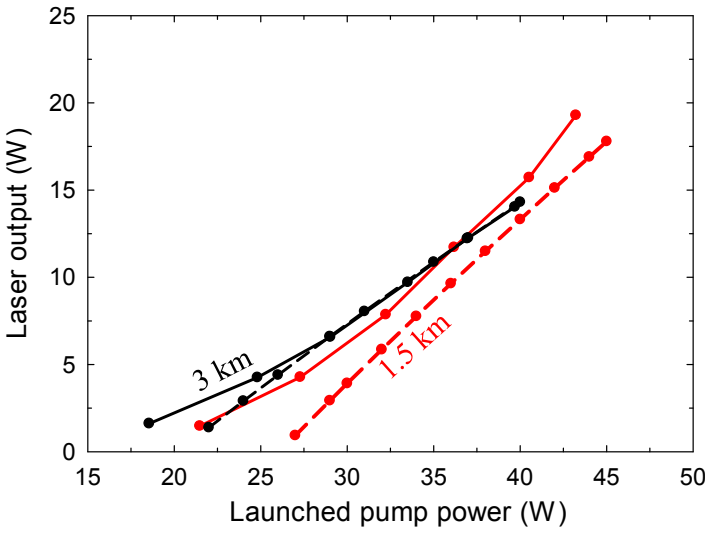

Figure 5.18 Analytic simulation (dashed line) compared with experimental results (solid line) of GRIN-MM FRL laser output with respect to the launched pump power. Fibre lengths are 3 km (black line) and 1.5 km (red line).

Despite the higher power achieved with the GRIN-MM fibre, the radiance (brightness) is actually higher with the DCRF thanks to the higher beam quality. This is a key attraction of DCRFs. Figure 5.19 shows simulation results for a 0.65 km long fibre with the parameters of the DCRF and the laser cavity that were used experimentally in the previous section. I used the pump and Stokes re-launch efficiencies as fitting parameters in order to obtain good agreement with experimental threshold and output power. I guessed values for the re-launch efficiencies in the high reflectivity end. It is then trivial to calculate the re-launch efficiency in the outcoupling end that results in a threshold of 33 W. The output power with 65 W of pump power was then calculated, and the whole procedure was reiterated until the output power became 6 W. In our case, with the pump distributed over the 1130 μm^2 inner-cladding area of the DCRF and assuming a pump re-launch efficiency of 30%, the 33 W threshold suggests a roundtrip cavity loss of 17.45 dB. Of this, the fibre propagation loss becomes 8.97 dB and the outcoupling 2.22 dB. This leaves a remaining loss of 6.26 dB. The fitted re-launch efficiencies become 90% (-0.46 dB) in the HR end and 26.33% (-5.80 dB) in the outcoupling end. The re-launching loss in the outcoupling end is surprisingly high. A re-launch loss of 5.8 dB in fibre end could well be expected with a nearly single-mode core, but in our case, also the inner cladding guides and amplifies light. Because the germanium content of the inner cladding is slightly smaller, both the

Raman gain and propagation loss can be expected to be a little lower, for overall similar laser threshold for cladding-modes. Thus, also cladding-modes can lase with a similar threshold, which means that it is the re-launch losses into the inner cladding rather than into the core that matter, and these are expected to be much smaller than 5.8 dB. Similarly as for the GRIN-MM fibre, the 44 W simulated threshold power is higher than experimentally obtained 33 W. Furthermore, the slope efficiency of 28% is higher than 19% experimental efficiency. This may be due to a poor overlap between some pump modes and the Stokes wave in the core.

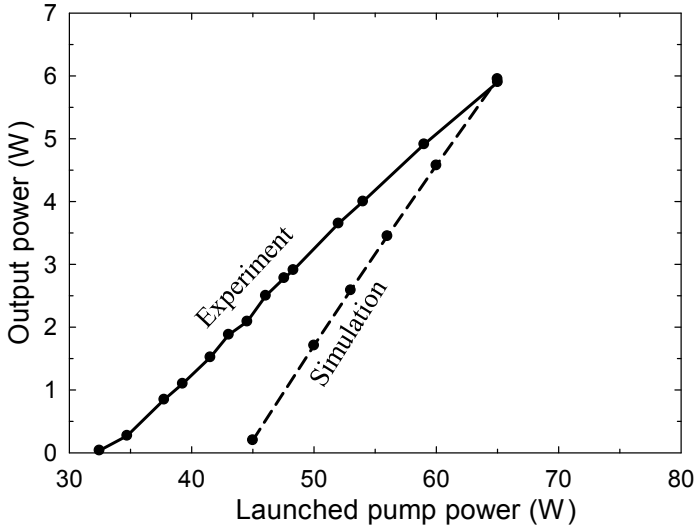

Figure 5.19 Experimental results (solid line) compared with the analytic simulation (dashed line), of DCRF FRL output with respect to the launched pump power.

5.4.3 Potential of output power scaling

Based on the results, the comparatively high propagation loss of the DCRF used here limits the output power and efficiency. While higher pump power in the fibre (to allow for shorter fibres) as well as lower loss are preferred long-term remedies for this, it is also interesting to see the maximum output power and the corresponding optimised fibre length with the present pump power level and fibre. Figure 5.20 shows the output power dependence on the fibre length for various outcoupling ratio and re-launching losses. When the fibre is short enough to make the propagation loss negligible, an over 43% conversion efficiency, which means about 28 W output power, can be theoretically possible with extremely small outcoupling (1%). Note here that the propagation losses are only negligible for the pump, whereas the losses can still be important for the signal

due to the high intra-cavity signal power in a high-Q cavity. On the other hand, with the 96% of output coupling from a perpendicularly cleaved fibre facet, the increase in threshold and fibre length and propagation loss reduces the efficiency to 10% with our parameters, even if there are no re-launching losses. The experimental outcoupling of 40% allows for 40% highest conversion efficiency with ~ 100 W of circulating signal power in 100 m of fibre without considering re-launching losses. However, in reality, the re-launching losses may well be significant. With the re-launching losses estimated in the last section, the maximum output power becomes 6.6 W at 500 m long optimum fibre length. This is slightly higher than the 6 W I obtained with 650 m of fibre.

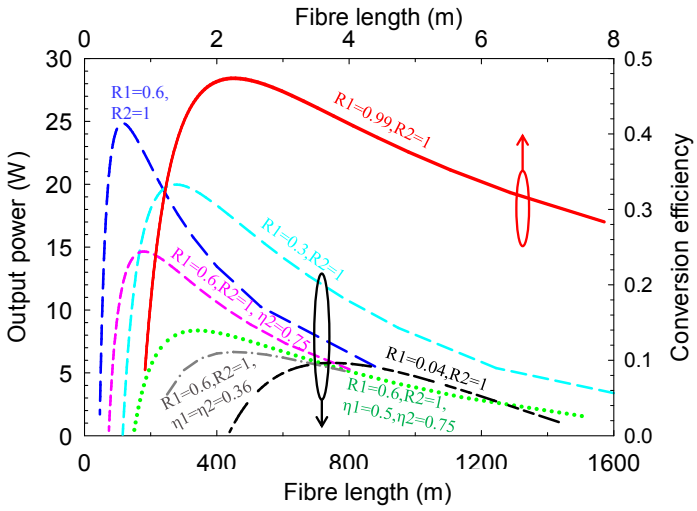

Figure 5.20 Output power *vs* fibre length for several outcoupling (R_1), re-launching efficiencies in the pump (η_1) and HR (η_2) ends when pumped by 65 W. Right axis indicates the conversion efficiency regarding to the output power.

Figure 5.20 exemplifies that reduced re-launch losses allow for large improvements. Further investigation with optimised outcoupling ratio for each fibre length is presented in Figure 5.21. The highest conversion efficiency of 43% shows good agreement with that achieved in Figure 5.20, when the loss in the cavity is minimised. Realistic re-launch losses still allow for a conversion efficiency of 12%, at an optimum fibre length of 550 m.

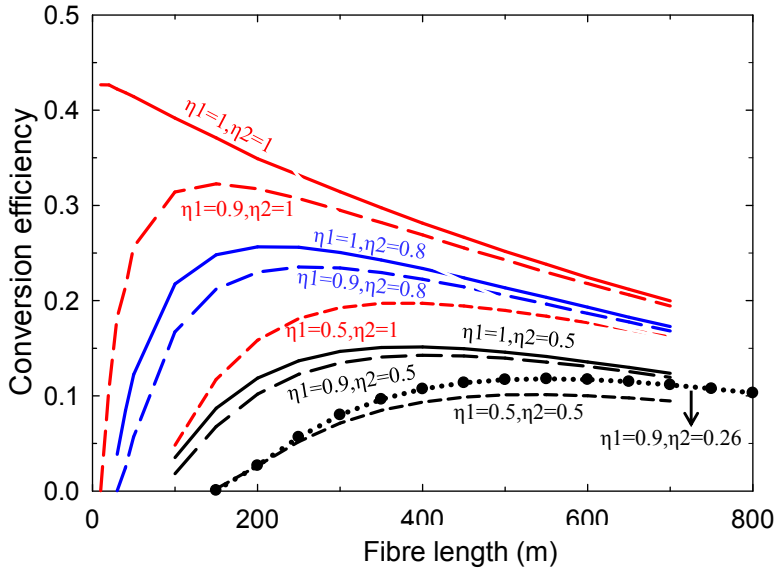

Figure 5.21 Output power *vs* fibre length for several re-launching efficiencies in the pump (η_1) and HR (η_2) ends with outcoupling optimised.

Still more efficient operation requires higher pump power (or intensity) or lower fibre loss. It is also possible to increase the Raman gain coefficient, which is equivalent to a higher pump power. For greater generality, I therefore introduce the normalised launched pump intensity as below:

$$I_{p0} = \frac{g_R P_{p0}}{A_{eff} \alpha_s} \tag{5.17}$$

Figure 5.22 shows how the optimised conversion efficiency depends on I_{p0} for different re-launching losses. This includes solutions that are optimised in terms of output coupling and fibre length. With I_{p0} = 4.726, which corresponds to our experiments with the DCRF, the maximum conversion efficiency agrees with the result shown above. However, higher than 50% conversion efficiency would be possible for I_{p0} over 14 even with re-launching efficiency of 50% in the pump launching end.

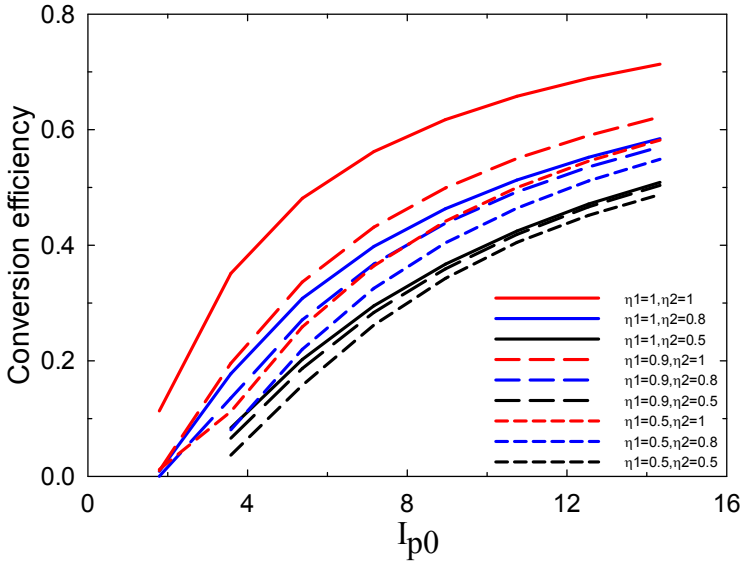

Figure 5.22 Conversion efficiency *vs* I_{p0} with optimised outcoupling and fibre length for different pump (η_1) & HR (η_2) ends re-launching efficiencies with actual pump and signal propagation losses ratio of 1.087.

5.5 Summary

In this chapter, I have demonstrated the first-ever FRL cladding-pumped directly by MM diodes as well as a high-power based on a GRIN-MM fibre. A high-brightness diode pump source was realized by the spectral beam combination in a VBG. Experimentally, brightness-enhanced Stokes output has been obtained. The slope efficiency with the GRIN-MM fibre reaches up to 80%, which is to our knowledge the highest slope efficiency of any MM-pumped FRL. An analytic solution of the coupled equations for FRLs has been derived using the Lambert *W* function. Further analysis of the laser cavity under more general conditions based on numerical simulations shows that under optimized conditions, the re-launching efficiency affects the output power significantly. The normalised launched pump intensity, matters, too, with the cavity parameters becoming less critical at higher normalised intensities. Even higher output power should be expected by optimising those factors. While this work demonstrated the feasibility of combining 975 nm pumps from high power commercial diodes to generate a single Stokes beam, in the future similar approaches and results will be possible at other low-loss wavelgnths where high-brightness diodes are available such as 0.8 μm.

5.6 References

1 C. A. Codemard, P. Dupriez, Y. Jeong, J. K. Sahu, M. Ibsen, and J. Nilsson, "High-power continuous-wave cladding-pumped Raman fiber laser," Opt. Lett. 31(15), 2290-2292 (2006).

2 V. R. Supradeepa and J. W. Nicholson, "Power scaling of high-efficiency 1.5 μm cascaded Raman fiber lasers," Opt. Lett. 38 (14), 2538–2541 (2013).

3 K. X. Liu and E. Garmire, "Role of stimulated four-photon mixing and efficient Stokes generation of stimulated Raman scattering in excimer-laser-pumped UV multimode fibers," Opt. Lett., 16(3), 174-176, (1991).

4 K. S. Chiang, "Stimulated Raman scattering in a multimode optical fiber: evolution of modes in Stokes waves," Opt. Lett., 17 (5), 352-354, (1992).

5 K. S. Chiang, "Stimulated Raman scattering in a multimode optical fiber: self-focusing or mode competition?," Opt. Commun., 95(4-6), 235, (1993).

6 B. Shiner, "High power fiber laser technology," presentation on Annual Department of Energy Laser Safety Officer (DOE LSO) Workshop, September 10, (2013).

7 S. I. Kablukov, E. I. Dontsova, E. A. Zlobina, I. N. Nemov, A. A. Vlasov, and S. A. Babin, "An LD-pumped Raman fiber laser operating below 1 μm," Laser Phys. Lett., 10, 085103, (2013).

8 S. T. Davey, D. L. Williams, B. J. Ainslie, W. J. M. Rothwell, and B. Wakefield, "Optical gain spectrum of GeO2-SiO2 Raman fiber amplifiers," Proc. Inst. Elect. Eng., 136(6), 301–306 (1989).

9 J. Bromage, K. Rottwitt, and M. E. Lines, "A Method to predict the Raman gain Spectra of germanosilicate fibers with arbitrary index profiles," IEEE Photon. Technol. Lett., 14(1), 24 (2002).

10 J. Ji, C.A. Codemard, J.K. Sahu, J. Nilsson, "Design, performance, and limitations of fibers for cladding-pumped Raman lasers," Optical Fiber Technology 16, 428-441, (2010).

11 A. Sevian, O. Andrusyak, I. Ciapurin, V. Smirnov, G. Venus, and L. Glebov, "Efficient power scaling of laser radiation by spectral beam combining," Opt. Lett., 33(4), 384-386, (2008).

12 R. M. Corless, G. H. Gonnet, D. E. G. Hare, D. J. Jeffrey, D. E. Knuth, "On the Lambert W function," Adv. Comput. Math, 5, 329-359, (1996).

13 C. Huang, Z. Cai, C. Ye and H. Xu, "Explicit solution for Raman fiber laser using Lambert W function," Opt. Express, 15(8), 4671-4676, (2007).

14 J. H. Zhou, J. P. Chen, X. W. Li, G. L. Wu, Y. P. Wang, "Exact analytical solution for Raman fiber laser," IEEE Photon. Technol. Lett., 18, 1097-1099, (2006).

15 J. AuYeung and A. Yariv, "Theory of cw Raman oscillation in optical fibers," J. Opt. Soc. Am. B, 69, 803-807, (1979).

16 See http://en.wikipedia.org/wiki/Lambert_W_function.

Chapter 6: Summary and future work

In the final chapter, I will begin with summarising the work presented in this thesis. Then I will present some possible ideas to approach the low QD in the future.

6.1 Summaries

The primary objective of my research demonstrated in this thesis was to construct and investigate the potential for the fibre laser sources with low QD based on tandem-pumped YDF and short-wavelength-pumped Raman fibre. Generally, even without fibre loss and nonzero non-radiative decay rate, the energy conversion process in lasers still generate heat due to QD, which is the photon energy difference between pump and signal. Thus the reduction of the QD would be attractive in terms of heat dissipation. Besides, this also provides a better understanding and potential for further power scaling. Although the Raman fibre is currently less troubled by the thermal generation than the RE-doped fibres like YDF, an approach to achieve low QD is also demonstrated, by utilising LDs at short wavelength as pump sources.

Lower thermal load and less spatial beam distortions may be possible in tandem-pumped high power YDFs. Besides, the lower peak excitation level with tandem pumping may mitigate PD, which otherwise increases rapidly as the result of high Yb excitation level when pumped at 910 - 980 nm [1]. Given these compelling advantages and demonstrations, both theoretical and experimental investigation of the reduction of the QD that tandem-pumping can offer is of considerable interest, and the subject of Chapter 3. Theoretically, the lowest QD in YDF with pure Al host is as low as 0.6% in the case of unity mode overlap between pump and signal. However the impact of model assumptions and errors in parameter values has not been assessed. Thus, a core-pumped YDFA was experimentally investigated using tuneable pump and seed sources in order to determine the minimum QD. In-house YDFs with various concentrations and compositions were investigated. Their fibre lengths wwere carefully selected to ensure sufficient, but not excessive, pump absorption. When seeded at 1050 nm, I show a good performance for 1030-nm pumping for a QD of less than 2%, which is a record for an efficient amplifier. The efficient amplification with 6-8 dB signal gain and over 95% slope efficiency has been achieved. In addition, I measured PD in a tandem pumped

YDFA. The results show a high dependence of PD on concentration. But this is only the initial step and further testing based on different types of YDFs is required.

Encouraged by the recent advances in high brightness diode sources, Chapter 4 and Chapter 5 present the experimental and theoretical work on FRLs pumped at 806 nm and 975 nm. The weak Raman gain and the significatn propagation are key factors. Restricted by the power capability of the 806 nm LD, I used synchronous pulse-pumping to reach a peak incident pump power of 30 W in 50 ns and 100 ns long pulses. A commercial Ge-doped HNLF with small core area of 10 μm^2 has been utilised as the Raman fibre. The pump launching efficiency is 10% and the background loss is 4.4 dB/km at the pump wavelength. The Raman gain coefficient has been calculated to around 4.0×10^{-13} m/W and 2.0×10^{-13} m/W for co-polarised and randomly polarised pump and Stokes waves, respectively. Therefore, to enhance the Raman gain, the SOPs of pump and Stokes waves were controlled. Stokes lasing at 835 nm was realised in both 944 m and 600 m long fibres. The QD is as lwo as 3.5%. With 100 ns pulse width, the slope efficiency can reach up to 65% in the 600-m long fibre and the threshold peak power can be 610 mW. The performance of 944 m fibre length is slightly worse but gives a lower threshold peak power of 440 mW with the same pulse duration. The output is MM and does not benefit from any beam clean-up effect. The average output power is limited due to the use of pulse bursts.

Further extensions and developments of power scaling and brightness enhancement are presented in Chapter 5. Two cw diodes at 975 nm are spectrally combined through a VBG, and then launched into the Raman gain fibres, which are GRIN fibre and DCRF. In the presence of high Ge concentration, the Raman gain coefficients corresponding to unpolarised waves are estimated to be 1.2×10^{-13} m/W and 1.31×10^{-13} m/W for GRIN fibre and DCRF, respectively. FRLs with 1.5 km long GRIN fibre shows 19 W output power at the 1st Stokes wavelength of 1019 nm. The QD becomes 4.3% and the slope efficiency reaches as high as 80%. Although the beam clean-up effect in GRIN fibre has helped a better output beam quality than pump, the output beam quality can be further improved in a DCRF. This is also the first diode-pumped FRL based on DCRF. It reaches nearly 6 W of output power and 19% slope efficiency. The beam quality M^2 becomes 1.9. The DCRF shows a huge potential for brightness enhancement from MM pump diode. Besides, in order to analyse the power evolution in the linear laser cavity, the analytic solution of the coupling equations has

been demonstrated by introducing both two branches of the Lambert *W* function for the first time. I finally discuss the influence of FRL cavity parameters based on modelling results. The novel approach of diode pumped FRLs seems very promising and definitely requires future investigations.

Overall the work carried out so far has presented a good proof of principle study with most of the measurements reported in this thesis being carried out for the first time. All in all, this work has demonstrated the flexibility and the substantial scope for generating low QD using tandem pumping for YDFA and diode pumping for FRLs.

6.2 Future work

6.2.1 Tandem pumped YDFA

Tandem-pumping with YDFLs, in which one YDFL pumps another, can allow for QD at the percent-level [2, 3]. This can be compared to the ~10% QD typical for direct diode-pumping. The immediate focus of future work should be power scaling. In Chapter 3, while QD of ~ 2% have been obtained with tandem pumping, experimental slope efficiencies are somewhat lower than this might suggest, and are furthermore difficult to measure with percent-level accuracy. Thus, the problematic heat generated in the core may well be considerably higher than the limit set by the QD. The calorimetric measurement of heat generation should be carried out. Dr You Min Chang has now measured ~3% heat generation at the 10 W power level [4]. Further investigation of tandem-pumping at the kW-level is the key next step, in which accurate heat may not be so critical or challenging [5, 6]. Alternatively, we have a multi-kW thin disk laser (Triumph) in our lab emitting at 1030 nm, which can be applied as the pump source.

6.2.2 Diode pumped FRL

Although the diode pumped FRLs with low QD have been studied in the thesis, a number of theoretical and experimental aspects still remain to be explored. To increase the output power, the improvement of the pump power without beam distortion can be achieved by operating in the quasi-cw regime with 10-100 μs long pulse width which nearly doubles the peak power. Alternatively, cascaded spectral beam combination

through several VBGs can be an option. This will lead to a broad pump linewidth, which might be challenging if it is significant compared to the Raman shift. Also, as mentioned above, the disk laser at 1030 nm would be applied as the pump source for FRL as well. Then the 1st Stokes wavelength locates at around 1080 nm, resulting in a QD of 4.6%.

In my experiments, the efficiency and the power scaling of the FRLs is also limited by the current Raman fibre with the relatively high background loss. Very often, the Ge doping of silica glass leads to an increased background loss which restricts the useable fibre length and, therefore, accentuates the requirement for high pump power. Nonetheless, with the recent advances in fibre fabrication, a new way could be found to incorporate more Ge into the glass while maintaining a low background loss to improve the device performance and to reach higher efficiency and lower threshold in laser configuration [7, 8]. Secondly, the waveguide design could be altered to increase the *NA* of the inner cladding. This will enable more pump power to be launched and therefore, increase the pump intensity. This can be realised either with a fluorine doped all-glass fibre or with an air-clad fibre [9, 10].

Finally, I show the analytic simulation of the Raman oscillation in optical fibres [11, 12]. This is with the assumption of single-pass pumping only. However, in reality, the laser cavity is constructed with pump feedback in the HR end for a lower pump threshold. The future direction on simulation should then focus on the explicit solution of the double-pass laser cavity. The power conversion during the SRS process and laser behaviour can then be modeled more precisely.

6.3 References

1 J. Koponen, M. Söderlund, H. J. Hoffman, D. A. V. Kliner, J. P. Koplow, and M. Hotoleanu, “Photodarkening rate in Yb-doped silica fibers,” Appl. Opt., 47(9), 1247-1256, (2008).

2 C. Codemard, J. K. Sahu, and J. Nilsson, “Tandem cladding-pumping for control of excess gain in ytterbium-doped fiber amplifiers,” IEEE J. Quantum Electron., 46(12), 1860-1869, (2010).

3 J. Nilsson, “Tandem-pumped Yb-doped fiber lasers with percent-level thermal load,” Fifth Annual SU2P Symposium, 2014.

4 Y. M. Chang, T. Yao, H. Jeong, J. Ji, S. Yoo, and J. Nilsson, “ Heat Generation Measurement for Tandem-pumped Ytterbium Doped Fiber Amplifier,” CLEO US, STh4N.7, San Jose, 2014.

5 C. Wirth, O. Schmidt, A. Kliner, T. Schreiber, R. Eberhardt, and A. Tünnermann, “High-power tandem pumped fiber amplifier with an output power of 2.9 kW,” Opt. Lett., 36(16), 3061-3063, (2011).

6 B. G. Ward, “Solid-core photonic bandgap fibers for cladding-pumped Raman amplification,” Opt. Express, 19(12), 11852-11866, (2011).

7 E. M. Dianov, “Advances in Raman fibers,” J. Lightwave Technol., 20(8), 1457-1462, (2002).

8 E. M. Dianov, D. G. Fursa, I. A. Bufetov, S. A. Vasiliev, O. I. Medvedkov, V. G. Plotnichenko, V. V. Koltashev, A. V. Belov, M. M. Bubnov, S. L. Semjonov, and A. M. Prokhorov, “CW high power 1.24μm and 1.48μm Raman lasers based on low loss phosphosilicate fibre,” Electron. Lett., 33(18), 1542-1544, (1997).

9 J. Wang, W. Zenteno, “All-glass high NA Yb-doped double-clad laser fibres made by outside-vapour deposition,” Electron. Lett., 40(10), 590-592, (2004).

10 V. A. Kozlov, J. Hernandez-Cordero, R. L. Shubochkin, A. L. G. Carter, and T. F. Morse, “Silica-air double-clad optical fiber,” IEEE Photon. Technol. Lett., 12(8), 1007-1009, (2000).

11 C. Huang, Z. Cai, C. Ye and H. Xu, “Explicit solution for Raman fiber laser using Lambert W function,” Opt. Express, 15(8), 4671-4676, (2007).

12 J. H. Zhou, J. P. Chen, X. W. Li, G. L. Wu, Y. P. Wang, “Exact analytical solution for Raman fiber laser,” IEEE Photon. Technol. Lett., 18, 1097-1099, (2006).

Appendix: List of publications

- T. Yao, J. Ji, and J. Nilsson, "Ultra-low quantum defect heating in ytterbium-doped aluminosilicate fibers," J. Lightw. Technol., 32(3), 429-434, (2014).

- T. Yao and J. Nilsson, "An 835 nm fiber Raman laser pulse-pumped by a multimode laser diode at 806 nm," J. Opt. Soc. Am. B, 31(4), 882-888, (2014).

- R. Steinborn, T. Yao, A. Webb, J. K. Sahu, and J. Nilsson, "Liquid-nitrogen-cooled high-concentration erbium-doped fibre laser", CLEO Europe, Munich, Germany, May 22-26, 2011.

- T. Yao, R. Steinborn, A. S. Webb, J. K. Sahu, and J. Nilsson, "Cryogenically cooled erbium-doped fiber lasers", CIOMP-OSA Summer Session: Lasers and Their Applications, Changchun, China, July 31-August 05, 2011.

- T. Yao, J. Ji, J. K. Sahu, A. S. Webb, and J. Nilsson, "Tandem-pumped ytterbium-doped aluminosilicate fiber amplifier with low quantum defect," CLEO US, San Jose, US, May 6-11, 2012.

- T. Yao and J. Nilsson, "Short-wavelength fiber Raman laser pulse-pumped by multimode laser diode at 806 nm," SOF, Colorado, US, June 17- 21, 2012.

- T. Yao and J. Nilsson, "Fibre Raman laser directly pumped by multimode laser diode at 975 nm" CLEO Europe, Munich, Germany, May 12-16, 2013.

- J. Nilsson, T. Yao, Y. M. Chang, J. Sahu, J Ji, and C Codemard, "Tandem-pumped Fiber Lasers with Low Quantum Defect," Advanced Solid-State Lasers Congress, Paris, France, October 27- November 1, 2013. (Invited)

- T. Yao and J. Nilsson, "High power, high efficiency fiber Raman laser pumped by multimode laser diodes at 975 nm," Advanced Solid-State Lasers Congress, Paris, France, October 27- November 1, 2013.

- Y. M. Chang, T. Yao, H. Jeong, J. Ji, S. Yoo, and J. Nilsson, " Heat Generation Measurement for Tandem-pumped Ytterbium Doped Fiber Amplifier," CLEO US, San Jose, US, June 8- 13, 2014.